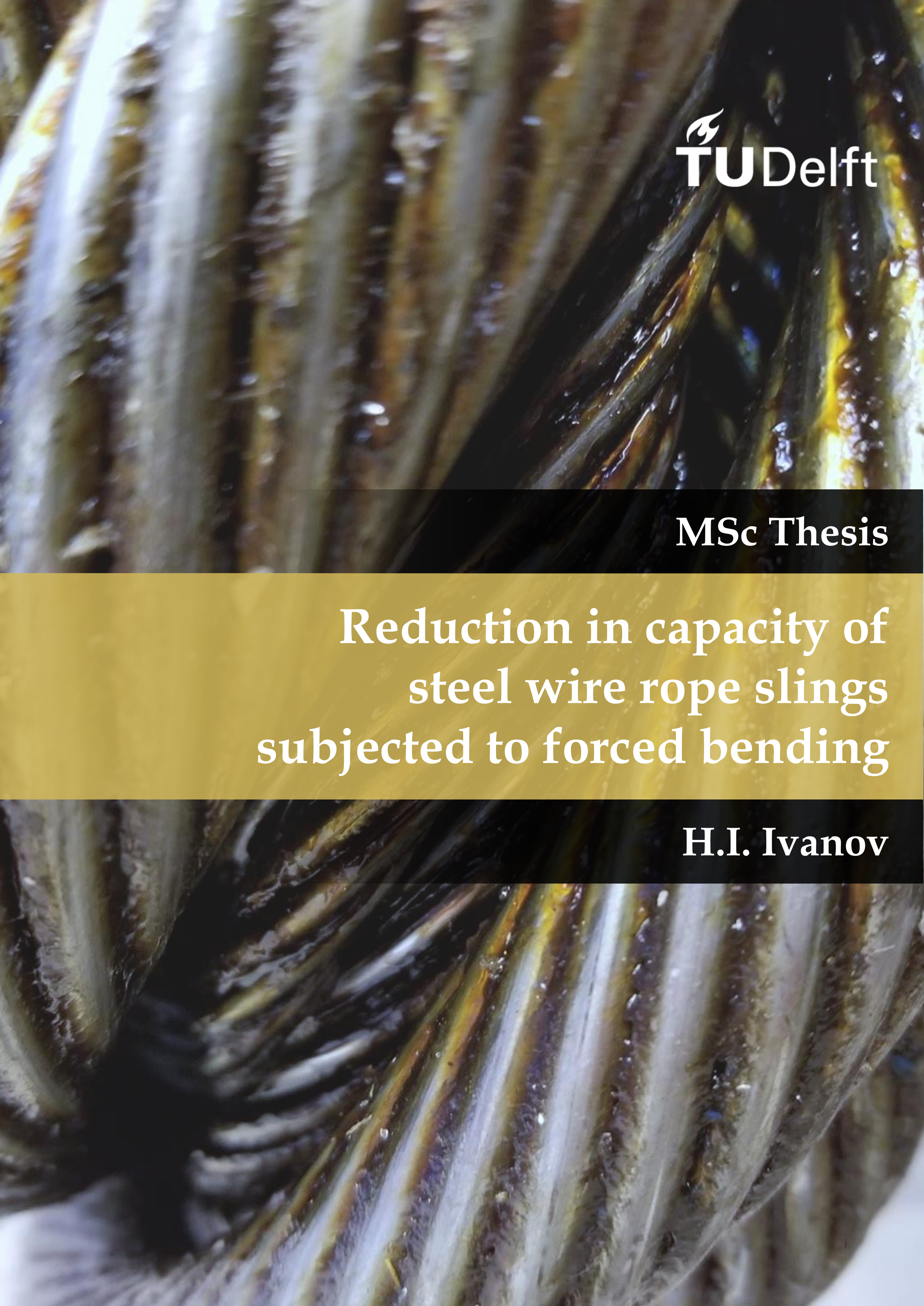

MSc Thesis

Reduction in capacity of steel wire rope slings subjected to forced bending

H.I. Ivanov

Reduction in capacity of steel wire rope slings subjected to forced bending

by

H.I. Ivanov

to obtain the degree Master of Science
at the Delft University of Technology,
to be defended publicly on Wednesday September 26th, 2018 at 2:30 PM.

Student number:	4628500	
Project duration:	November 13th, 2017 – September 26th, 2018	
Thesis committee:	Prof.dr. A.V. Metrikine,	TU Delft, chairman
	Ir. P.C. Meijers,	TU Delft
	Dr.ir. K.N. van Dalen,	TU Delft
	Dr.ir. J. Breukels,	Allseas Engineering B.V.

This thesis is confidential and cannot be made public until September 26th, 2023.

ABSTRACT

Wire rope slings are commonly used lifting tools in all sorts of engineering applications. Usually, slings are either loaded axially or they are bent around a load bearing element such as a shackle or pipe. In the latter case, the combination of bending and axial loading introduces additional stresses within the wire rope that cause a reduction in capacity. In the offshore industry, this reduction is currently taken into account using a safety factor recommended by standardization societies such as DNVGL and IMCA. However, the expression to derive this factor solely depends on the rope's curvature around the bend. Given that steel wire ropes can come in many different geometric configurations and their behavior is nonlinear, it is questionable to assume that this reduction is only based on a single parameter. Consequently, the main research question of this thesis is:

How does the wire rope capacity reduction due to forced bending recommended by DNVGL and IMCA standards compare to analytical and experimental results obtained for wire ropes of different sizes and configurations?

The approach to answering this question starts with a literature study, creating a predictive analytical model and then performing experiments for validation. Findings from the literature study uncover the main parameters affecting wire rope behavior such as lay angles, wire diameters and stress-strain relations. With these insights, an analytical model is created to predict the reduction in capacity of steel wire ropes subjected to forced bending. The model analyzes individual wire behavior and then applies a failure criterion to determine when the entire rope cross-section would fail. Finally, small and full-scale experiments are conducted that test different rope configurations (6x25F-IWRC & 6x36WS-IWRC) with different rope sizes ($\emptyset 20\ mm$ & $\emptyset 77\ mm$).

Knowledge gained from the literature study, the analytical model and the experiments was combined to come up with conclusions pertaining to the main research question. It was found that rope configurations, specifically wire to rope diameter ratios, played a vital role in the capacity reduction of steel wire rope slings. Additionally, results indicate that the capacity of slings increases with higher lay angles. The results also indicated that expressions recommended by the standards are not conservative enough for certain curvature ranges and ropes. Building on the research question, several observations pertaining to rope ovalization and consistency of failure location raised ideas for further investigation.

PREFACE

This thesis has been written as a final step to obtaining my MSc in Offshore and Dredging Engineering from the Delft University of Technology. The graduation committee overseeing my work consists of the following members:

Prof. Dr. A.V. Metrikine	Chairman	Delft University of Technology
Ir. P.C. Meijers	University supervisor	Delft University of Technology
Dr.ir. K.N. van Dalen	University supervisor	Delft University of Technology
Dr.ir. J. Breukels	Allseas supervisor	Allseas Engineering B.V.

The topic of this thesis originated from an interest expressed by Allseas to gain more knowledge about steel wire rope slings. By partnering up with the Delft University of Technology, I was given an opportunity to carry out this research for them. For the ten months that I was involved with this project, many people have helped and influenced my work and I would like to extend my appreciation to them.

I spent a large portion of my time within the innovations department at the Allseas Engineering office in Delft. I would like to first thank Allseas for the opportunity to conduct this research and for providing me with a working environment where crazy ideas and innovation go hand in hand. Many thanks go out to Jeroen Breukels who has supported me from day one all the way to the end. Thank you for your guidance and for encouraging me to create my own path and follow my intuitions. I would like to also thank Natalia Ermolaeva for all the support and interesting discussions during our meetings and for her enthusiasm throughout the entire project.

Many thanks go out to all the people from the Delft University of Technology who were involved in the research. Peter Meijers, thank you for all the encouragement and support you have provided during our many meetings. Our conversations always gave me the confidence I needed to keep pushing towards progress. I would like to thank the laboratory supervisor, Peter de Vries, for his unconditional help in making the crazy logistics of my experiments possible and for also showing great interest in the project. Many thanks go out to John Hermsen, Louis den Breejen, Jack van der Toorn, Fred Schilperoort and Kees van Beek who were all involved in the setup and execution of my experiments. Thank you for helping me come up with solutions whenever there was a problem and for all your efforts throughout the process.

~ Hristo Ivanov
September 26th, 2018

CONTENTS

LIST OF FIGURES

LIST OF TABLES

1.0 INTRODUCTION

Lifting tools play a pivotal part in a vast amount of engineering applications. Perhaps one of the most popular lifting tools is the rope. This invention has found its roots in early civilizations and has been continually evolving even to this day. The reason a rope is considered so useful is mainly due to a combination of its load carrying capacity and bending flexibility. This allows it to be used in applications such as cranes, slings, bridges, overhead conductor lines and more.

In the offshore industry, steel wire rope slings are often used to carry out lifting operations. A sling is a steel wire rope with a relatively short length and specific end terminations on each side. An example of a sling with Flemish eye end terminations is shown in Figure 1.1.

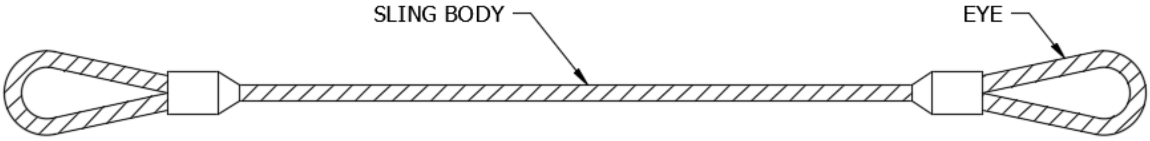

Figure 1.1 - Typical sling made using a Flemish eye termination (FERPS).

Slings are commonly used as supplementary tools in lifting operations. For instance, Figure 1.2a shows how several slings can be combined to keep a container level as it is being lifted. Alternatively, Figure 1.2b displays a sling body being bent around a shackle. Each scenario imposes loads on the steel wire rope differently and consequently causes it to react differently.

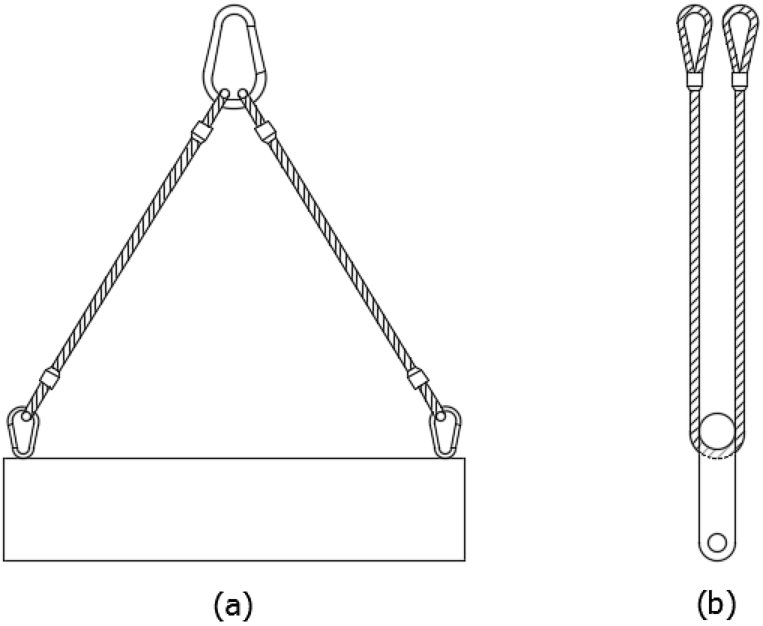

Figure 1.2 - Lifting examples of slings in (a) tension and (b) combined tension and bending.

Without going into too much detail, this chapter focuses on introducing the basics of steel wire ropes. First, a brief history streamlines their evolution and introduces their present-day form. Then, the details of how steel wire ropes are made, and their specific configuration or geometry is explained while highlighting some key characteristics. Next, the main research question of this thesis is explained followed by a definition of the research goals and the approach that was taken. Finally, an outline of each chapter contained in this thesis is provided.

1.1 STEEL WIRE ROPE

Once dissected, it becomes evident that steel wire ropes are complex tools. To begin understanding how they work, a brief history is presented showcasing the progression of how steel wire ropes developed to their modern-day forms. Then, the components that make up the rope are explained along with the different ways that they can be combined. Finally, a quick overview of the manufacturing process of steel wire ropes is provided.

1.1.1 History

Ropes of all shapes and forms have been used for practical applications from the beginning of human civilization. Sometime during the era of the Ancient Egyptians, the evolution of ropes in its early stages starts with the use of hairs bonded together. By the time the Middle Ages came around, the development of ropes had slowed down and was practically unaltered up until the 1600s [1]. Around this time and up until the 1900s is when most of the major technical breakthroughs occurred and gave birth to the wire rope designs and configurations that are still in use today [2].

The first instance of the modern wire rope came in the form of Albert Ropes, which were used as hoisting cables in the silver mines of Harz Mountain in Germany. These ropes were handmade by first twisting three wires around each other to form a strand, and then twisting three or four of those strands around each other to form a rope. This construction was later improved by Englishmen Andrew Smith and Robert Newall, who developed the six-strand configuration twisted around a fiber core. The popularity of wire ropes had grown immensely thanks to the boom of the railroad industry. In the United States, signs of the commonly known Warrington configuration had begun to take root. John Roebling came up with the idea of using alternating wire diameters to better fill the void space in between the layers. With this insight, several other inventors branched off and made their own alterations of what they thought was the ideal configuration. Over time, rope types developed in such a way where each had its own advantages and disadvantages and was used based on a specific application. Today, this has become evident as there are many different configurations built for applications in numerous industries.

1.1.2 Configuration

The configuration of a wire rope is perhaps what best exemplifies its main advantage as a lifting tool. First, consider a typical chain-link rope. Here, almost no redundancy exists because the failure of one chain link causes the entire system to fail. On the other hand, observing the cross-section of a steel wire rope shows that its makeup consists of multiple load bearing components. Consequently, if one wire in a cross-section fails, the load is quickly redistributed to the remaining wires. Although this phenomenon seems intuitive, it is important to note that a wire rope exhibits a much more interesting redundancy measure. For instance, a wire rope can have each one if its wires broken yet still be considered in good working condition. This is possible because a wire restores its full bearing capacity just millimeters away from the element breaking point [3]. Therefore, in the case where the wire breaks in a cross-section are sufficiently spread out over the entire length, the rope can continue to carry its original capacity. This phenomenon can be best described by Figure 1.3.

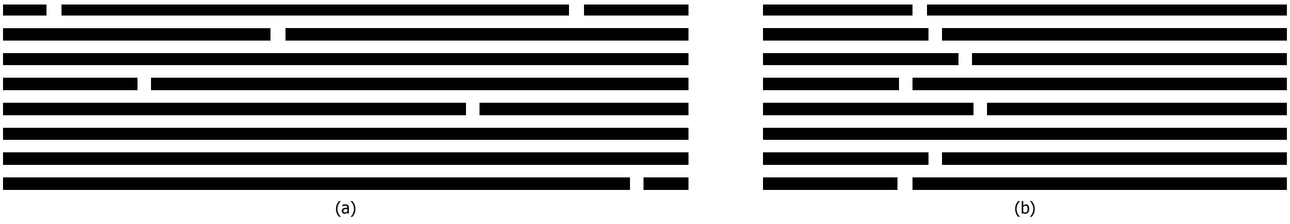

Figure 1.3 - Simplified view along length of steel wire rope showing staggered element breaks (a) and concentrated element breaks (b).

In part (a), the rope is considered to be in good condition because each element break is staggered throughout the length of the rope, which only causes a local reduction in capacity of about 1% [3]. The remaining wires of the cross-section can easily redistribute the load. In part (b), however, the element breaks occur at a concentrated area along the rope length. In this case, the close proximity of the breaks causes the cross-sectional capacity to be significantly reduced and can lead to sudden failure.

The type of geometric configuration of a rope also has a direct link to its behavior. Understanding the geometry of a steel wire rope begins with its core component, the wire. To achieve higher strength, wires are bundled together to form a strand. A simple strand consists of a layer of wires that are wrapped around a core in such a way that they form a single helix. To form a conventional wire rope, strands are then wrapped helically around a core as shown in Figure 1.4.

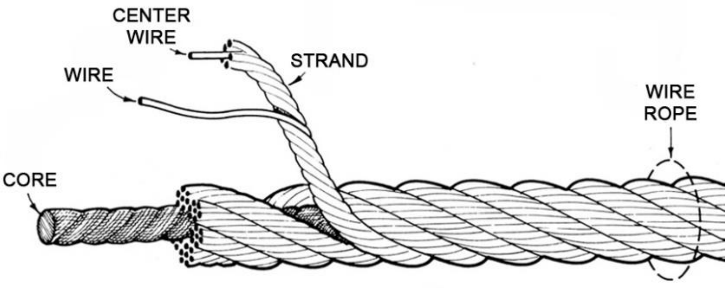

Figure 1.4 - Breakdown of main components that make up a steel wire rope [4].

Taking this into account, it can be deduced that the amount of different ways these elements can be combined is high. Regardless, the configurations found in Figure 1.5 are the most common ones seen today. This figure shows the build-up of different types of strands which are ultimately used to classify the configuration of the entire rope. These strands, which carry the majority of axial loading, are helically wrapped around a steel or fiber core to form what is considered the steel wire rope. The difference in each strand configuration is the way in which the layers and size of wires are arranged so as to best fill up the void space inside the cross-section.

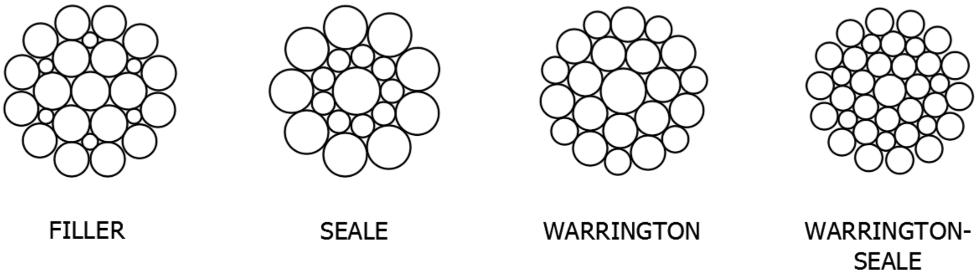

Figure 1.5 - Common strand configurations used in steel wire ropes.

Going into more detail, the terminology can be defined using a 6x36WS-IWRC rope as an example. The naming refers to a rope with 6 outer strands that have 36 individual wires each. WS means the wires in each strand are arranged in a Warrington-Seale configuration and the IWRC refers to the rope having an independent wire rope core. Figure 1.6 illustrates the cross-section of this rope configuration as well as a 6x25F-IWRC and labels some of the main geometric terminology. As can be seen, both of these ropes have an identical IWRC, however, the outer strands are different. Since the 6x36WS has more wires, it can match the diameter of the 6x25F by using smaller diameter wires. Alternatively, the 6x25F has less wires and less layers so it needs larger individual wire diameter size. In the end, both configurations can have the same strength, but one might be better than the other depending on the specific application.

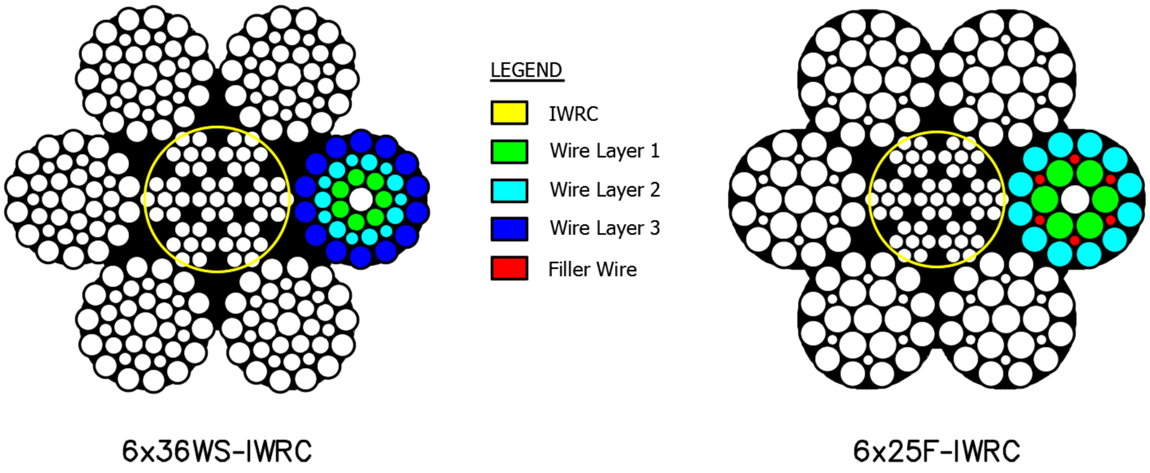

Figure 1.6 - Terminology of geometric properties of steel wire rope configurations.

Another significant geometric property of wire rope is the lay length. Considering a simple strand, this is defined as the length along the axis of the strand in which a wire completes one full rotation. Figure 1.7 illustrates this parameter (h_w) as well as how it can be derived. Alternatively, it is also common to use the lay angle (α) instead since conversion between the two variables is straightforward.

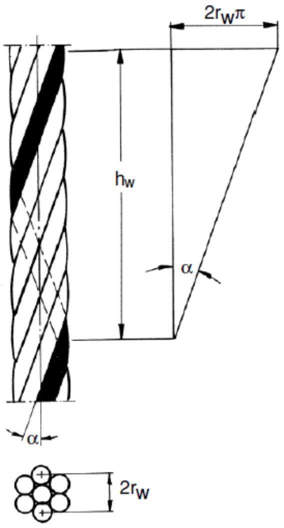

Figure 1.7 - Illustration of the lay length of a wire rope [5].

In addition to the lay length/angle, the lay direction is also of importance. In stranded ropes, there are several orientations in which the wires and strands can be arranged as shown in Figure 1.8. The symbols "z" and "s" refer to right and left lay direction of the wires in an outer strand, respectively. Similarly, the symbols "Z" and "S" refer to either right or left lay direction of the outer strands in a rope. In langs lay ropes, the lay direction of both the wires and strands is the same (zZ or sS). Alternatively, in ordinary lay ropes, the wires and strands are laid in opposite directions (sZ or zS). Another common naming convention is through abbreviation such as RHOL for right hand ordinary lay or LHOL for left hand ordinary lay.

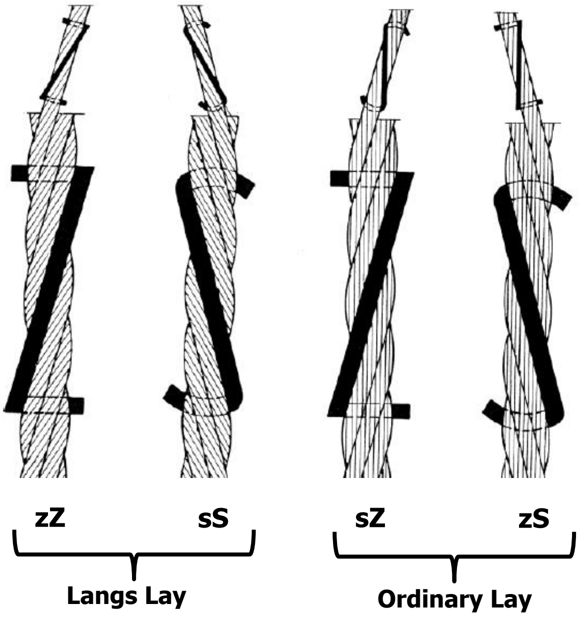

Figure 1.8 - Illustration of the four configurations of lay direction for stranded wire ropes [5].

Each configuration causes the rope to exhibit different behavior and therefore has its own advantages and disadvantages. For instance, ordinary lay ropes are more commonly used because wire breaks usually first occur on the outer layer. This allows inspectors to more easily check the rope's condition and apply the appropriate discard criteria. Alternatively, langs lay ropes are more advantageous in applications where a high constant tension is maintained or in multi-layer spooling.

1.1.3 Manufacturing

Figure 1.9 below provides an overview of the main stages of the manufacturing process starting with the raw steel material and ending with the complete wire rope.

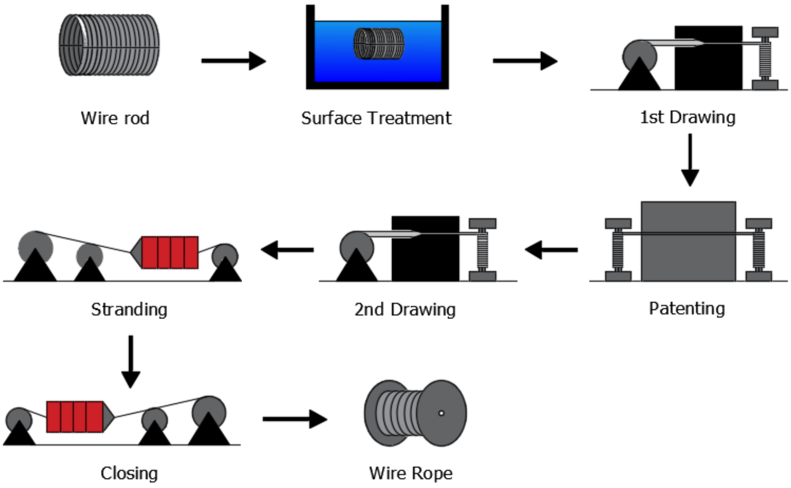

Figure 1.9 - Overview of manufacturing process of steel wire ropes [6].

The manufacturing process of steel wires begins with first cold-rolling or drawing steel rods. Most commonly, these rods are made of high-strength non-alloy carbon steel with a high carbon content (0.35-0.95%). A surface treatment may be applied to thoroughly clean and remove any unwanted dirt and debris before the next stage. Then, the rods are subjected to a patenting process in preparation for the drawing stage. In the patenting process, the rods are first heated to a temperature of about 900°C, then placed in a lead bath to abruptly reduce to a temperature of 500°C [5]. Finally, they are taken out and cooled to room temperature as shown in Figure 1.10.

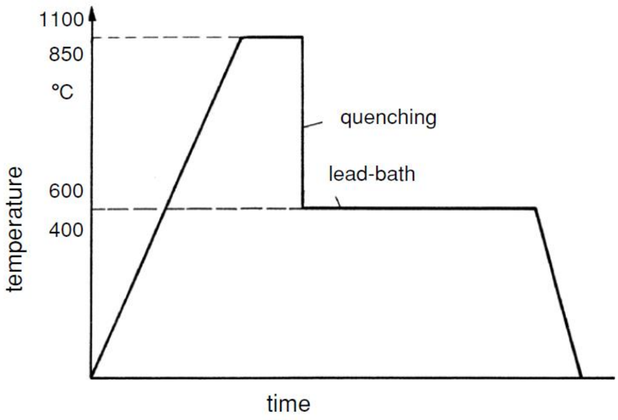

Figure 1.10 - Temperature variation of typical patenting process for steel rods [5].

The result from patenting modifies the structure of the steel rod in such a way that it becomes more favorable for the drawing process. During drawing, the cross section of the rod is reduced by pulling it through what is known as a drawing die (Figure 1.11). Additionally, this reduction in diameter also adjusts the mechanical properties by increasing yield and tensile strength. The rod will go through several stages of patenting and drawing until the final cross section is obtained.

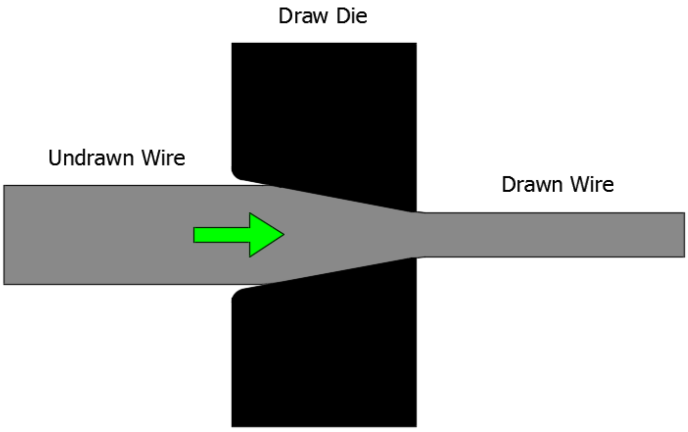

Figure 1.11 - Simple illustration of the drawing process where a rod goes through a drawing die.

Afterwards, the individual wires go through another machine so that they can be twisted around each other to form a strand. This stranding process varies greatly based on the type of wire rope as there can be many different combinations of wire diameters, lay lengths, and lay directions. Finally, the separate strands are wrapped around a core (steel or fiber) to form a conventional wire rope.

1.2 PROBLEM DEFINITION

Being that steel wire ropes play such a significant role, it is important to understand their behavior. When choosing a rope, perhaps the most critical factor is the capacity or how much force it can sustain before failure. In the industry, a commonly referred to parameter is the minimum breaking load (MBL).

Engineers in the offshore industry use these ropes in many different ways. Take, for instance, two simple scenarios as shown in Figure 1.12. The first illustrates the most common situation where a rope is subjected to axial tension due to an applied loading. Here, the loading can directly be related to the capacity of the rope. In the second scenario, the rope is bent around a load bearing element such as a shackle. Considering the free-body diagram, each leg of the rope would carry half of the loading imposed by the shackle.

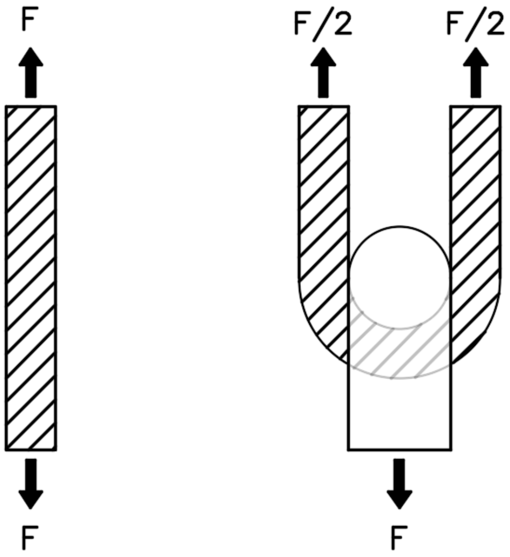

Figure 1.12 - Free body diagrams of two simple loading cases of ropes.

However, when bending the wire rope around a shackle, additional stresses are introduced. Consequently, this reduces the available capacity that the rope can use to resist the applied loading. For many situations encountered in the offshore industry, this reduction becomes quite significant and therefore requires proper accounting.

Currently, this reduction is applied through a safety factor, which is derived from a standard written by DNVGL. In the standard DNVGL-ST-N001 [7], the reduction factor due to bending is calculated according to Equation (1).

$$\gamma_{b,DNVGL} = \frac{1}{1 - \frac{0.5}{\sqrt{D/d}}} \tag{1}$$

A recent update of a similar standard (IMCA LR 008-2016 [8]) uses the expression given by Equation (2). The *D/d* ratio refers to the diameter of the bend over the diameter of the wire rope as illustrated in Figure 1.13.

$$\gamma_{b,IMCA} = \frac{1}{1.07}\,\gamma_{b,DNVGL} \tag{2}$$

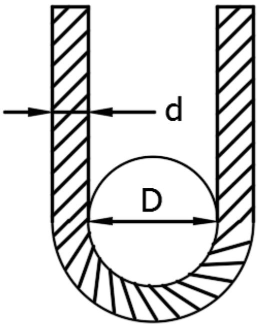

Figure 1.13 - Illustration of D/d ratio.

Figure 1.14 displays the relationship of the reduction factor based on the *D/d* ratio. According to both standards, the reduction factor used in lift calculations should be the governing reduction due to either end terminations or bending. Hence, there is a range of *D/d* ratios where the end termination of a certain sling could govern this reduction rather than the bending. Additionally, the *D/d* ratios most commonly used in offshore operations for slings vary between 1.33 to 1.55. Consequently, the *D/d* ratios of interest have a narrow range associated with very sharp curvatures.

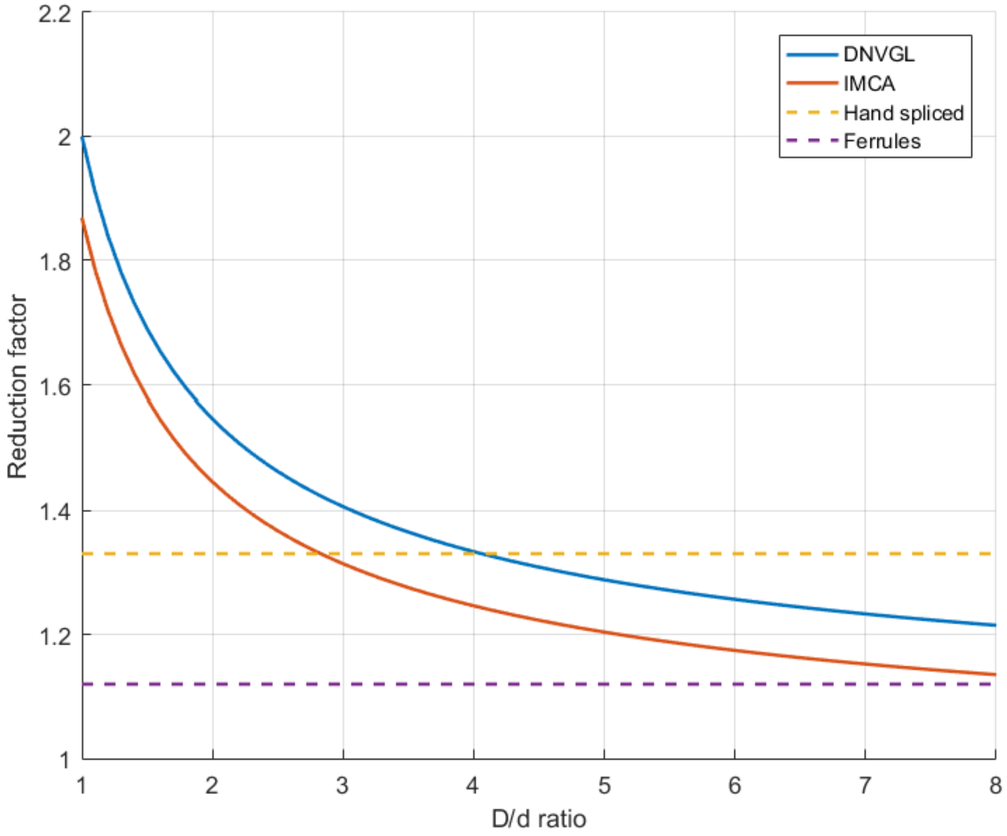

Figure 1.14 - Reduction factor due to bending suggested by current industry standards.

Generally, this reduction factor decreases as the *D/d* ratio increases. Moreover, the only variable is the *D/d* ratio, which means that this expression can be applied to wire ropes of all sizes and configurations. Being that wire ropes are complex tools, it is questionable to assume that this simplified expression accurately describes reality. The behavior of steel wire ropes is notoriously nonlinear, therefore, the extrapolation of the expression by DNVGL and IMCA to be applicable to all types and sizes of wire ropes requires further investigation.

1.3 RESEARCH GOALS & APPROACH

The offshore industry is constantly evolving and pushing boundaries resulting in larger diameter wire ropes required to handle heavier lifts. However, as size increases so does cost. Consequently, knowing the actual capacity of lifting tools becomes of great importance so as to help avoid unnecessary expenses due to oversizing or, alternatively, evade unsafe situations due to under-sizing.

As described earlier, there are questionable points that merit the investigation of the current reduction factor expression's applicability to all steel wire ropes. The main focus of this thesis is to answer the following research question:

How does the wire rope capacity reduction due to bending recommended by DNVGL and IMCA standards compare to analytical and experimental results obtained for wire ropes of different sizes and configurations?

To answer this question, the approach of this thesis will be split into three main parts consisting of a literature study, analytical modelling and experiments.

Literature Study
A review of past research and literature will be conducted. The goal of the literature study is to understand the behavior of steel wire ropes when subjected to different loadcases. This will yield possible parameters/characteristics of the steel wire rope that should be considered when calculating the reduction in capacity due to bending.

Analytical Modelling
Building an analytical model that can produce reasonably accurate results is a main goal of this thesis. Careful considerations when modelling the wire rope will be taken as the many nonlinearities present are difficult to predict. Hence, appropriate assumptions will need to be applied.

Experiments
The best way to determine the reduction in capacity is to test it in reality. To do so, experiments were performed at the Delft University of Technology on steel wire rope slings of different sizes and types in similar load scenarios as illustrated by Figure 1.12. The first test will subject the rope to pure tension and load it until break to measure its nominal capacity. The second test will apply combined tension and bending. Then, the results from each test can be compared and the reduction in capacity calculated.

1.4 REPORT OUTLINE

A brief summary of each chapter can be found below.

- **Chapter 1** – A brief introduction into steel wire ropes and the problem definition followed by the research goals and approach.
- **Chapter 2** – Literature study of steel wire ropes by summarizing previous research, defining important characteristics and investigating the specific behavior of wire ropes during bending.
- **Chapter 3** – The analytical model created is described and then applied using several case studies.
- **Chapter 4** – A full overview of the experiments conducted including setup, results and observations for both small and full-scale versions.
- **Chapter 5** – Discussion and comparison of results between previous literature, the proposed analytical model and the experiments conducted.
- **Chapter 6** – Overall summary of the main conclusions found in this thesis.
- **Chapter 7** – Recommendations concerning further improvements of current model, alternative studies and suggestions for additional experiments.

2.0 BEHAVIOR OF STEEL WIRE ROPE

Steel wire ropes are heavily relied upon in many applications. Consequently, understanding their behavior is of upmost importance to the engineers who use them. This chapter will focus on shedding light onto the considerations that must be taken when using steel wire ropes. First, a brief overview of previous research in cable modelling is presented. Then, the key characteristics which govern the behavior and capacity of steel wire rope are discussed. Finally, specific theories derived from previous research are examined with the goal of describing the behavior of steel wire rope under the bending scenario being considered in this thesis.

2.1 PREVIOUS RESEARCH

With the growing popularity of steel wire ropes in the 20th century also came the interest in their behavior. The stresses and strains experienced by ropes became important for engineers as the reliance of these tools became critical in many applications. The 1950s gave birth to some of the first models, which considered ropes as strings loaded in tension. This was a great simplification as many of the rope's inherent properties such as bending and torsional stiffness were ignored. With time, researchers improved on these assumptions and new modelling methods were proposed that offered a much more realistic representation. Spak et al [9] provides an extensive review of the past research conducted on steel wire rope modelling. Overall, the different models can be categorized into the following distinct categories,

1. String/beam models,
2. Thin-rod models,
3. Semi-continuous models and
4. Finite element models.

Figure 2.1 provides a representative timeline of how each model has evolved with highlights of some key literature works. These works will be briefly elaborated, but it is important to note that there has been extensive research conducted beyond what is discussed here.

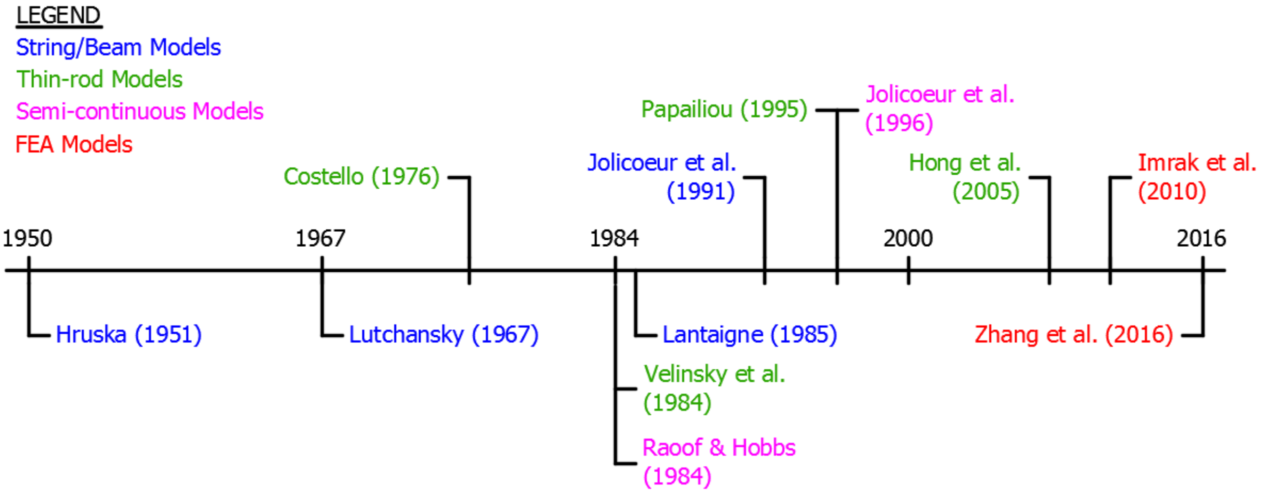

Figure 2.1 - Timeline showing development of various steel wire rope models.

2.1.1 String/beam models

The string models were the first attempts at trying to analytically capture the behavior of wire ropes. As mentioned, most of these basically considered the rope as a bundle of individual wires modelled as strings loaded in tension. This approach ignored the bending and torsion rigidity of the wires and is commonly referred to as a fiber response. Some of the main contributors to these types of models included Hruska [10] and Lanteigne [11]. This model incorporated numerous simplifications, but perhaps the most significant was the omission of bending and torsional stiffness. The general equation of motion used for this method is

$$m\ddot{w} - Tw'' = 0. \tag{3}$$

where m is rope mass, w is displacement and T is axial tensile force. To improve on some of these simplifications, beam models were introduced. This approach considered the wires to act as a bundle of individual beams rather than strings. Consequently, bending and torsional stiffness properties could now be incorporated into the beam elements. Lutchansky [12] was one noteworthy author who helped develop this approach. General equations of motion for the beam models are

$$\rho A\ddot{w} + EIw'''' - Tw'' = 0 \tag{4}$$

and

$$\rho A\ddot{w} - KGA(w'' - v') = f(x,t), \;\; EIv'' + KGA(w' - v) = 0 \tag{5}$$

where ρ is cable material density, A is cross-sectional area, w is displacement, EI is bending stiffness, T is axial tensile force, v is rotation of beam centerline due to shear and bending, K is shear coefficient and G is bending moment in bi-normal direction. These equations incorporate the Euler-Bernoulli or Timoshenko beam assumption, respectively.

Overall, these methods were a simplistic first approach to modelling steel wire rope behavior. All of these studies were focused on simple strands loaded axially by tension. Jolicoeur and Cardou [13] performed experiments on simple, straight strands to validate the accuracy of these models and discovered that the fiber response assumption of the wires yielded a good correlation with the results. However, the complex geometry of ropes requires considerations of inherent properties neglected here.

2.1.2 Thin-rod models

The development of thin-rod models was a direct result of the need for incorporating more of a wire rope's inherent properties. This began with the work of Costello and Philips [14] who developed a model based on the nonlinear equations of equilibrium of thin helical rods first derived by Love [15]. Figure 2.2 shows the internal loads produced by the twist and curvature of a rod. Summing these internal forces translates to force and moment equations which can then be used in conjunction with stiffness matrices to calculate the axial and torsional response. Some key assumptions were that the bending stiffness was composed of each individual wire bending around its own neutral axis, thus assuming a frictionless rope.

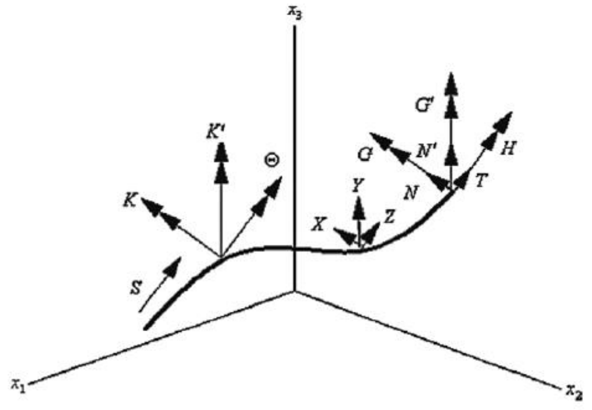

Figure 2.2 - Internal forces produced by a helical rod loaded in tension [16].

Velinsky [17] and Velinsky et al [18] extended this model by incorporating multi-strand rope construction. The methodology was to first calculate the response of a simple straight strand loaded axially. Then, the response of a wound strand was approximated by considering it as a single outside wire wrapped around a core (like in a simple strand). This basically assumed the mechanical relations computed for a straight strand can be applied to the wound strand.

These pioneering thin-rod models presented a breakthrough in wire rope research. Bending and torsion stiffness was better incorporated and the varying behavior due to different cable geometries was captured. When considering ropes loaded axially, the correlation with experimental results was quite good. However, in certain applications like transmission conductor lines, the simplification of a frictionless rope was not accurate enough. To overcome this, Papailiou [19] added friction into the thin-rod model by introducing a nonlinear stick-slip regime based on the bending curvature of a rope. This was later improved by Hong et al. [20] who concluded that the theoretical minimum bending stiffness is never reached and is actually governed by the coefficient of friction between wires.

The complexity of modern thin-rod model equations allows them to incorporate a significant amount of detail. This can include friction, interwire/intrawire contact, change in lay angle, etc. However, it has been shown that some of these considerations have a relatively small effect on the global behavior of the rope. Regardless, it is important to know when and which assumptions can be applied depending on the specific application and use of a steel wire rope.

2.1.3 Semi-continuous models

The semi-continuous model was another approach to cable modelling that attempted to simplify the idea of the thin-rod model. Created by Raoof and Hobbs [21], this model transformed each layer of wires in a strand into an orthotropic, hollow cylinder. This cylinder has properties that try to match the corresponding wire layer, ultimately mimicking that layer's behavior within the rope. The idea behind this model is illustrated in Figure 2.3.

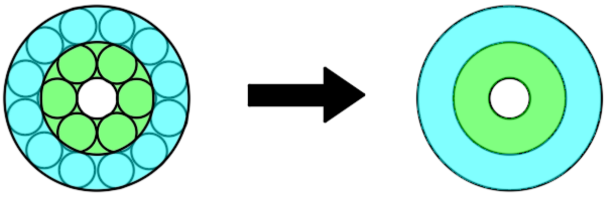

Figure 2.3 - Illustrative summary of semi-continuous modelling approach of strands.

This simplification presents an interesting way to model wire ropes. Using contact mechanics combined with material elastic properties, equations were derived that aimed to predict the behavior of these orthotropic cylinders under different loadings. Unlike thin-rod models, which use a specific method to calculate cable response, the semi-continuous model allows the analysis of constitutive equations using several methods [9]. Ultimately, it helped to greatly simplify the calculations necessary to predict the cable's behavior analytically.

Jolicoeur and Cardou [22] also contributed to the semi-continuous model through some modifications. Instead of considering the layers as thin orthotropic sheets, they assumed a higher thickness so the sheets can be modelled as cylinders. However, this assumption was proven to be significant only for seven wire strands while being negligible for strands containing large numbers of wires such as in ACSR conductors [22]. The authors differentiate their work based on new theoretical expressions they have introduced that allow for a better analysis of the bending behavior of strands by considering the range of possible bending stiffness values.

The semi-continuous models developed showed an alternative way of predicting rope behavior. Results of this model compared to other analytical models and experiments of strands showed good correlation when considering tension and torsional loading [22]. Furthermore, a study was done which concluded that thin rod models were more reliable for helical cable analysis that involved small diameter cables with fewer strands while semi-continuous models showed much better correlation with large diameter strands having nineteen or more wires [23]. Nevertheless, semi-continuous theories focused on spiral cables which consisted of single helixes whereas the ropes of interest in this thesis are stranded and contain more complex geometry.

2.1.4 Finite element models

Naturally, finite element analysis (FEA) was eventually applied to predicting the behavior of steel wire ropes. FEA offers a very different approach to the models previously discussed because its computations are numerical rather than analytical. Consequently, this yields huge advantages for FE wire rope models since they require much less simplifications and can therefore incorporate many effects neglected by analytical models. This can include core-wire contact, wire-wire contact within each layer, friction, exact geometry, local contact deformation and more. However, this comes at a great cost as the more complex the FE model is, the more computational time and power necessary to find a solution.

Starting with the 1990s, there have been several studies that have utilized FEA with varying model complexities in the past two decades. Most studies were aimed at reconstructing the behavior of simple strands subjected to axial loading. A model created by Jiang et al. [24] focused on analyzing the complex wire-wire and wire-core contact and concluded both were influential for the specific configuration tested. Imrak and Erdonmez [25] were the first to create a FE model that takes into account the double helical configuration of stranded ropes. Their model correlated well to the elastic region of analytical models and the overall behavior found from experimental results. Naturally, to model such a complex geometry a sacrifice was made in terms of rope length. This poses some questions such as whether the helical contraction is properly accounted and to what extent boundary conditions influence the results.

FE models that try to predict bending behavior are even more computationally expensive. The balance between complexity, model length and incorporating contact interaction effects are vital to producing realistic results. A fairly recent study by Zhang & Ostoja-Starzewski [26] investigated the bending stiffness of a simple strand using a FE model. They applied different levels of contact interaction and compared the results with past analytical research. An interesting conclusion was that incorporating certain contact interactions yielded more accurate results only for certain lay angles. For instance, as the lay angle increases, wire-wire contact starts to have more of a significant influence and should not be neglected.

Overall, FE models have the greatest potential in accurately predicting wire rope behavior. As has been seen in the past, computational power has greatly increased over time allowing for more and more complex FE models to be created. If this trend continues, FE models have the potential to become robust enough to incorporate all nonlinearities and very accurately predict wire rope behavior.

2.2 GLOBAL CHARACTERISTICS

Past research has provided many great insights into the behavior of steel wire ropes. It is important to also reflect on some of the key characteristics that govern this behavior. Perhaps the most significant parameter to digest is the effect of the helical structure, which gifts a rope its unique properties. Furthermore, the material behavior of wires and ropes is observed through their distinctive stress-strain relationships. Since capacity is a major point of interest in this thesis, the most common failure mechanisms are also highlighted.

2.2.1 Helical structure

The helical structure of a wire rope is where the ingenuity of this extremely useful tool originates. This characteristic has two major effects that will be discussed, which are the

- Decrease in bending stiffness and
- Decrease in axial strength/stiffness.

Perhaps the most important characteristic of a wire rope is flexibility. Although rods can also carry axial loads, ropes are much more widely used because they can be easily bent into a desired shape and are more lightweight making them a more practical choice in most applications. A rope’s flexibility can be explained by considering a simple scenario. First, imagine a thick beam subjected to bending, which results in the exaggerated, deflected shape shown in Figure 2.4a. In Figure 2.4b, the beam is cut into smaller segments and the same loading is applied. Assuming no friction, the smaller segments exhibit much smaller strains because they bend around their own neutral axis rather than the central axis.

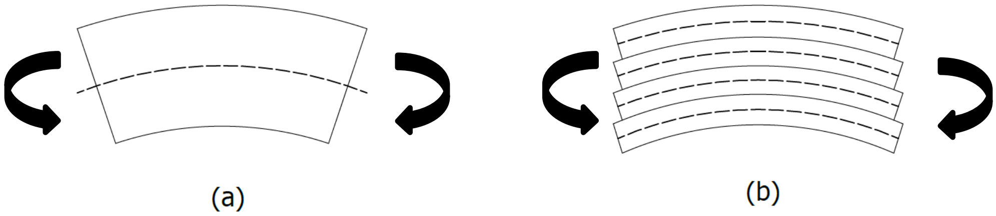

Figure 2.4 - Regular beam in bending (a) and bundle of wires in bending (b).

However, because the boundary conditions at both rope ends are usually fixed in most practical applications, the smaller segments will not be allowed to rotate freely and will therefore act as a beam. To overcome this problem, the helix is introduced. By forming a helix, each individual wire will be equally in both the tension and compression zone during bending causing the induced strains to cancel each other as illustrated in Figure 2.5. Essentially, the wire shifts its relative position without experiencing any elongation. This eliminates the effect of the fixed boundary conditions discussed before. Although neglected here, friction also plays an important role and will be discussed in a later section.

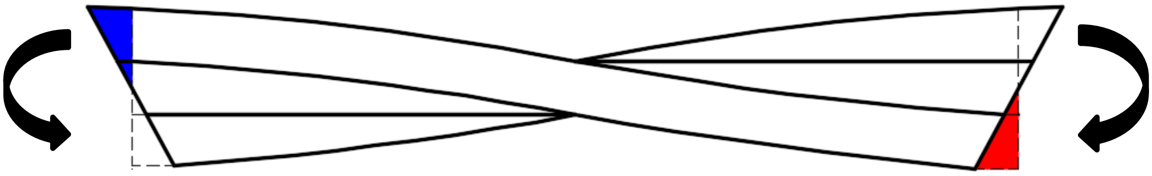

Figure 2.5 - Original (dashed) and deformed shape of helical wires subjected to bending. Colors highlight tension and compression zone.

Another effect that is important to note is the decrease in axial strength and stiffness. This is obviously a negative characteristic of the helical structure as it reduces the capacity of the wire rope. The reason behind this reduction is the lay angle influence on the distribution of stresses throughout the layers in a rope. This phenomenon will also be further elaborated later.

2.2.2 Material behavior

The material behavior of steel wire rope is an important parameter to analyze. Its core component, the wire, exhibits a stress-strain relationship that typically follows the curve shown in Figure 2.6. This behavior is somewhat different when compared to structural steel because of the manufacturing process of the wire in combination with its chemical composition. Nevertheless, the typical characteristics of an elastic-plastic material can be clearly defined. First, the wire experiences elastic elongation following Hooke's Law up to its yield point. Past this point, nonlinear plastic deformation takes place until the ultimate stress of the wire is reached indicating failure.

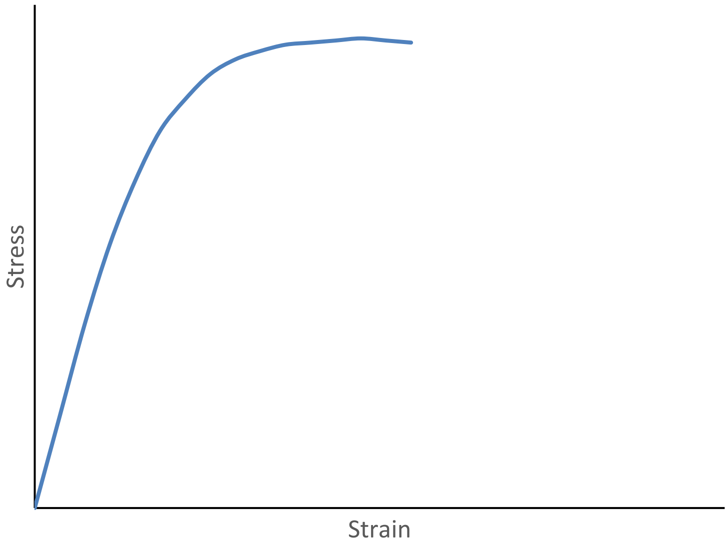

Figure 2.6 - Typical stress-strain relationship of individual steel wire.

However, when examining the stress-strain relationship of an entire steel wire rope as shown in Figure 2.7, notable differences can clearly be defined. Here, the curve can be separated by three distinct regions of

1. Initial extension,
2. Elastic extension,
3. Plastic extension.

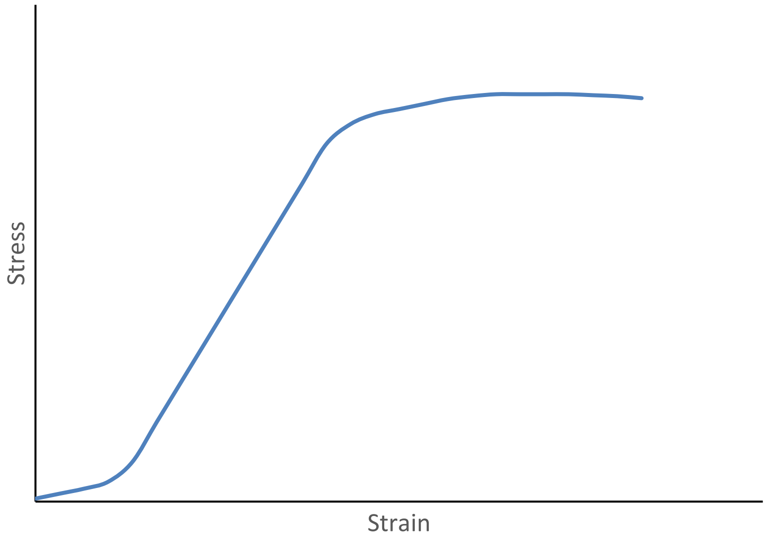

Figure 2.7 - Typical stress-strain relationship of steel wire rope.

Initial extension is a nonlinear phenomenon that is most commonly observed when loading a new rope. During construction of a rope, gaps are created between the individual wires and strands due to imperfect alignment. Consequently, when the rope is loaded for the first time, the helical structure of the wires contracts. During this process, the rope's diameter decreases as the gaps are eliminated while also causing an extension in the longitudinal direction as the helical lay is lengthened. This elongation continues until adjacent wires create a sufficiently large bearing area with respect to each other to resist the radial force imposed by the helical structure. To help reduce this initial extension, wire ropes are pre-stretched by the manufacturer by loading them up to a certain percentage of their MBL. This allows wires to settle into their final position so that the initial extension is minimized during actual loading.

Once the wires have made sufficient contact with each other, the elastic extension commences. At this stage, the entire rope elongates in approximate compliance with Hooke's Law up until the yield limit is reached. It is important to notice that the slope of this curve is less steep than that of an individual wire indicating that the rope exhibits a more ductile behavior. This can be explained by the behavior of a helical structure, which causes the individual wires to elongate differently relative to each other. Moreover, this is also the reason why the elastic range is not characterized by a typical linear relationship of the stress and strain. A tangent Young's modulus can be calculated between two load points chosen within reasonable distance. It is also important to note that since the slope of this line is affected by the interaction of the helically wrapped wires, each rope configuration and diameter will exhibit a unique behavior.

Finally, past the yield point, the wire rope experiences permanent, plastic deformation. In this phase, the relationship between stress and strain becomes evidently nonlinear and accelerates the overall extension of the rope as loading is applied. As the ultimate strength is approached, individual wires break once they reach their elongation at rupture forcing the load to redistribute. This process of wire breaking continues until the cross-sectional area cannot handle any further redistribution of the load at which point the rope fails suddenly.

2.2.3 Types of failure

As described by Timoshenko, the failure of a material is governed by its resistance to sliding and resistance to separation [27]. These two mechanisms can be illustrated by Figure 2.8. Separation failure occurs when a crack propagates along the material perpendicular to the direction of applied loading. In the case of sliding failure, the cross-sectional area of a material reduces in proportion to the applied loading until fracture. For ductile materials, the resistance to separation must be greater than the resistance to sliding. This ensures that the material will elongate up until the reduced cross-sectional area causes the resistance to separation to become lower than the resistance to sliding. At this point, fracture will occur causing the material to separate. It is important to also note that the resistance to sliding is a property that can be affected by rate of loading and temperature [27]. Hence, if a material is loaded suddenly and at a low temperature, the resistance to sliding may increase so that it surpasses the resistance to separation. This causes the material to lose its ductility and fail suddenly without much plastic deformation. However, in the context of this thesis, these effects are considered negligible.

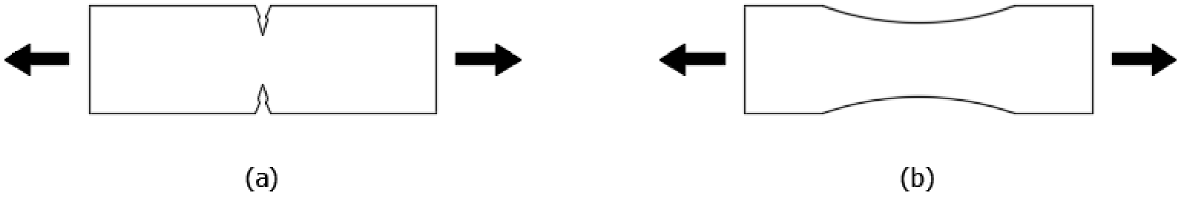

Figure 2.8 – Separation failure (a) and sliding failure (b).

In the case of wires, failure is achieved by following the appropriate stress-strain diagram corresponding to the specific material grade. Once the wire is loaded past its yield point, plastic extension occurs up until the ultimate yield point where fractures transpire, and the material separates. Depending on the material grade, the total elongation of the wire can vary between 1.5-4% and the ultimate strength can be 105-133% higher than the specified grade strength [5]. It is interesting to note that although wires are made of steel, they exhibit a much more brittle behavior. As mentioned previously, this is related to the manufacturing process the wires go through which causes them to change their mechanical properties. The result is that the wires have a much higher yield stress, but at the cost of a high reduction in ductility.

Based on previous experience, the main failure modes of individual wires are split into two categories. The first is called cup-and-cone failure, which is illustrated by Figure 2.9. This type of failure is associated with overload or necking of wires caused by an axial tensile loading. Necking, which refers to the reduction in diameter of the cross-section as it elongates, is then followed by small microvoids that appear in the center of this area. These eventually combine to form a bigger void at which point sudden fracture occurs in the form of a shear plane angled at 45 degrees. This failure causes the ends of both pieces to resemble a cup and cone.

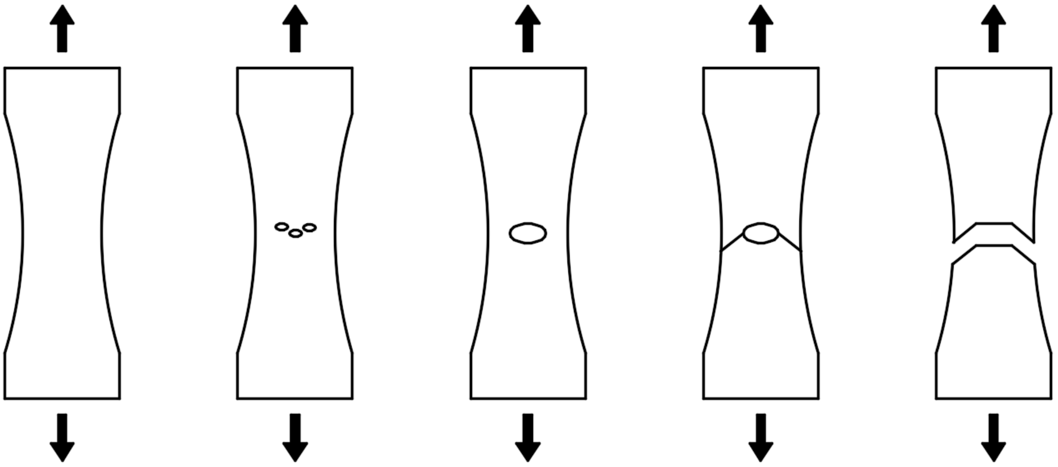

Figure 2.9 - Different stages of axially tensioned material that results in cup-and-cone failure.

The second main failure mode of wires is shear (Figure 2.10). In this case, the fracture plane is not normal to the cross-section but rather at an angle near 45 degrees. This failure more would occur when an opposing force like friction acts on a portion of the outer surface of the wire.

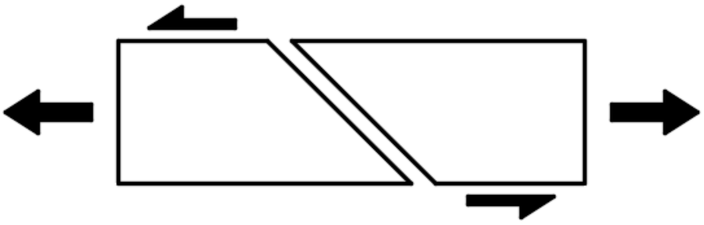

Figure 2.10 - Typical shear failure of material under combined loading.

Depending on the specific use and application of wire ropes, additional failure mechanisms can occur. For instance, ropes subjected to the harsh offshore environment can be greatly affected by corrosion. This causes the outside surface of the wires to deteriorate, thus reducing its load-bearing capacity. Through galvanization and other similar techniques, the damage due to corrosion can be minimalized. However, there are situations where the severity of the environment can be extreme enough to significantly reduce the lifetime of a rope if not properly maintained.

Fatigue is normally a governing failure mode for many engineering applications using steel wire ropes. However, when considering steel wire rope slings, this is not the case. The reason behind this is that current industry practice considers slings as consumables that are usually used for single operations. Hence, the number of cycles and fluctuating stresses associated with fatigue are not applicable and the governing failure mode then becomes the ultimate strength capacity.

2.3 BEHAVIOR UNDER BENDING

Although wire ropes can be used in various applications, the selection of a specific rope is governed by the loading/stresses it will experience. It is therefore important to understand the stresses a rope will incur based on the loading applied. In the context of this thesis, the scenario of interest is a sling body bent around a circular pin.

The helical configuration of the individual wires adds a degree of complexity when identifying the different stresses in this scenario. To start, consider a simple strand loaded in tension. If examining the response of the outer wire to the applied loading, the resulting force components are as shown in Figure 2.11. Here, in addition to the normal force, a radial component is also observed.

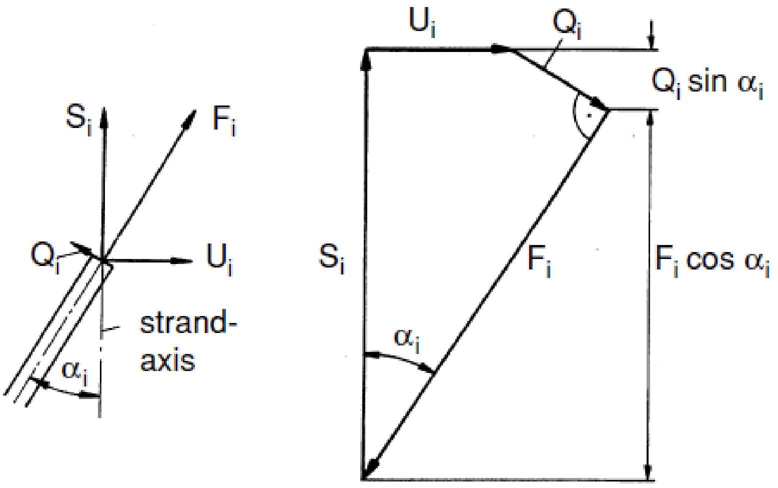

Figure 2.11 - Simplified free-body diagram of outer wire due to loading of strand by force (S_i) [5].

This radial component arises from the contraction induced by the helical structure of the outer wires. In turn, this causes a coupling where the axial loading applied to the strand also induces shear, torque and moment. Expanding on this simple example and taking into consideration the bending scenario of interest, the main stresses experienced by a steel wire rope can be categorized into:

- Axial loading stress;
- Bending stress;
- Stress due to friction;
- Ovalization stress;
- Stress due to torsion, moment and shear.

2.3.1 Axial loading stress

If considering a single, straight wire loaded in tension, the resulting stress can simply be found by applying:

$$\sigma = \frac{F}{A}. \tag{6}$$

Additionally, this equation will hold if several straight wires are bundled together. However, once that bundle of wires becomes wrapped around a core and forms a helix, a difference in stress can be observed. This can be explained by cutting a cross-section of the two different scenarios as depicted by Figure 2.12. In Figure 2.12a, the stresses throughout the wires are the same because each individual wire cross-section is identical. However, in a strand, the representative cross-sections of the outer wires exhibit a different shape than the core as shown in Figure 2.12b.

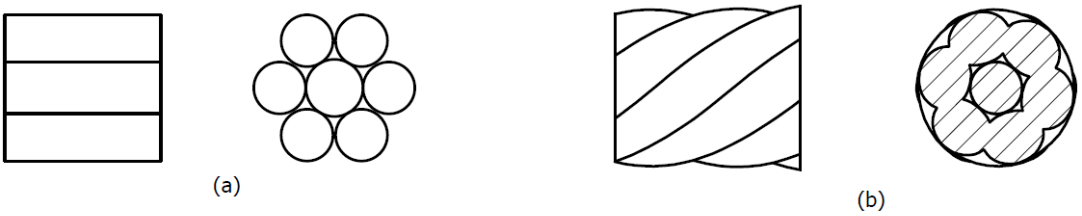

Figure 2.12 – Strand with parallel bundle of wires (a). Simple strand with helical structure (b).

To translate this effect of the helical structure into resulting normal stresses in each individual wire, Equation (7) below is used when considering stranded wire ropes. The force in each wire k in strand l is

$$F_{kl} = \frac{\dfrac{\cos^2 \beta_l}{1 + v_l \sin^2 \beta_l} \dfrac{\cos^2 \alpha_{kl}}{1 + v_{kl} \sin^2 \alpha_{kl}} E_{kl} A_{kl}}{\sum_{j=0}^{n_s} \left(z_j \dfrac{\cos^3 \beta_j}{1 + v_j \sin^2 \beta_j} \sum_{i=0}^{nw_j} z_{ij} \dfrac{\cos^3 \alpha_{ij}}{1 + v_{ij} \sin^2 \alpha_{ij}} E_{kl} A_{kl} \right)} S \tag{7}$$

where β_l is lay angle of strand in relation to rope, α_{kl} is lay angle of wire in relation to strand, E is modulus of elasticity of wire, A is cross-sectional area of wire, z is number of strands/wires, v is Poisson's ratio and S is force applied to entire rope.

As can be seen from Equation 7, the lay angle plays an important role in determining the force in each individual wire. Figure 2.13 shows how the lay angle influences the stresses of a simple strand loaded in tension. The distribution of stresses between the core wire and the outer wires exhibits a nonlinear relationship. As the lay angle increases, the effective area of the simple strand decreases due to the change in area of the outer wires. Consequently, the outer wires can resist less of the applied loading and will elongate causing an increase in stress in the core wire.

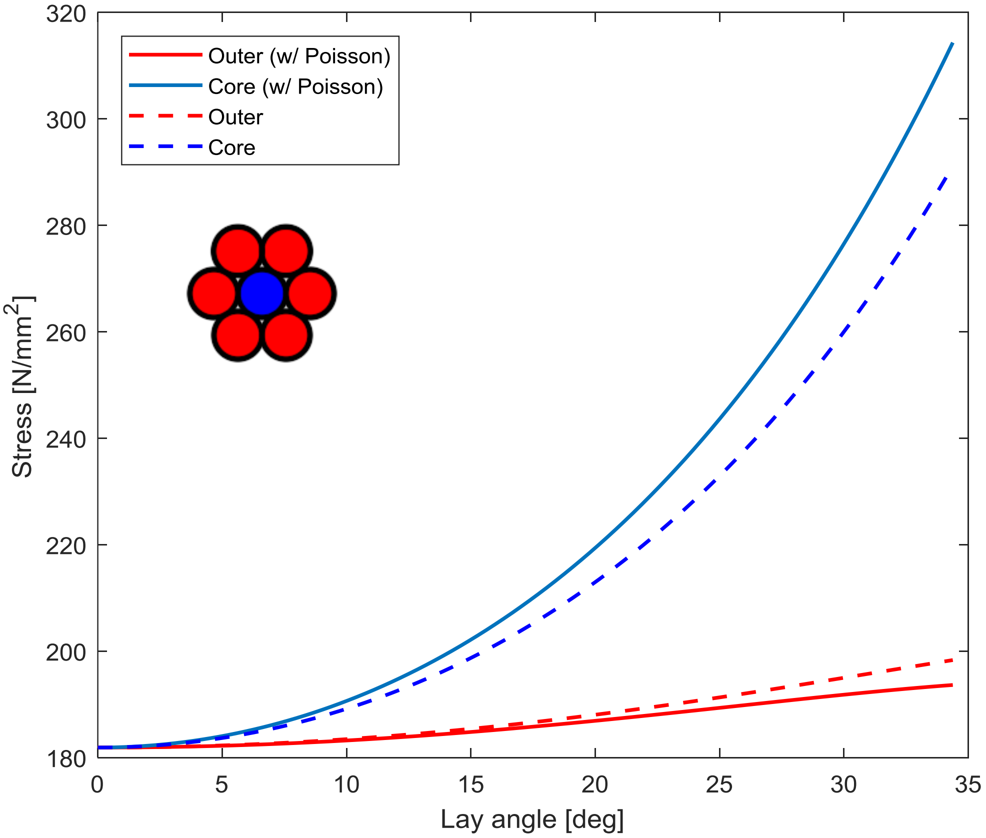

Figure 2.13 - Effect of Poisson's ratio on stresses in a simple strand due to lay angle of outer wires.

It is important to note that often the effect of Poisson's ratio of both wires and strands is neglected. This assumption has been investigated by several authors and proven to have minimal error in relation to the actual stresses. This simplification is also convenient because the Poisson's ratio for strands differs from the nominal value for steel, which can be used for the individual wires. Depending on the rope type and configuration, strands can have a much higher ratio. However, especially for ropes with steel cores, the influence this has on the resulting stresses is low enough to be considered negligible [5]. Figure 2.13 also illustrates the deviations in stresses when the Poisson's ratio is ignored or not. Indeed, the differences in stresses are small, but do become more pronounced as the lay angle increases. Additionally, it is interesting to note that neglecting the Poisson's ratio increases the stresses in the outer wires while decreasing the stress in the core.

2.3.2 Bending stress

Calculating the bending stresses of wires in a rope is not a trivial task. Numerous approaches have been taken, but the most famous equation is the one proposed by Reuleaux [28], which provides a rough approximation due to its simplicity. The expression calculates the bending stress of an individual wire as

$$\sigma_b = \frac{\delta}{D} E \tag{8}$$

where δ is wire diameter, D is diameter of rope axis bent around sheave and E is modulus of elasticity. The major criticism of this equation is that it assumes the wire does not have a helical shape. After investigation, several authors have concluded that the bending stress is both smaller and larger than the Reuleaux stress depending on the cross-sectional location of the wire. Figure 2.14 shows that although each author's results show deviations, the differences are small enough in most cases to conclude that the Reuleaux stress provides a good overall representation of the bending stress.

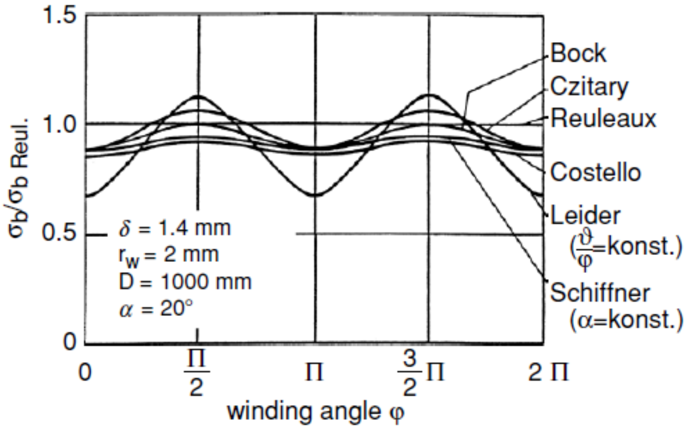

Figure 2.14 - Comparison of bending stress calculations by different authors [29].

Although the results presented are promising and show good correlation, they may not be applicable to all scenarios. When considering a sling body being bent, rope curvatures reach values that are very high in comparison to other applications. For instance, if a wire of 1 mm inside a 20 mm rope is bent around a pin with a *D/d* ratio of 1, the resulting Reuleaux stress is unrealistically high. A resulting 2.5% strain confirms it is already within the plastic region. Regardless, this would mean the wire would be on the brink of failure and cannot carry any more load. Realistically, this is not the case, therefore, the Reuleaux stress assumption has limitations and may not be precise enough for all applications.

More in-depth attempts at analytically calculating the bending stress have proven to yield more realistic results. The key to this calculation is related to the curvature of a wire before and after bending. Initially, a wire inside a straight rope has a prescribed curvature that is dependent on its helical lay angle. During bending of the rope, this wire curvature changes as wires and strands start displacing relative to each other (Figure 2.15). To determine the bending stress, the change in curvature of a wire from initial to final position must be found. Part of the reason this is a complicated calculation is because the initial and final rope curvature vectors are not parallel. Additionally, most wires have a double helical arrangement when considering a stranded rope, which is commonly used.

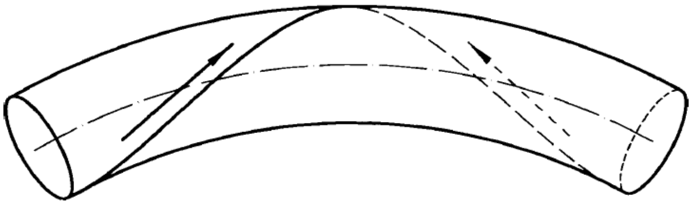

Figure 2.15 - Displacement of helical wires during bending [19].

As mentioned, the initial curvature of the wires in a stranded rope must first be determined so that a baseline for comparison can be established for calculating the bending stresses. For a single helix strand wrapped around a straight core, the classical expression used by most researchers is

$$\frac{1}{\rho_0} = \frac{\sin^2 \beta}{r_s} \tag{9}$$

where ρ_0 is initial radius of curvature, β is lay angle of strand and r_s is winding radius of strand in rope. Equation (9) provides a simple formula for calculating the initial curvature that is solely based on the lay angle in combination with winding radius. To better understand this relationship, Figure 2.16 describes how the initial curvature of the outer wires of a spiral rope are affected by these two parameters. As expected, the initial curvature increases as the lay angle increases. Additionally, the winding radius is also plotted for three different distances as a function of the diameter of the core wire. In this spiral rope example, the diameters of wires in all layers is assumed to be the same (1 mm). Here, a more interesting observation can be made which shows that the lay angle has less of an influence on the initial curvature as the distance to the center of the strand is increased.

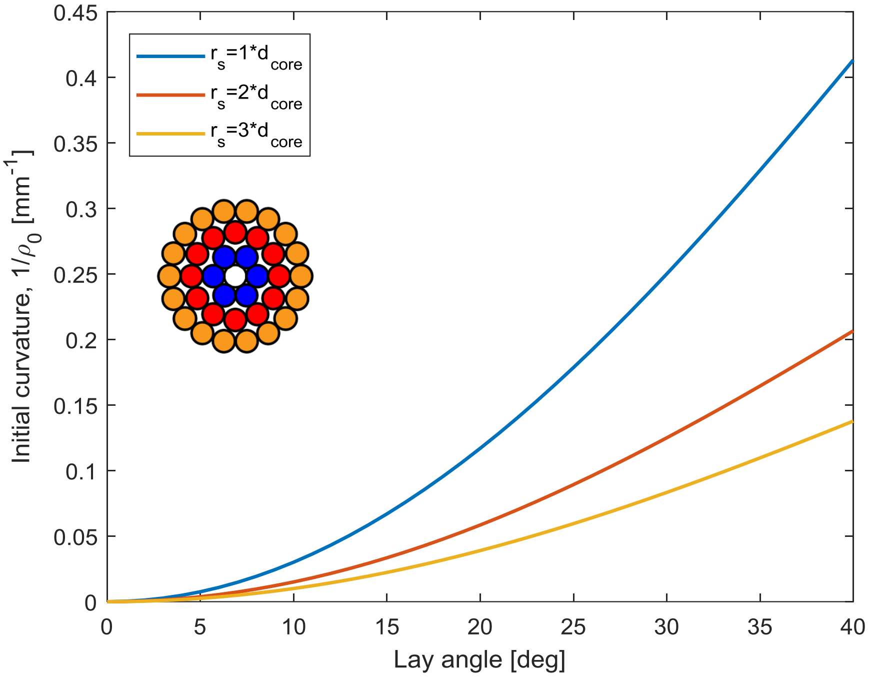

Figure 2.16 - Initial curvature of outer wires in a spiral rope based on lay angle and winding radius.

Once a wire rope is bent around a sheave or pin, the wires assume a new curvature, which generates bending stresses in the wires. To come up with this new curvature, another classical derivation is made which considers the space curve of a single helix bent around a circular curve. This derivation was worked out by Wiek [30] and later redefined by Hobbs and Nabijou [31] and results in the final curvature as

$$\frac{1}{\rho} = \frac{\sqrt{G - H}}{Q}, \tag{10}$$

where

$$G = 1 + c\cot^2\beta\,\{4c + 2\cos\varphi - 2c\cos^2\varphi + c\ \cot^2\beta\,(1 + c\cos\varphi)^2\} \tag{11}$$

$$H = \frac{c^2\cot^4\beta\,\sin^2\varphi\,(1 + c\cos\varphi)^2}{1 + \cot^2\beta\,(1 + c\cos\varphi)^2} \tag{12}$$

$$Q = \ r\{1 + \cot^2\beta\,(1 + c\cos\varphi)^2\} \tag{13}$$

with

$$\varphi = \frac{\pi R}{2l}\theta + \varphi_0, \qquad c = \frac{r}{R} \tag{14}$$

where β is lay angle, R is rope radius of curvature, θ is wrap angle of the rope around the sheave, l is lay length, φ_0 is polar angle coordinate of wire inside the rope cross section and r is winding radius of wire. To illustrate the effects the lay angle, bending radius and winding radius have on the final curvature, the same spiral rope used to calculate the initial curvature is considered in Figure 2.17. The first observation from the plots is that as the winding radius increases, the influence of the lay angle on the final curvature decreases. This relationship was also seen when calculating the initial curvature and makes sense that it stays true here. Secondly, the influence of the *D/d* ratio appears to decrease as the lay angle increases regardless of winding radius. Additionally, as the lay angle increases, the difference between *D/d* ratios remains approximately constant for each winding radius.

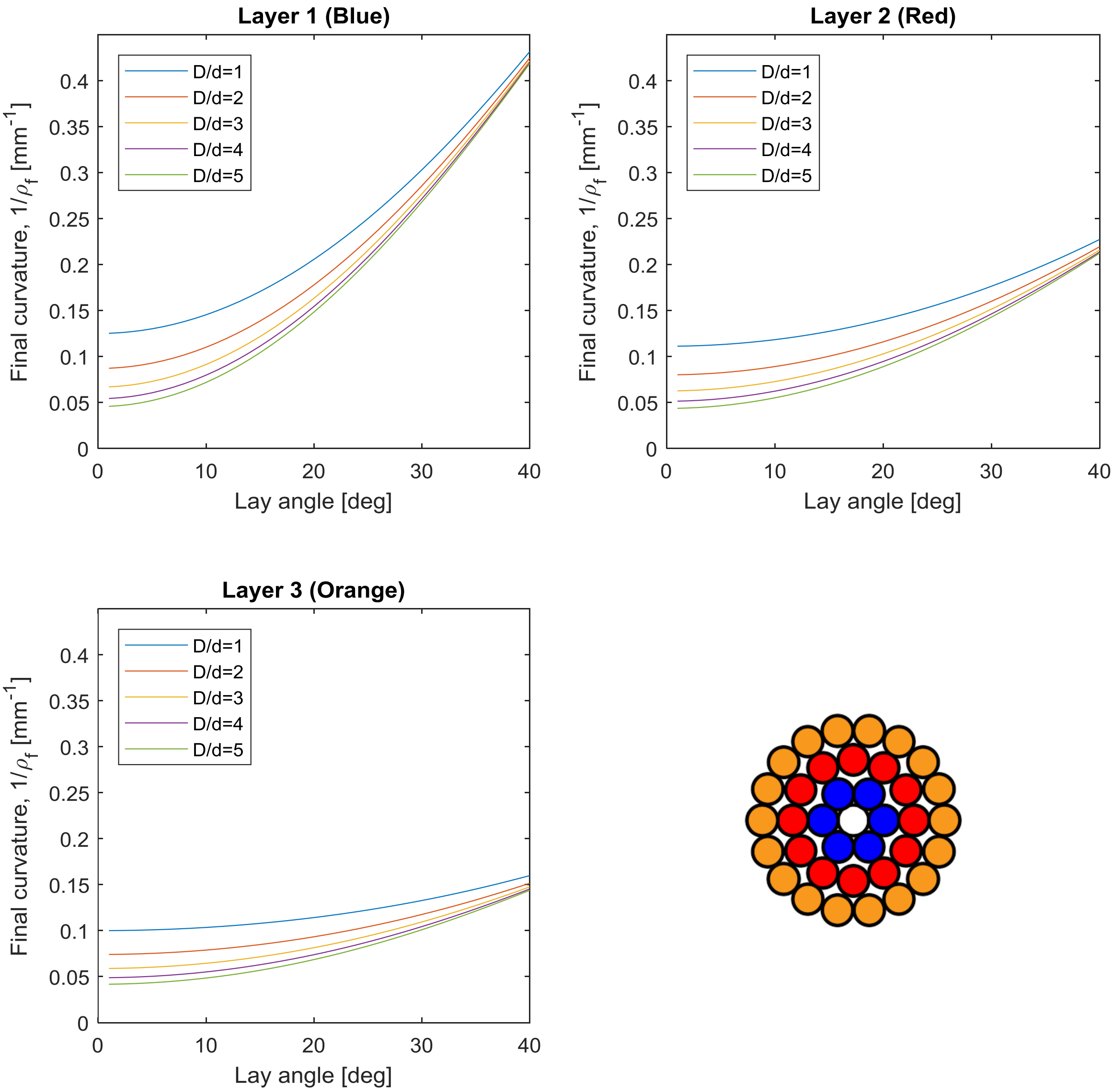

Figure 2.17 - Final curvature of wires in each layer of a spiral rope bent with varying D/d ratios.

Now that both the final and initial curvature has been defined, the bending stresses of the wires can be determined. The bending stress of a wire in layer l can be calculated as

$$\sigma_{b,l} = \left(\frac{1}{\rho_f} - \frac{1}{\rho_0}\right)\frac{1}{2}d_l E_l \tag{15}$$

where $\frac{1}{\rho_f} - \frac{1}{\rho_0}$ is the difference in curvature, d_l is the wire diameter and E_l is the modulus of elasticity.

Continuing with the spiral rope example already established, Equation (15) is implemented and the results are plotted in Figure 2.18 as bending strains instead of stresses. Looking at the plots, it is evident that as the lay angle increases, the strain due to bending decreases significantly. This phenomenon further helps to explain why the helical structure of wires plays such a vital role when talking about a rope's flexibility. This decrease becomes less pronounced as the winding radius increases, but it is still significant nonetheless. Another intuitive observation is that the higher the *D/d* ratio, the smaller the strain due to bending. Depending on the rope configuration, wire rope manufacturers often recommend a minimum *D/d* ratio to ensure proper lifetime of the rope. In this spiral rope example, it can actually be seen that the given *D/d* ratios are too low and that most wires will become overstrained and fail. The reason for this is because the diameter of each individual wire is too large in relation to the rope diameter. If the wire diameter was decreased and the rope diameter was kept the same by adding another wire layer, the resulting bending strains would be much lower. This is because the distance to the extreme fiber of the wire would be decreased due to the smaller diameter. Although the logic behind this is quite intuitive, it helps exemplify why wire rope configuration plays such an important role. It is also important to note that the bending stress calculations discussed here are based on the assumption of a frictionless rope. The influence of friction will be discussed in the following section.

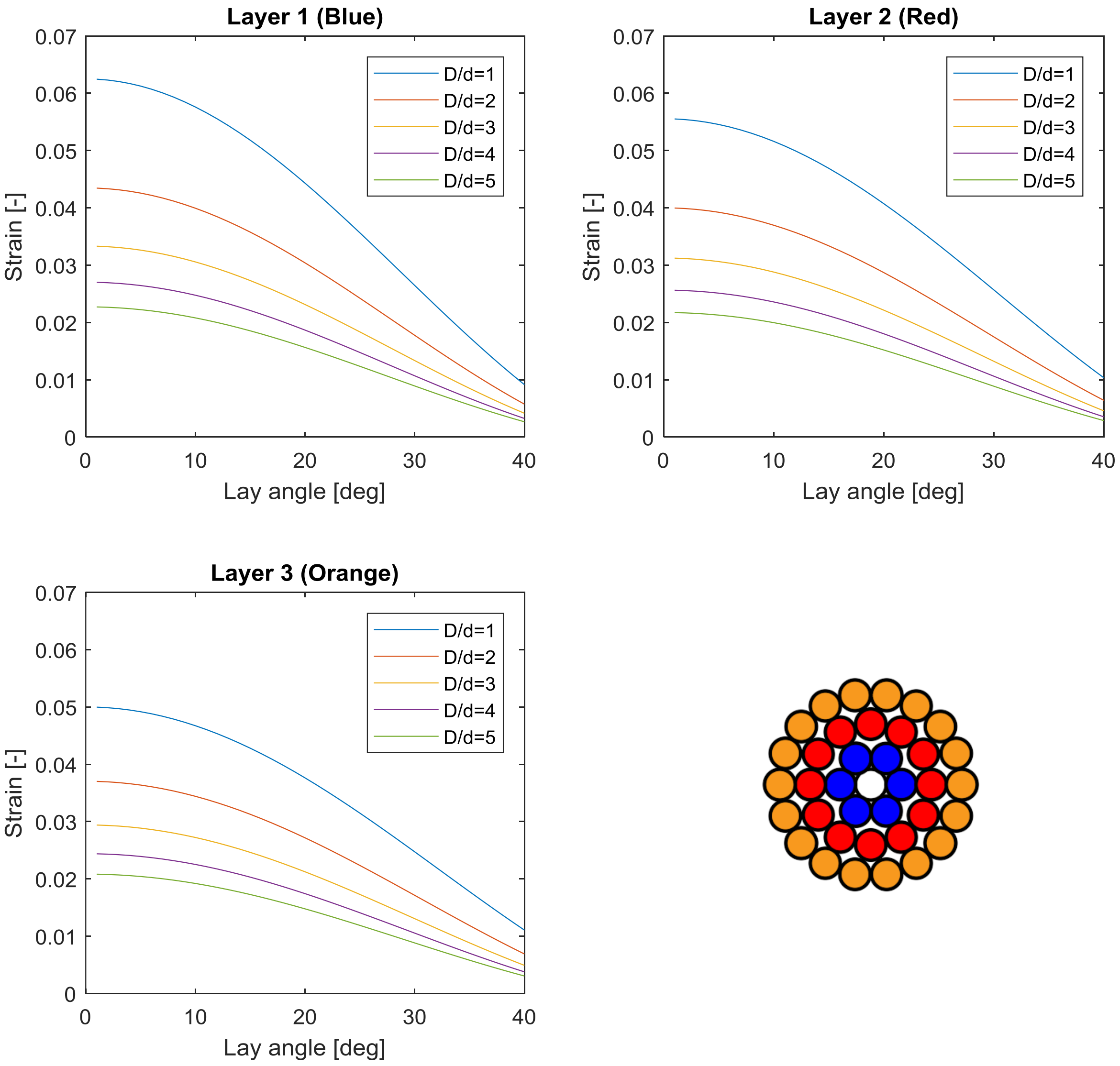

Figure 2.18 - Bending strain of wires in each layer of a spiral rope bent with varying D/d ratios.

2.3.3 Secondary stress (stress due to friction)

Yet another highly debated topic is the influence of friction in a steel wire rope. This stress is commonly referred to as secondary tensile stress in literature. Different authors have come up with different conclusions about the influence of friction in their models. Generally, Costello's theory that friction plays a minimal role has been proven to be quite accurate when considering steel wire ropes loaded in pure tension. However, this assumption has raised questions when considering ropes in bending. To date, one of the most widely recognized models that incorporates friction during bending is the one found in Papailiou [19].

Papailiou made several significant assumptions in his model. First, he considered that wires are only in contact with adjacent layers and that wires within the same layer do not interact. This assumption is questionable and its validity is highly dependent on the specific rope geometry. Another simplification made is that there is continuous contact between wires in adjacent layers. Papailiou studied this effect and concluded that it holds true especially for parallel lay ropes.

The theory behind the friction model starts with deriving the radial force contribution due to the helical structure during axial loading. This derivation has been based on the work done by Leider [32] and is simplified to a simple strand consisting of one center wire with six outside wires in a helix. Using the tensile forces in the individual wires resulting from a rope axial loading, a radially oriented distributed load can be derived as

$$p_L = \frac{Z_L}{\rho_L} \tag{16}$$

where Z_L are wire tensile forces in a layer and ρ_L is radius of curvature of a wire helix. All associated parameters are illustrated by Figure 2.19.

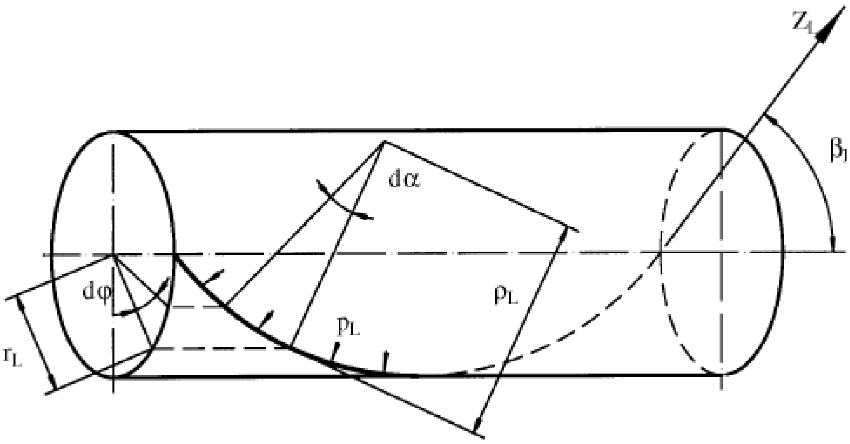

Figure 2.19 - Resulting radial pressure of wires due to helix [19].

The distributed load acting on a wrap angle $d\alpha$ can then be simplified into a normal force as

$$dN_L = p_L \rho_L d\alpha. \tag{17}$$

Taking into considerations the geometric relations shown by Figure 2.19,

$$\frac{r_L d\varphi}{\rho_L d\alpha} = \sin\beta_L \text{ and } \rho_L = \frac{r_L}{\sin^2\beta_L} \tag{18}$$

where r_L is the winding radius, φ is the incremental helix angle and β_L is the lay angle [33]. Combining these relations, the normal force is redefined as

$$dN_L = Z_L \sin\beta_L \, d\varphi. \tag{19}$$

Using the normal force, a resulting friction force can be derived through a coefficient of friction μ_L that best describes the surface interaction between the steel wires. Considering statics, the free body diagram of a wire element can be described by Figure 2.20.

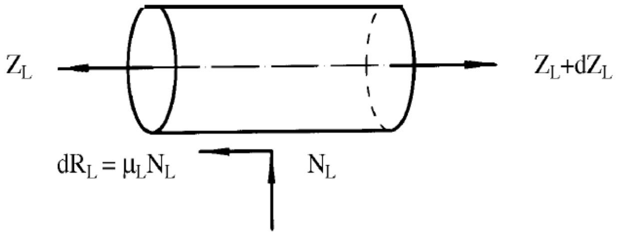

Figure 2.20 - Free body diagram of outer wire element in a simple strand [19].

Finding the balance of forces from the free body diagram results in

$$Z_L + dZ_L - Z_L = dZ_L = \mu_L Z_L \sin\beta_L \, d\varphi \tag{20}$$

Applying the proper boundary conditions ($\varphi = 0, Z_L = Z_{d,L}$) after integrating (20) over φ results in the maximum total tension that can be resisted by friction at every point φ

$$Z_L(\varphi) = Z_{d,L} e^{\mu_L \sin\beta_L \varphi} \tag{21}$$

where $Z_{d,L}$ is the individual wire tensile force as calculated in 2.3.1. However, to isolate the fluctuating variable tension force generated by friction of a single wire ($Z_{zus,L}(\varphi)$) leads to

$$Z_{zus,L}(\varphi) = Z_L(\varphi) - Z_{d,L} = Z_{d,L}(e^{\mu_L \sin\beta_L \varphi} - 1) \tag{22}$$

and the corresponding wire stress can simply be found by

$$\sigma_{zus,L}(\varphi) = \frac{Z_{d,L}}{A_{d,L}} \left(e^{\mu_L \sin\beta_L \varphi} - 1\right). \tag{23}$$

It is assumed that this stress remains uniform over the entire wire cross section as a pure tension stress but varies with the different positions of the wire along its helix.

It is important to discuss several key characteristics of this model in order to understand its limitations. Firstly, this so called secondary stress can only exist when a rope experiences bending. As a rope bends, the wires in each layer are stretched differently, thus forcing them to displace relative to each other. To achieve relevant displacement between wires, this secondary stress must be overcome. In Papailiou, the curvature at which this stress is overcome is of great importance. His model was specifically developed for overhead transmission lines where the goal was to accurately predict the bending stiffness as the rope curvature changes. The conclusion was that the bending stiffness had three distinct regions that were governed mainly by the friction coefficient between wires and the applied pre-tension. This phenomenon was also confirmed by Hong et al. [20] and is nicely illustrated by Figure 2.21. The first region represents a high, constant stiffness where friction prevents wires from displacing relative to each other. The second region is defined as a transition region where only some of the wires overcome friction while others are still sticking together. The final region represents the curvature at which all wires have overcome friction and can displace relative to each other, which leads to a much smaller bending stiffness as the wires each bend around their own neutral axis.

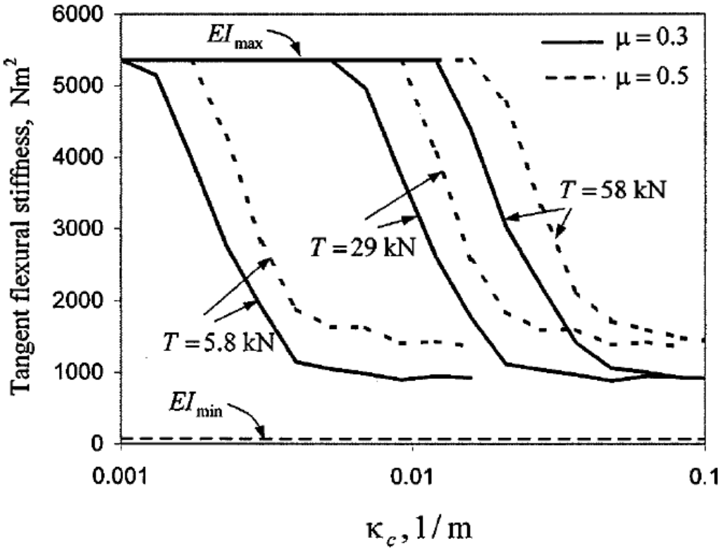

Figure 2.21 - Bending stiffness as a function of curvature with variable pre-tension and friction coefficient [20].

In that application, the wire ropes have a constant pre-tension and experience relatively small curvature changes in comparison to the topic of this thesis. The scenario in this thesis considers a curvature range where friction has been overcome and all wires are slipping. Consequentially, the important theory to extract from [19] is the actual stress that must be overcome because this remains in the wires throughout the bending process. Additionally, the friction coefficients for steel wire rope slings are lower due to the lubrication applied between wires throughout the rope. For steel-on-steel contact a value of 0.3 is normal. However, with lubrication, a friction coefficient between 0.15-0.2 provides a more reasonable estimate of the actual value and has been used by previous researchers [34] [35].

2.3.4 Ovalization stress

Although the relative movement of wires in a rope has mostly been discussed as an advantage, there are situations where inherent consequences arise. When a rope is bent over a pin or sheave and an axial tension is applied, its nominally round shape can become oval in a process called ovalization. As wires are forced onto a sheave, the rope gradually begins to take on the shape of the groove. In this process, bending and torsion stresses arise due to the change in shape from circular to oval and can be calculated by finding the change in curvature of the wires [29]. A simple expression to determine the ovalization stress at the bottom of the groove for the center wire of a strand is

$$\sigma_{b,ov} = \left(\frac{\sin^2 \beta_{ov}}{r_{s,ov}} - \frac{\sin^2 \beta}{r_s}\right)\frac{\delta}{2}E \tag{24}$$

with

$$r_{s,ov} = r - \frac{d_s}{2} \text{ and } r_s = \frac{d}{2} - \frac{d_s}{2} \tag{25}$$

where δ is wire diameter, β is strand lay angle, d is rope diameter, d_s is strand diameter, r_s is strand winding radius and E is modulus of elasticity [5]. Figure 2.22 illustrates the ovalization phenomenon.

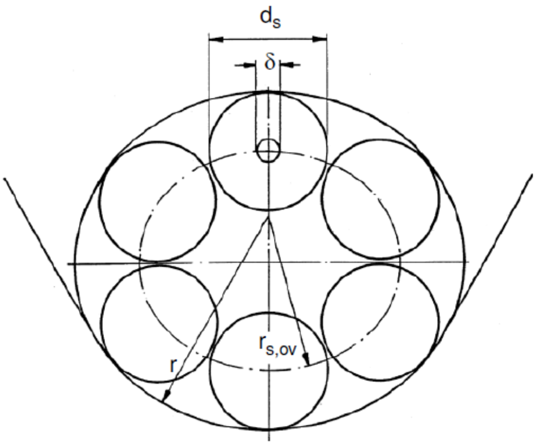

Figure 2.22 - Ovalization of a steel wire rope in a groove [5].

Assuming that the change in lay angle due to ovalization is negligible, the stress is governed by the radius of the groove. To study this effect, Figure 2.23 was created for a 20 mm rope. Here, the ovalization stress of the 1 mm center wire of an outside strand at the bottom of the groove is shown as a function of the groove radius over rope diameter ratio.

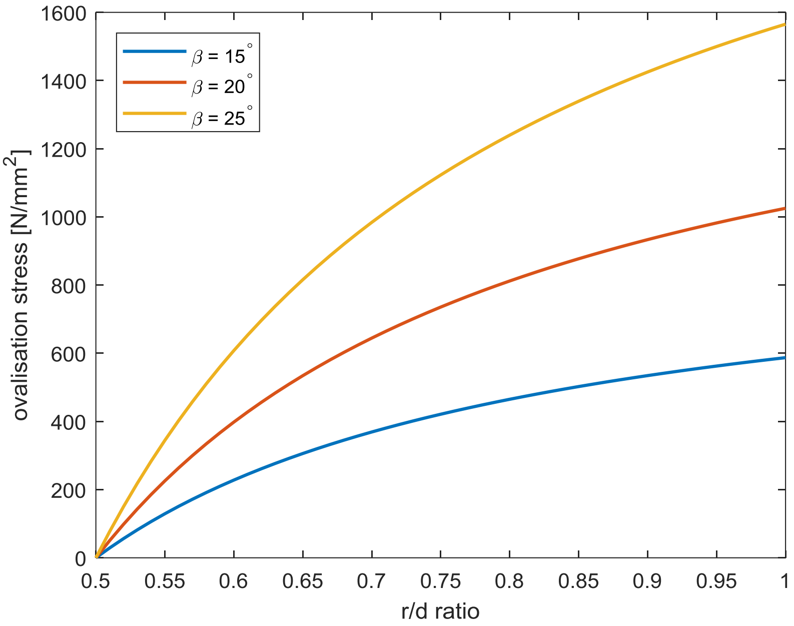

Figure 2.23 - Ovalization stress in center wire of outside strand.

Looking at the figure, the resulting ovalization stress in the wire is very sensitive to the *r/d* ratio. As the groove radius starts becoming slightly larger than the rope, the stress increases sharply and in a nonlinear fashion. This is because as the fit between the groove and rope gets looser, wires will experience larger changes in curvature as they try to conform to the groove. Additionally, it is observed that as the lay angle increases, the stresses become larger and more sensitive to the *r/d* ratio. This indeed makes sense because the curvature change will be larger for a wire with a smaller angle with respect to the compressive force applied by the sheave.

Several authors have also performed experiments to examine what the effect of ropes running over sheaves with varying *r/d* ratios has on bending fatigue (Figure 2.24). This plot reconfirms that deviation from the perfect snug fit (*r/d*=0.5) results in a sharp reduction in capacity. Also, the behavior of the nonlinear relationship of the fatigue capacity evolves in a similar manner to the bending stress increase observed in Figure 2.23.

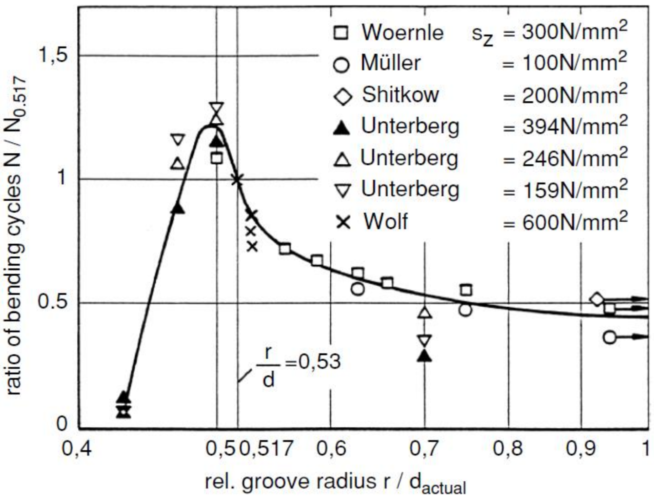

Figure 2.24 - Influence of groove radius on bending fatigue capacity [5].

In practice, it is commonly accepted to have an *r/d* ratio of 0.53. This is done to accommodate the difference between the actual diameter and nominal diameter of a rope while keeping the fit as snug as possible to minimize the stresses. Additionally, it is important to note that ovalization is a very nonlinear phenomenon that is difficult to predict accurately and will most likely vary between the different wire rope configurations. For instance, it has been observed that ovalization is of greater importance for ropes with a fiber core than those with an IWRC [5]. In the context of this thesis, the rope is bent around a pin, which results in an *r/d* ratio that goes towards infinity. Theoretically, this yields unreasonably high stresses in the wires. Hence, an analytical approach to determining the actual stresses for this scenario is very difficult due to the nonlinearities involved.

2.3.5 Torsion, moment and shear

As discussed earlier, the introduction of the helix structure imposes secondary stresses when a rope is subjected to a tensile loading. Referring back to Figure 2.11, Czitary [36] derives the forces resulting from the helix and concludes that the corresponding torsion, moment and shear stresses can be considered negligible. The reason for this is because the stresses result from the change in lay angle that is caused by rope elongation during axial loading, which is relatively small. To check this effect, the torsional stress for a wire in a rope similar to the one used in 2.3.4 is calculated as

$$\tau = \left(\frac{\sin\beta\cos\beta}{r} - \frac{\sin\beta_0\cos\beta_0}{r_0}\right)\frac{\delta}{2}G \tag{26}$$

where β is lay angle, r is winding radius, δ is wire diameter, G is shear modulus and index 0 indicates the initial state before loading [36]. Using the equation, Figure 2.25 illustrates the torsional stress experienced by the center wire of an outer strand due to axial elongation of the rope. From the plot, it can be seen that the stress due to torsion increases linearly with the axial elongation. Assuming a linear modulus of elasticity, this relationship is as expected since the change in lay angle will increase with rope elongation. Furthermore, it is also observed that the torsional stresses are higher for larger wire helical lay angles. Intuitively, this is expected since a larger helical lay results in a higher radial component. Nevertheless, the contribution of torsion to the overall stress is indeed small enough to be considered negligible in most cases.

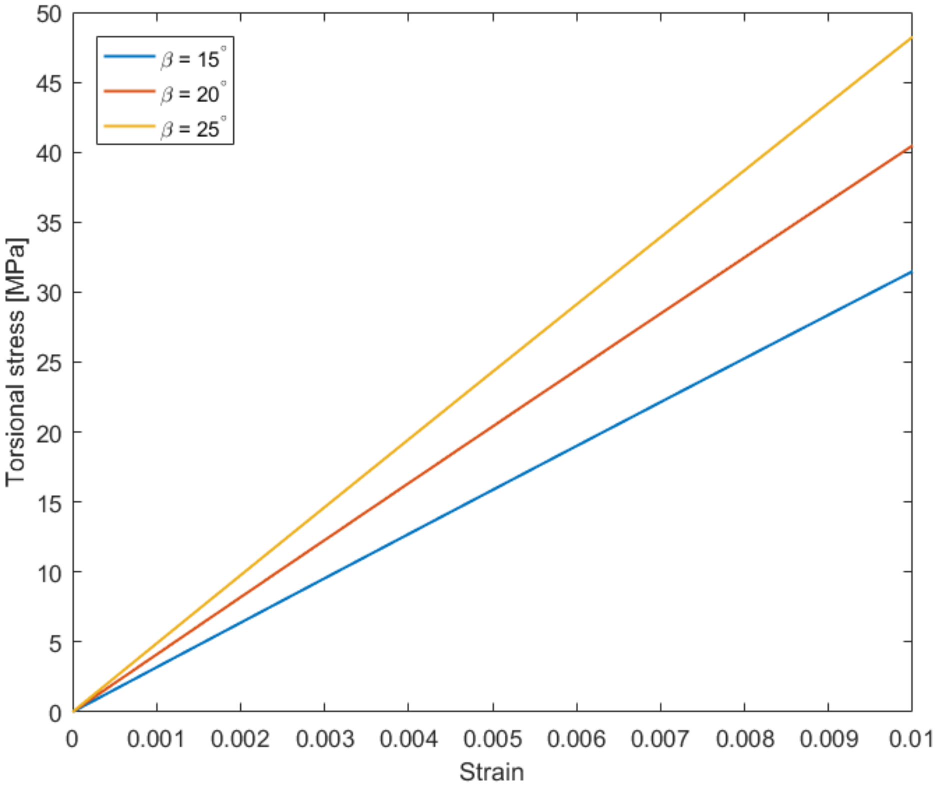

Figure 2.25 - Torsional stress of center wire in outer strand due to strain caused by axial loading of wire.

3.0 ANALYTICAL MODELLING

As previously discussed, many authors have contributed their own approaches to modelling the behavior of wire rope. However, even to this day, there is no clear answer as to which approach best predicts this elusive tool. Moreover, much of the research conducted has been focused on trying to predict specific characteristics of the rope rather than global behavior.

In the context of this thesis, an analytical model is presented that aims to predict the capacity of a steel wire rope sling. The scenario in question involves trying to determine the reduction in capacity when the body of a sling is bent around a pin. Hence, the analytical model first predicts the capacity under axial loading and then compares it to the capacity of the rope in bending. In this chapter, an overview of the analytical model is given by outlining the theory and assumptions. Then, the results of the following rope configurations are presented and discussed:

- 20 mm 6x25F-IWRC,
- 20 mm 6x36WS-IWRC,
- 77 mm 6x36WS-IWRC.

3.1 MODEL DESCRIPTION

The analytical model presented here attempts to combine several insights from previous research into one complete model that can predict the reduction in capacity of a steel wire rope when bent. To come up with the reduction factor, the model needs to calculate the capacity for two different processes.

Before going into depth, it is important to define the main assumptions that are incorporated in this model. As discussed in 2.3, there are many different stresses involved when a steel wire rope is subjected to loading. However, the main stresses considered in this model are:

- Axial stresses;
- Bending stresses;
- Frictional stresses.

As previously mentioned, the secondary stresses resulting from the helical structure of the rope are usually minimal. Therefore, stresses due to torsion, moment and shear have not been included in the analytical model. The ovalization stress was a phenomenon that was defined for ropes bending over sheaves. However, it was shown that these analytical expressions were not valid for a rope bending over a pin where the groove radius approached infinity. Excluding this stress from the model yielded reasonable results so it was also considered negligible, but this effect requires further investigation.

Figure 3.1 is a flowchart that describes the logic behind calculation of the rope capacity during pure axial loading. The process starts with the user input of relevant parameters associated with the specific rope construction, wire material properties and applied loading. See Appendix A for an elaboration of the required parameters. Using these inputs, the program then determines several geometric properties of the rope. At this stage, all the constant parameters have been defined and are fed into an iterative loop where the loading is applied incrementally. The first step involves determining how the applied loading of the current time step is redistributed among each individual wire. Then, this applied wire loading is added to the overall wire force based on the previous time step. Using this overall force, the current apparent modulus of elasticity of each wire is calculated at each time step. Knowing the force and Young’s modulus, the resulting elongation of each wire is determined. Finally, the elongation state of each wire is checked to see if it has reached a certain failure criterion. If a wire has reached failure, its effect is then captured at the next iteration step when the applied rope loading is redistributed to the individual wires. At the end of the loop, a function is used to determine the load at which the entire rope is considered to fail.

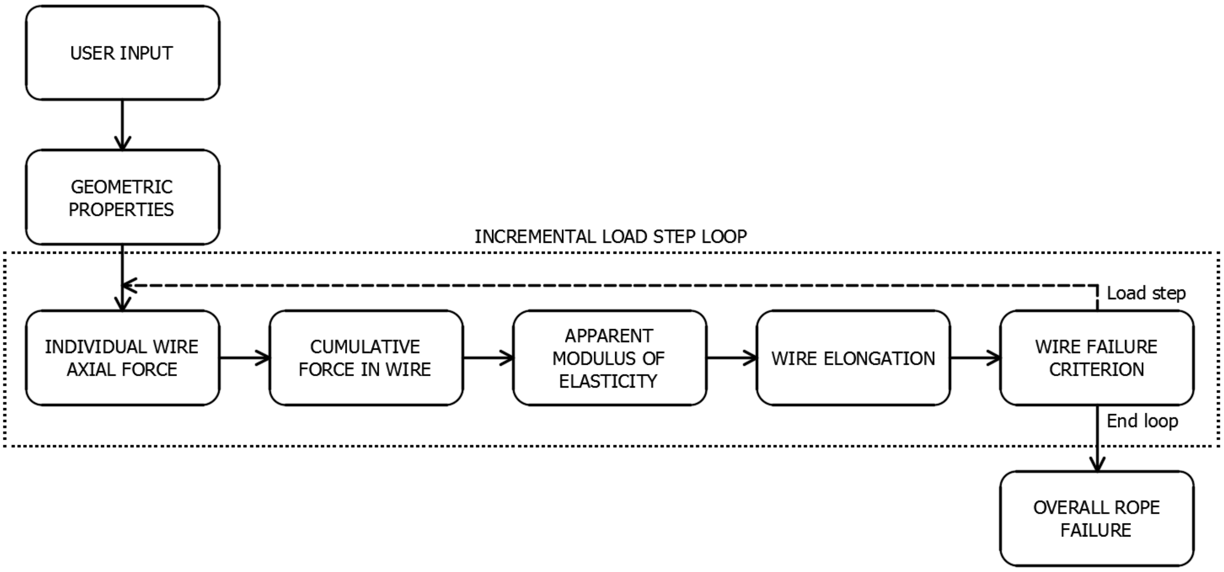

Figure 3.1 - Flowchart of pure axial loading capacity calculation.

To predict the capacity of a steel wire rope sling in the bending scenario, it is important to first describe the way this process is interpreted. The process is simplified by splitting it into two separate phases as shown by Figure 3.2. In Phase 1, the rope is taken from a straight position and bent around the pin. Note that this will require the application of some tensile loading to help overcome the bending stiffness of the rope. Once the rope has fully conformed to the curvature of the pin, Phase 1 ends and Phase 2 commences. Here, the elongation of the rope is mainly governed by the axial loading applied.

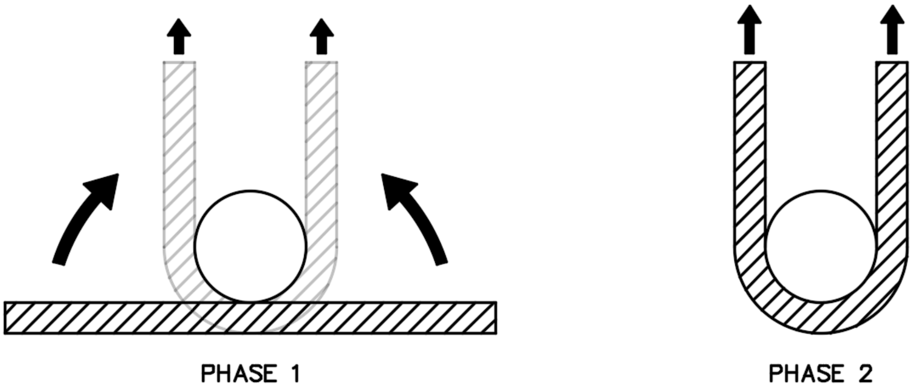

Figure 3.2 - Illustrative interpretation of the bending scenario of a steel wire rope.

With the two different phases defined, the flowchart of the bending scenario is constructed in a similar manner as before. Here, friction effects and bending strains must be incorporated in addition to the axial tensile loading. As shown in Figure 3.3, this is done inside the iterative loop. It is also important to note that these two additional forces occur only during Phase 1. The reasoning behind this will be explained in the next few sections.

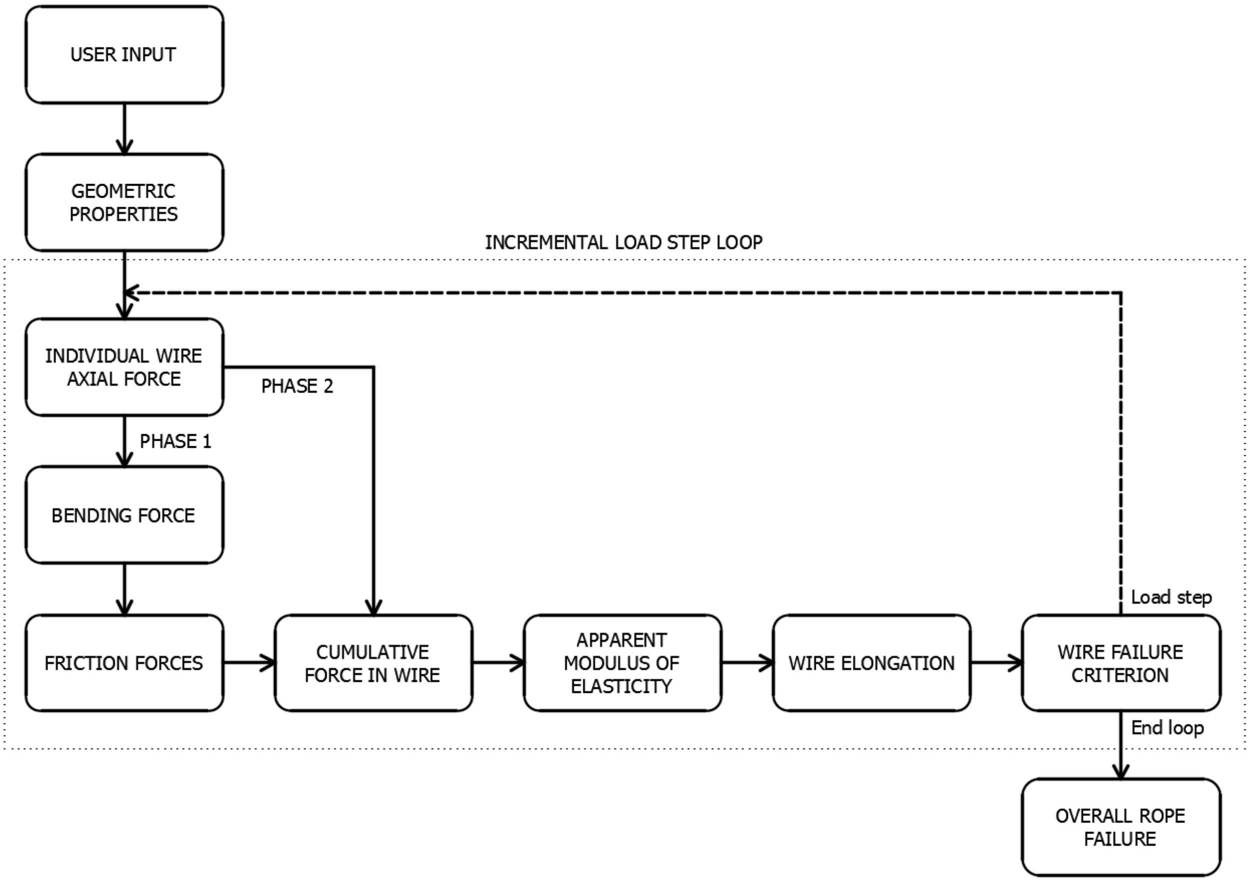

Figure 3.3 – Flowchart of bending capacity calculation.

3.1.1 Individual wire tensile load

This calculation represents the axial force in a wire due to the overall loading applied to the rope. The equations and theory behind this calculation discussed in 2.3.1 have been directly implemented into this analytical model. Poisson’s ratio has also been included, however, an important assumption has been made. As previously discussed, the Poisson’s ratio of wires can be compared to that of steel, but the ratio in the strand level can be significantly different. Nevertheless, it is assumed that the Poisson’s ratio for strands and wires is the same since the rope configurations considered here all have a steel core. Additionally, the influence of this ratio can also be considered small depending on the lay angle (Figure 2.13).

3.1.2 Bending strains

The bending stress experienced by the steel wire rope is of particular interest in this scenario. Slings are commonly bent with *D/d* ratios that are extremely low, which results in very sharp bends and significant stresses. As discussed in the previous chapter, accurately predicting these stresses is difficult due to the nonlinearities involved. Regardless, an attempt is made to approximate the stresses most likely to be experienced by the wires using several assumptions, which shall be discussed throughout this section.

First, the change in curvature must be derived for a stranded rope. This type of rope configuration involves wires in a double helix, while the expression derived in the previous chapter was applicable to wires in a single helix. To overcome this, [30] proposed to cleverly use his single helix formula in an iterative manner in order to come up with the curvatures for wires in a stranded rope. The iteration can be summarized like so,

$$\kappa_{rope}$$

$$\kappa_S = \frac{\sqrt{1 + c_S \cot^2 \alpha_S \left(2(c_S + 1) + c_S \cot^2 \alpha_S \left(c_S + 1\right)^2\right)}}{r_S\left(1 + \cot^2 \alpha_S \left(1 + c_S\right)^2\right)} \quad \text{with} \quad c_S = r_S \kappa_{rope} \tag{27}$$

$$\kappa_W = \frac{\sqrt{1 + c_W \cot^2 \alpha_W \left(2(c_W + 1) + c_W \cot^2 \alpha_W \left(c_W + 1\right)^2\right)}}{r_W\left(1 + \cot^2 \alpha_W \left(1 + c_W\right)^2\right)} \quad \text{with} \quad c_W = r_W \kappa_S \tag{28}$$

$$e = \Delta \kappa_W y$$

where κ is centerline curvature, r is winding radius, α is lay angle, y is distance to extreme fiber, e is wire bending strain and the subscripts S and W refer to strand and wire, respectively. First, the curvature of the rope due to bending around a pin can be determined based on the pin diameter. Then, by considering the outer strand forming a single helix around the rope core axis, the strand radius of curvature is determined. Next, the same equation is applied by considering the individual wire forming a single helix with the core of the strand. The key to capturing the double helix effect is through the use of the constants, c_S and c_W, which relate the winding radius to the curvature of the core being considered. This results in the final curvature of the wires when the rope is bent, however the initial curvature of the wires before bending must also be determined in order to find the strain experienced by the wires. To do so, the same iterative process is used except this time the rope curvature is taken to approach zero. This way, the curvature of the individual wires is calculated when the rope is in a straight position.

To complete the bending strain calculation, the distance to the extreme fiber needs to be considered. To reduce conservatism and simplify strain calculations, this analytical model considers an average bending strain that is constant on each side of the tension and compression zone of a wire bending around its own neutral axis as shown in Figure 3.4. When considering all the strains acting on a wire cross section, the compression zone caused by bending will be countered by the axial tensile loading. Hence, the only consequential loss of information occurs in a small section on the tensile zone of the wire. Moreover, this section makes up less than 20% of the total area.

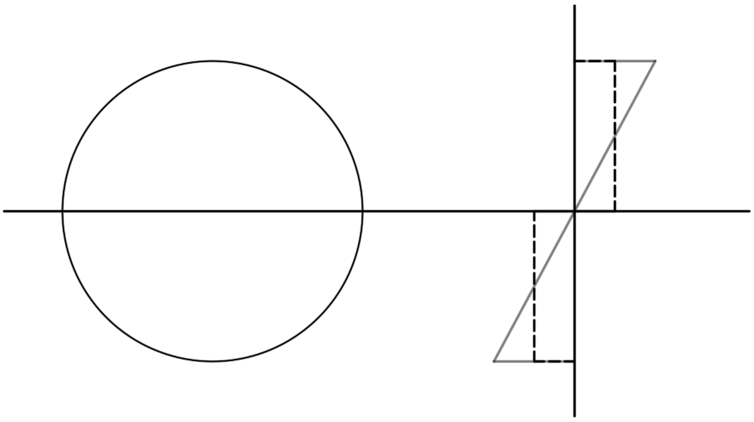

Figure 3.4 - Approximation of bending strains (dashed) in a wire cross section.

Knowing the rope curvature is an important aspect to the calculation of the bending strain. This model uses the diameter of the pin to determine the final curvature of the rope. However, applying these strains directly does not reflect what is actually happening. As previously described, the rope is bent during Phase 1. To better understand the process, the terms forced and free bending must be defined. Free bending occurs when the rope is initially bent from its straight position. Here, the stresses induced in the wires are caused by the bending stiffness of the rope as it changes its curvature. Forced bending occurs once the rope wraps around the pin and is forced to conform to its curvature. Trying to model the process precisely is a complicated task, so another simplification is applied instead. First, the total bending strains due to forced bending around the pin are calculated. Second, the total bending strains are equally divided by the number of load steps in a predetermined threshold loading and then applied incrementally in a linear fashion. The threshold loading is the applied axial force needed to fully wrap the rope around the pin. This is basically the end of Phase 1 and the beginning of Phase 2. The value of the threshold loading is approximated to be roughly 25% of the MBL. This was empirically determined through the observation of the forced bending phenomenon during experimental testing (Chapter 0).

3.1.3 Secondary stress due to friction

In 2.3.3, the secondary stress was defined based on the model by Papailiou [19]. Its limitations were also discussed in relation to the scenario being observed in this thesis. In the context of this current model, the stick phase is considered negligible and all wires are assumed to be displacing relative to each other. In order for this displacement to occur, wires need to overcome the friction force.

The first challenge in implementing the friction model by [19] involves the rope configuration. His model was developed for overhead conductor lines, which are predominantly spiral ropes as opposed to the stranded rope configurations being considered here. To overcome this, a similar iterative approach previously taken with the bending strain calculation is applied.

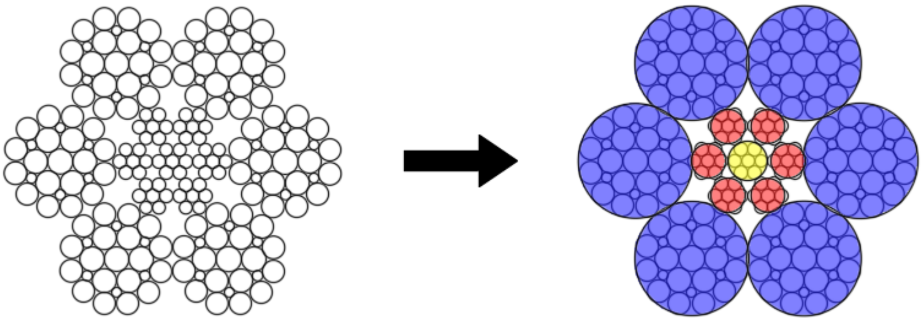

Figure 3.5 - Strand level simplification of rope for calculation of friction forces.

The method described here was based on previous research done by Bart de Jong [37]. First, the stranded rope is simplified to a spiral rope as shown by Figure 3.5. This is done by considering the outsides strands as whole elements that are wrapped around one core element. Now, the friction forces between outer strand layers can be determined as if it was a spiral rope. Next, to get to the wire level, each individual strand must be isolated and the analysis repeated. The key step is to take into account the friction force that was calculated at the strand level. In other words, the input axial tensile wire force is based on the strand axial force plus the calculated friction force. Depending on the strand location within the helix, this total strand force will be larger or smaller than the nominal axial strand loading imposed by the rope force. The strand with the highest tensile forces will be chosen to complete the calculation for the input wire force as it will likely be the first to fail.

Another important aspect of this secondary stress is that it occurs only while the rope is bending. Hence, if the rope experiences no change in curvature, the secondary stress is negligible. Therefore, proper accounting of this force is achieved in a similar way as the bending strains by phased application. Since bending only occurs in Phase 1, the secondary stress is applied along with the bending strain exclusively during this stage. During Phase 2, the secondary stress is omitted since there is no change in rope curvature.

3.1.4 Modulus of elasticity

The stress-strain relationship of wires is an integral part of the model. With it, the necessary conversion between the two parameters can be established via the modulus of elasticity. However, there are a few challenges that must be overcome.

As previously discussed, the drawing process changes the mechanical properties of wires drastically. This is what allows them to achieve high tensile grades, but it also drastically decreases their ductility in comparison to normal steel behavior. Moreover, this results in nonlinear stress-strain curves where a typical elastic analysis will not accurately capture the wire behavior or its actual capacity. Additionally, wire rope manufacturers tend to use wires of different tensile strengths throughout the strand layers.

To overcome these obstacles, the model considers each wire on an individual basis. This can be achieved if the user can provide all the different stress-strain curves of wires used throughout the rope. In most cases, this data is available for each layer of the outer strand. As an example, Figure 3.6, which was taken from a separate study, shows the stress-strain diagrams of each wire in an outer strand of a 6x36WS-FC rope. This is a good illustration of the extent of deviations between wires in different layers and further exemplifies why this is important to capture.

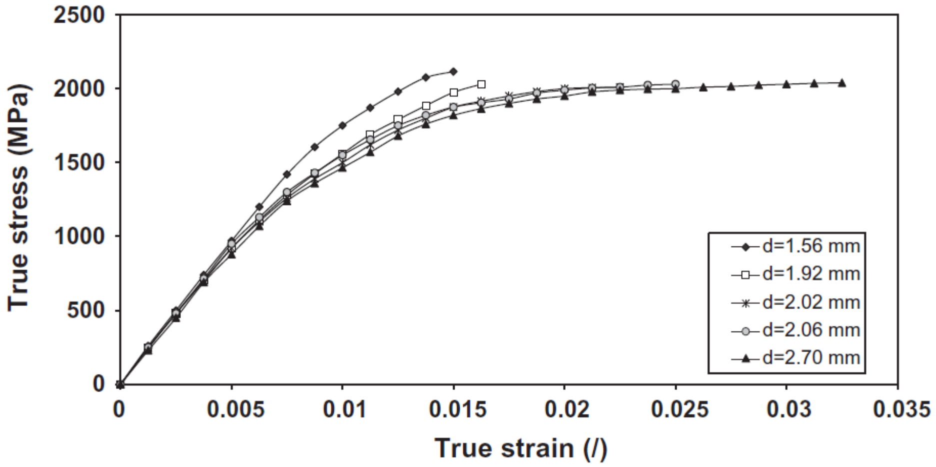

Figure 3.6 - Stress-strain diagram of wires in an outer strand of a 6x36WS-FC rope [35].

The conversion between stresses and strains is done linearly through the modulus of elasticity. Given that most wires exhibit a nonlinear slope, it is difficult to conclude a single representative value. However, by using a sufficiently small time step, this nonlinearity can be linearized by finding a tangent modulus of elasticity at each iteration. At each time step, the tangent modulus of elasticity is calculated for each individual wire based on its current stress state from the applied loading. This value is then used throughout the rest of the iteration to convert between stresses and strains.

3.1.5 Failure criterion

Once the resulting elongation for each wire is obtained, it must pass through a failure criterion before the next load step. This is an integral part of how the rope is predicted to behave so it is important to understand the assumptions being made in this model.

The first point of discussion is global rope elongation behavior versus individual wire elongation. As explained in the previous chapter, wires are stressed differently based on their geometric properties when an axial loading is applied to the rope. When translating these stresses directly into strains, this results in wires having different elongations. Hence, even though a sling with two end terminations will have a uniform extension throughout the rope cross section along the rope axis, the individual wires will elongate differently along their own local axis based on their lay angle. This insight exemplifies the key role in using wire grades with different stress-strain relationships throughout the strand layers in order to achieve a balance. Regardless, fluctuations in stresses between the wires cannot be avoided and some wires will fail before others.

The next important topic is taking into consideration how the failure of a wire effects the global behavior of the rope. As explained in 1.1.2, wire ropes have a unique redundancy property that allows them to redistribute the loading in the case of a wire failure. An attempt is made to replicate this property by taking advantage of the incremental load step loop found in this model's structure.

The failure criterion used in this model is based on the state of the wire in relation to its stress-strain relationship. At this point of the iterative loop, the apparent modulus of elasticity of each wire is determined for the current load step. If a wire has reached a certain threshold modulus value, it is considered to have failed. This threshold value is empirically determined and is based on the average axial stress increase of the wires over 0.2% strain from one load step. If the corresponding slope is below this value, the wire has reached the plastic region where it is not able to carry any more of its loading and only elongates. The idea is that although the wire has technically not completely failed since it has not reached its strain at rupture, it has a minimal contribution to the axial stiffness of the rope.

With the failure point of a wire defined, the resulting consequence to the overall rope behavior is applied. Basically, the indication of failure triggers the program to set the area of the corresponding wire to zero. This is reflected in the next iteration of the loop when the overall rope loading is transferred to each individual wire. Now, the failure of the wire causes a stress increase in other wires as the overall rope loading has to be redistributed to a smaller number of wires.

3.2 RESULTS FROM CASE STUDIES

Using the analytical model, three different steel wire ropes were analyzed. The data required for the user input was obtained from certificates provided by the wire rope manufacturer and summarized. First, the nominal capacity of the rope is calculated by the analytical model and a snapshot of the resulting force distribution of individual wires within the rope cross-section was created. Finally, the reduction in capacity due to bending is determined for all three ropes and the differences are discussed.

3.2.1 Rope configurations & properties

The analytical model is made in such a way that it can work for almost all common steel wire rope configurations used today. The rope configurations under investigation are listed in Table 3.1 along with some of their main characteristics. Figures found in section 3.2.2 provide a visual representation of the strand constructions described here. Using these ropes, two general relationship can be observed. The first is the difference in geometries between the 6x25F and 6x36WS ropes, which are the same diameter. The second is the relationship between the small and large diameter 6x36WS ropes. It is important to take into account that not all parameters remain consistent between rope geometries when observing these relationships.

Table 3.1 - Wire rope configurations and properties used in the analytical model.

	20 mm 6x25F-IWRC	**20 mm 6x36WS-IWRC [37]**	**77 mm 6x36WS-IWRC**
Lay type	RHOL	RHOL	RHOL
Strand lay angle	18°	27.5°	17°
Strand construction	1-6-6F-12	1-7-7+7-14	1-7-7+7-14
Grade	1960 N/mm^2	1960 N/mm^2	SUPER TITAN (mix)
Coating	Galvanized	Unknown	Galvanized
Lubrication	A2	Unknown	D / Bitumin Lube

The specific geometric properties of the rope are critical to how it will behave. With ropes being comprised of so many individual wire elements, the combinations are overwhelming. This is why ropes of the same configuration could sometimes behave differently depending on their manufacturer. Table 3.2 and Table 3.3 provide the wire diameters and ultimate tensile strengths of two of the above rope configurations. Specific data such as wire diameters and ultimate tensile strengths for the 20mm 6x36WS-IWRC rope was not available so an educated assumption was made where necessary.

Table 3.2 – 20 mm 6x25F-IWRC individual wire properties of outer strand.

Wire Diameter (mm)	Ult. Tensile Strength (N/mm^2)
1.26	2061
0.56	1991
1.36	2202
1.42	2168

Table 3.3 – 77 mm 6x36WS-IWRC individual wire properties of outer strand.

Wire Diameter (mm)	Ult. Tensile Strength (N/mm^2)
4.39	2131
2.73	2114
3.53	2113
3.62	2082
4.81	2064

As explained in section 3.1.4, the actual stress-strain relationship is what is needed to differentiate the behavior between wires of different layers. Without conducting actual tests on the individual wires, this data cannot be obtained. To overcome this, the stress-strain relationship described by Figure 3.6 is combined with the data in the tables above and used as input for the analytical model.

3.2.2 Force distribution in individual wires

The wire stresses arising from axial loading to the rope are an important aspect of its failure mechanism. Observing how the wires are stressed within each layer can provide better insight into how the loading is distributed throughout the cross-section. The following figures illustrate exactly this phenomenon for each of the wire rope configurations and sizes in question. The parameter S/d^2 refers to the axial loading on the rope divided by the square of the nominal rope diameter.

$$\frac{S}{d^2} = 50\ N/mm^2$$

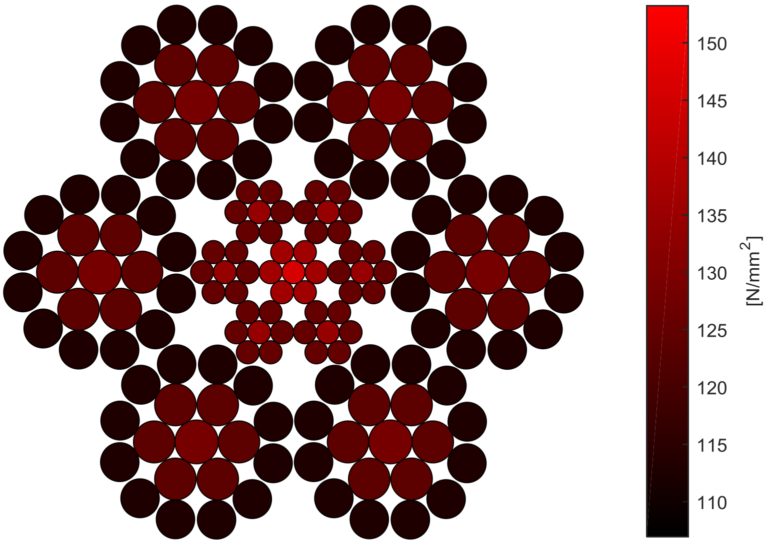

Figure 3.7 – Wire axial stress distribution of 20 mm 6x25F-IWRC rope.

Figure 3.7 and Figure 3.8 represent the wire stress distribution for the two different 20 mm rope configurations. The first point to note is that the core strands experience higher stresses than the outer strands for both configurations. However, the range of stresses is higher for the 6x36WS sling than the 6x25F sling. Both of these observations fall in line with the predicted relationship discussed in Section 2.3.1. As show in Figure 2.13, the stress in the core wire increases while the stress in the outer wires/strands decreases as the helix angle is introduced. Additionally, this difference in stress becomes more pronounced the higher the lay angle. Since the strand lay angle in the 6x36 sling is higher, the core accumulates more stress since the outer wires/strands contribute less to the axial stiffness.

$$\frac{S}{d^2} = 50\ N/mm^2$$

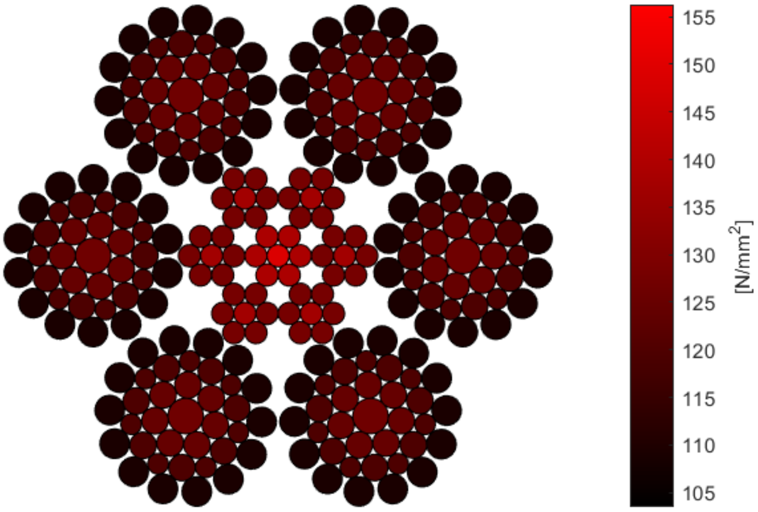

Figure 3.8 - Wire axial stress distribution of 20 mm 6x36WS-IWRC rope.

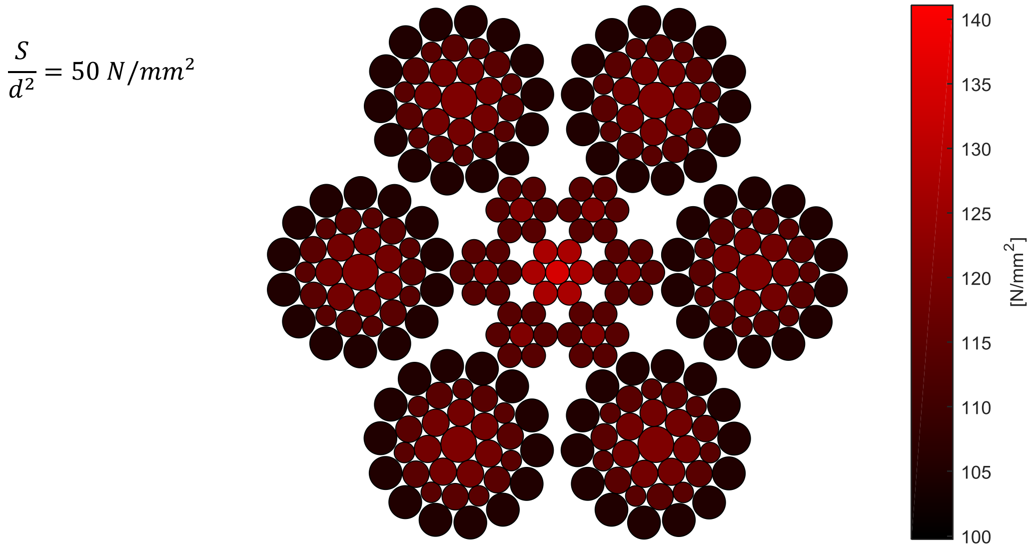

Figure 3.9 - Wire axial stress distribution of 77 mm 6x36WS-IWRC rope.

It is interesting to also compare the results of the small and large diameter 6x36WS-IWRC ropes. Although the configurations are the same, there is a notable difference in how the axial stresses are redistributed throughout the cross section. Again, this is heavily influenced by the lay angle of the strands and wires. The 77 mm rope has a smaller strand lay angle than the 20 mm rope. This influence is reflected in Figure 3.9 where the range of stresses is smaller since the outer strands contribute to more of the axial stiffness due to the smaller lay angle.

3.2.3 Bending reduction factor

The reduction in capacity (R) is calculated as

$$R = 1 - \frac{F_b}{2F_m} \tag{29}$$

where F_b is the measured break load of the bent test and F_m is the measured break load of the proof load tests. Both F_b and F_m are calculated in the model analytically through the use of the failure criteria described in the previous section. Figure 3.10 represents this reduction in capacity calculation for the three different ropes of interest. As a reference, the corresponding formulas imposed in the DNVGL and IMCA standards are also plotted.

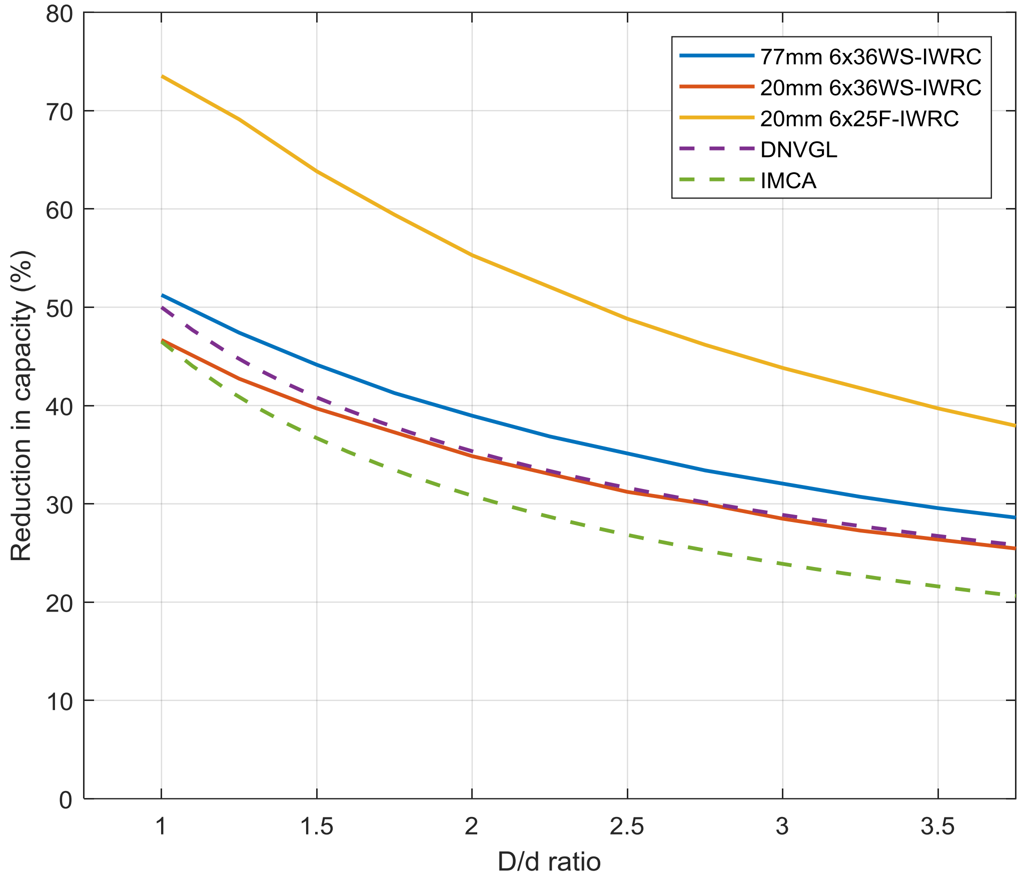

Figure 3.10 - Analytical prediction of reduction in capacity due to bending of different rope configurations.

From the figure, it can be seen that the reduction in capacity is different for each rope configuration. Since bending strain plays a major role in the model, it is the governing parameter that causes this difference. A reason the 20 mm 6x25F rope has such a high reduction in capacity compared to the others is because it has both a smaller lay angle and relatively larger wire-to-rope diameter ratios. These two factors are theorized to reduce the capacity of the individual wires and consequently the rope. The main difference between the two 6x36WS configurations is that the 77 mm diameter rope has a smaller lay angle, which ultimately causes it to have higher bending strains due to the larger change in curvature of wires during bending.

To see the effects of these selected parameters, a sensitivity study was done based on the 77 mm 6x36WS-IWRC configuration. First, the influence of the lay angle on the reduction in capacity is plotted by Figure 3.11 for three different *D/d* ratios. The results shown here exhibit behavior previously discussed in 2.3. The most evident observation is the increase in capacity as the lay angle increases. This is mainly due to the fact that the bending strains decrease as the helical lay angle increases. Additionally, the influence of the *D/d* ratio on the capacity reduces as the curvature of the rope increases.

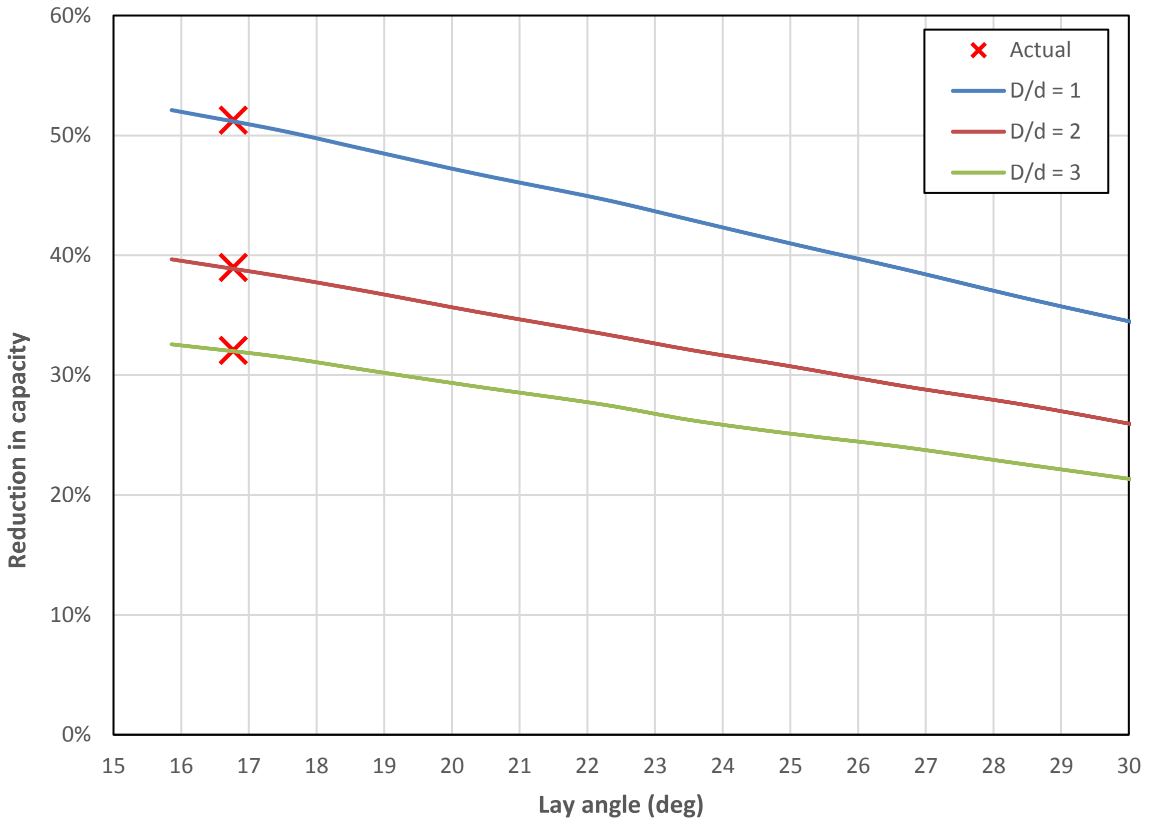

Figure 3.11 - Reduction in capacity based on outer strand lay angle of 77 mm 6x36WS-IWRC rope.

Another important parameter that was identified was the ratio between outer strand wire diameters relative to the nominal rope diameter. Based on solid mechanics, the bending strain of a cross section increases linearly with the distance from the neutral axis. Hence, the larger the wire diameter, the greater the distance to the extreme fiber. Consequently, the bending strains become higher resulting in a higher reduction in capacity. One way to observe this phenomenon is by isolating its effect on the bending strains. To do this, the three different rope geometries were set to have the same lay angle (20°) and the reduction in capacity was calculated by the analytical model. As seen in Table 3.4, both 6x36WS-IWRC ropes exhibit very similar reductions while the 6x25F-IWRC rope is still significantly higher. The reason for this is because the 6x25F-IWRC rope has one less layer in its outer strands which means it needs larger wire diameters in order to achieve the same rope size as a 6x36WS-IWRC rope.

Table 3.4 - Capacity reduction when identical outer strand lay angle is used for all rope types.

Rope Type	Lay angle	Reduction in capacity (D/d=1)
20 mm 6x25F-IWRC	20°	69%
20 mm 6x36WS-IWRC	20°	48%
77 mm 6x36WS-IWRC	20°	47%

Through isolation of the selected parameters discussed above, several insights have been discovered about the differences in capacity reductions between ropes of different geometries. The main difference that separates the reductions of the 6x36WS-IWRC ropes is the lay angle. The outer strand wire diameters scale relatively linearly with the rope size so any difference due to wire diameter ratios is almost negligible. For the 6x25F-IWRC rope, both the lay angle and larger wire diameter ratio are the main contributors to the much higher reduction in capacity.

An additional sensitivity study was done on a different type of user input. The parameters previously investigated are usually known because they are part of the rope's geometric configuration. However, this is not always the case. For instance, the coefficient of friction is also a user input, but the value of this property is not so easily identified. As discussed previously, ropes are heavily lubricated during manufacturing in order to reduce friction between wires so they can more easily shift relative to each other. Although this concept has been proven effective, it is hard to justify that the lubrication uniformly affects the wire interactions throughout the entire rope. Hence, there will be some variation of this friction value. To explore how this effects the reduction in capacity, Figure 3.12 was created for the 77 mm 6x36WS-IWRC rope.

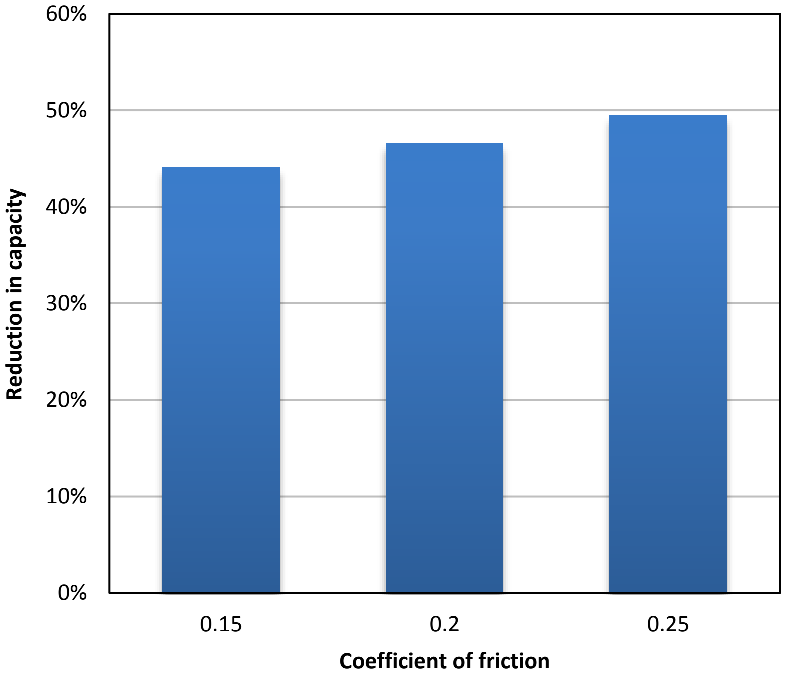

Figure 3.12 - Sensitivity study of reduction in capacity due to change in friction of a 77 mm 6x36WS-IWRC rope with D/d=1.5.

The plot above shows that as the coefficient of friction increases, the reduction in capacity also increases in a relatively linear fashion. Since this analytical model assumes Coulomb friction, a higher coefficient of friction means that a higher friction force will be generated from the same normal force. Consequently, the wires need to overcome this higher friction force in order to shift thus increasing stresses and ultimately reducing the rope performance. Since a coefficient of 0.25 is close to that of steel-on-steel contact, the more realistic values range between 0.15-0.2 for lubricated ropes. In this range, the difference between capacities is not insignificant, but it still relatively small nonetheless.

4.0 EXPERIMENTS

In addition to the analytical model, experiments were conducted on steel wire rope slings. The goal of the experiments is to test the actual capacity of slings in large curvature bending and to validate the proposed analytical model. Two different types of experiments were conducted. First, small-scale tests were carried out on 20 mm steel wire rope slings. Then, a full-scale experiment was carried out on 77 mm steel wire rope slings. The results of each experiment were then processed and several observations were highlighted.

4.1 SMALL-SCALE EXPERIMENT

The small-scale experiment is done on 20 mm 6x25F-IWRC steel wire rope slings. The goal of these tests is to determine the reduction in capacity due to bending for small-scale (20 mm) slings. The different setups of the whole experiment are explained first followed by the major results and observations. More detailed drawings of the test setups can be found in Appendix B. A short additional study on the ovalization phenomenon was also incorporated into these experiments. The setup and custom test bench pieces were based on designs by de Jong [37]. All tests were performed using a 60-ton universal tensile testing machine inside Stevin Lab II located in the Delft University of Technology (Figure 4.1). The loading was controlled by displacement for all tests.

Figure 4.1 - 60-ton tensile testing machine used during small-scale experiment.

4.1.1 Setup #1 – Proof load test

The slings had to first be proof tested to determine their actual breaking capacity. Depending on the rope configuration and manufacturer, this can be up to 15% higher than the MBL [5]. Hence, it is important to know the actual capacity so that the reduction can be accurately calculated later. Figure 4.2 illustrates the loading scenario of the slings and Table 4.1 describes the specimens that were tested.

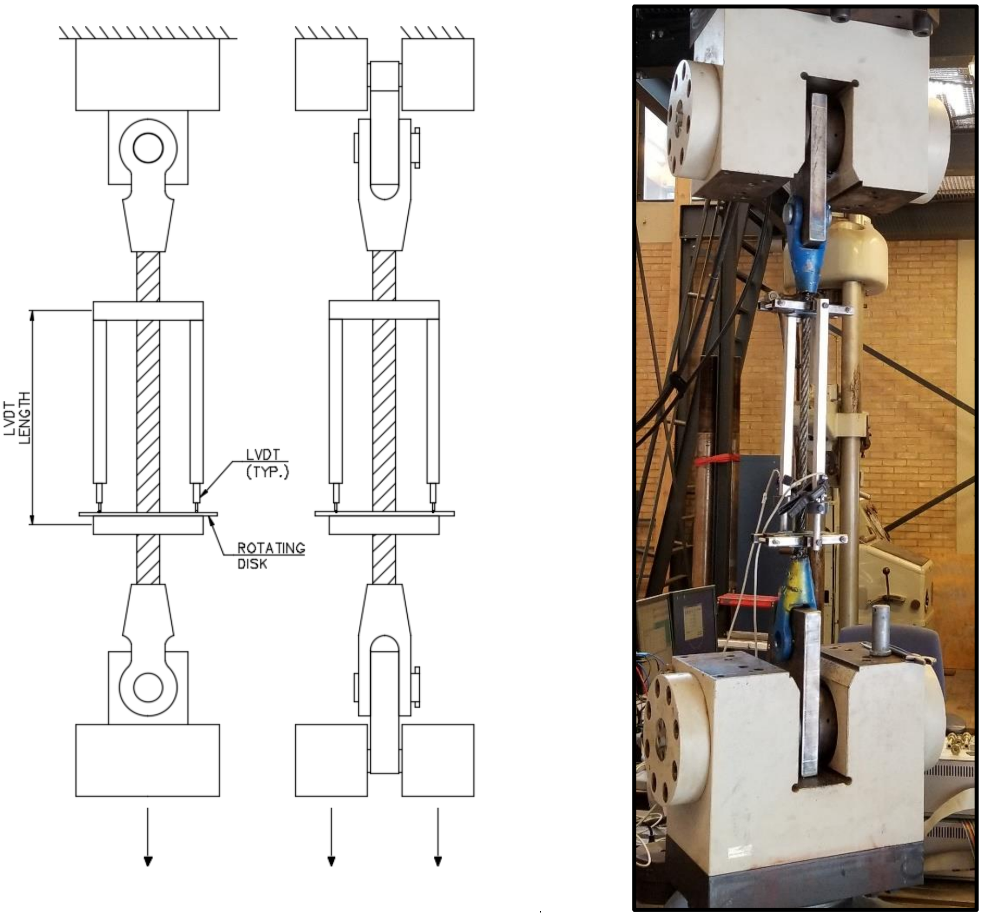

Figure 4.2 – Proof load test setup for small-scale experiment.

Besides obtaining the breaking load, capturing the load-deformation behavior was also of interest. The test bench automatically records and outputs this behavior. However, this recording includes possible displacements from components other than the actual rope, which can introduce error. To see if this is significant, another measuring technique was applied that directly measured the rope elongation. This system consisted of two linear variable differential transformer (LVDT) devices attached as shown in Figure 4.2. One difficulty with this setup is that as the rope elongates, there is a significant twist. To overcome this, a circular disk was attached to the bottom clamp, which provides a level reference plane for the LVDTs even when the rope is twisting. Afterwards, the data from the sensors is averaged in order to come up with the actual elongation of the rope. In the end, the load-deformation behavior was recorded by both machine and sensors and then compared.

Table 4.1 - Description of small-scale proof load test slings.

Sample #	Rope Type	MBL (kN)	Rope Length (mm)	LVDT Measurement Length (mm)
P1	20 mm 6x25F-IWRC	279	600	525
P2	20 mm 6x25F-IWRC	279	600	530
P3	20 mm 6x25F-IWRC	279	600	538

4.1.2 Results of proof load test

The proof load tests of the 20 mm 6x25F-IWRC samples were successfully completed. To eliminate the initial settlement of wires, all samples were subjected to a loading cycle up to 10% MBL (30 kN) and back down to zero before the final loading cycle until failure. Table 4.2 provides a summary of the main parameters of interest. Several obscurities were observed such as the difference in strain between the machine and sensors as well as a premature failure of sample P3.

Table 4.2 - Summary of proof load test for 20 mm 6x25F-IWRC slings.

Sample	Break force (kN)	Machine elongation	Sensor elongation	Comments
P1	326	0.0548	0.0374	Clean break (x = 200 mm)
P2	324	0.054	0.0357	Clean break (x = 200 mm)
P3	313	0.0512	0.0276	Outer strand slipped out of socket

First, it is important to discuss what is defined as a clean break. According to ISO 10425:2003(E), a clean break means that the estimated origin of rupture is a certain distance away from the end termination defined as

$$x \geq 6d_r \tag{30}$$

where d_r is the rope diameter. Both Samples P1 & P2 broke approximately 200 mm away from the nearest end termination, which constitutes a clean break. However, Sample P3 experienced premature failure as one of the outer strands failed at the socket end termination. Even though Sample P3 failed at a load higher than the MBL, it was disregarded when performing a statistical analysis.

The actual breaking load was between 13-16% higher than the MBL provided by the manufacturer. As explained previously, this is within the expected range predicted by literature.

Figure 4.3 provides the load-elongation curve of Sample P2. Figures for all samples can be found in Appendix C. The different curves represent the outputs from the machine and the two LVDT devices. All curves show the three distinct regions that were described in 2.2.2. The initial settlement of wires can be seen from the first loading cycle up to 10% MBL. Then, the elastic region can be defined by the linear relationship followed by a transition into the plastic region where the rope elongates until failure with only a small increase in force. Additionally, the small drops in force seen in the plastic region correlate to the wire breaks that occur as the rope shows signs of reaching failure.

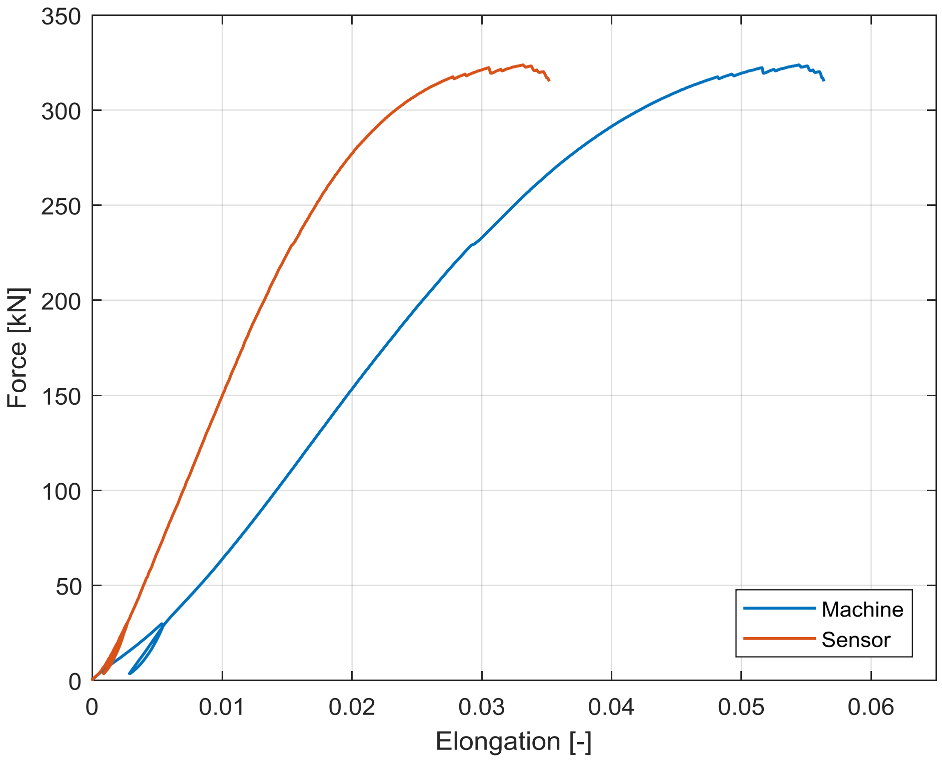

Figure 4.3 - Load-elongation curves of Sample P2 from test bench and LVDT output.

A significant difference between the machine elongation and sensor elongation was observed. The machine strain was between 1.7-2.2% higher throughout the tests. This can usually be attributed to the additional displacements introduced by the test setup and the internal slippage of the machine components. Possible sources of error include rope pullout from the sockets as well as elastic deformation of the components in the test assembly.

4.1.3 Setup #2 – Bending test

After the proof load capacity of the slings was determined, the slings were then subjected to loading under bent conditions. Figure 4.4 provides a general illustration of the loadcase and corresponding setup. The rope is doubled up around a circular pin and has both of its end terminations attached to the upper block of the testing machine. This setup is meant to mimic the body of a sling being bent around a load bearing element such as a shackle.

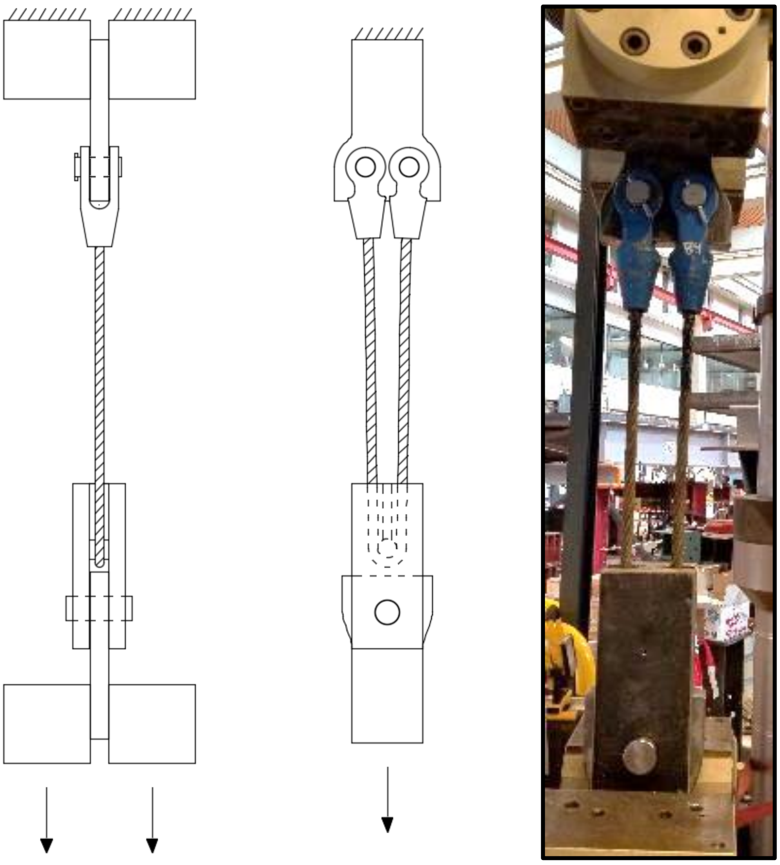

Figure 4.4 - Bending test setup for small-scale experiment.

To make a proper comparison with the DNVGL standard, the relationship between capacity and *D/d* ratio needs to be observed. For slings used in practical applications by Allseas, the most interesting *D/d* ratios ranged from *D/d*=1.33-1.55. Consequently, three different *D/d* ratio were chosen in the vicinity of this specified range. This was achieved by varying the diameter of the circular pin where the rope is bent. A summary of the test samples is given by Table 4.3.

Table 4.3 - Description of test samples for bending test.

Rope Type	Diameter (mm)	# of Samples	Total Length (mm)	D/d
6x25F-IWRC	20	3	1200	1
6x25F-IWRC	20	3	1200	1.5
6x25F-IWRC	20	3	1200	2

Additional measurement techniques were applied in an attempt to capture the behavior of individual wires during bending. First, random samples were spray-painted white around the area of the bend while the rope was in a straight position. This allows for better color contrast during video recording and also marks the starting location of the outside wires and strands before bending. Then, a thin black line was painted around the circumference of the rope at a location near the bend while the rope is still straight. Measurements and images of this area were recorded at several stages of the experiment and later compared. The idea behind these techniques is trying to observe the relative shifting between wires during bending. If the wires do have some relative displacement, then this will cause the black strip to be misaligned along the diameter of the rope. Additionally, if the width of the black stripe changes, this can also give an estimate of the strains experienced by the outer fiber of the outside wires.

4.1.4 Results of bending test

The loading scheme for the bending tests was similar to the proof load tests. First, a loading cycle up to 10% MBL (30kN) was introduced to eliminate the initial settlement of wires. The following load cycle loaded the rope until failure starting from zero. Additionally, a pretension of 6 kN was initially applied before the first load cycle to install the rope and achieve the setup illustrated by Figure 4.4. With the nominal breaking capacity of the rope determined, a comparison was made with the results of the bending test to come up with the reduction in capacity due to bending. Table 4.4 summarizes the main results obtained from these experiments.

Table 4.4 - Summary of bending test for 20 mm 6x25F-IWRC slings.

Sample	D/d	Break load [kN]	Machine elongation [-]	Capacity Reduction
B1	1	373.3	0.0383	42.6%
B2	1	366.2	0.0352	43.7%
B3	1	365.2	0.0392	43.8%
B4	1.5	376.8	0.0354	42.0%
B5	1.5	346.3	0.0283	46.7%
B6	1.5	339.6	0.0285	47.8%
B7	2	357.9	0.0298	44.9%
B8	2	380.5	0.0297	41.5%
B9	2	386.6	0.0302	40.5%

The capacity reduction due to bending is plotted and shown in Figure 4.5. Comparing the results with both the DNVGL and IMCA standard, the experimental values generally show that the reduction in capacity is higher than predicted.

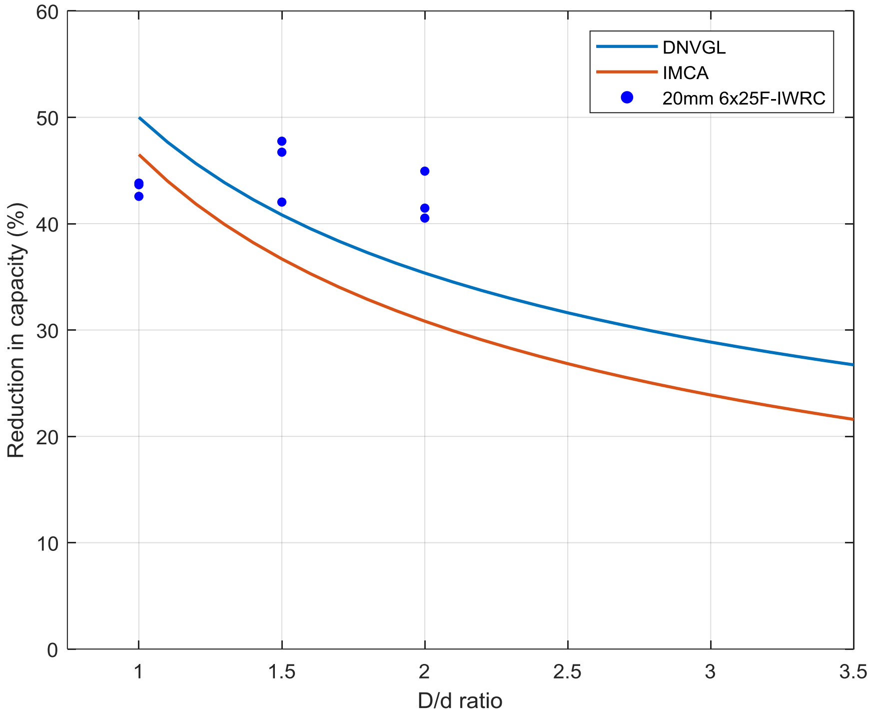

Figure 4.5 - Reduction in capacity due to bending of 20 mm 6x25F-IWRC slings.

Figure 4.6 shows the load-elongation curves of the samples tested with a *D/d*=2 setup. Graphs for all samples can be found in Appendix C. Samples B8 & B9 exhibited almost identical behavior and break load while Sample B7 differed slightly due to its lower break load. Interestingly, the relatively gradual slope usually characteristic of the initial settlement region can still be seen even after application of the first loading cycle. This is because this region correlates to the loading applied as the rope is fully conforming around the pin. As this process develops, the elastic region becomes clearer until it becomes the governing relationship almost all the way up until failure. It is interesting to note that the plastic region for all samples is significantly small compared to what is expected from typical rope failure.

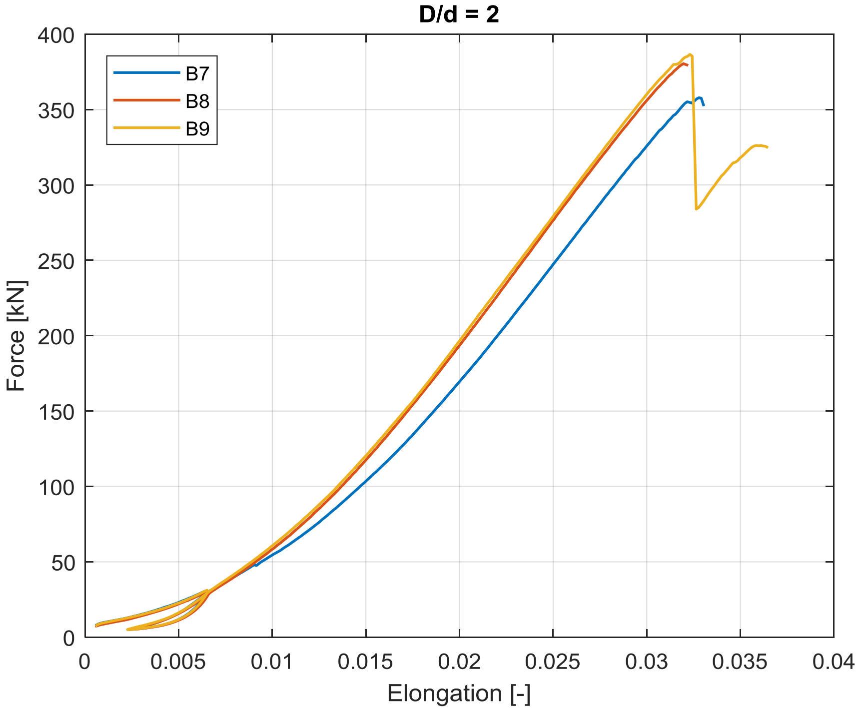

Figure 4.6 - Load-elongation curves of 20 mm 6x25F-IWRC samples tested using a D/d=2.

The additional measurement techniques applied during this experiment proved to yield some interesting observations. For instance, the relative shifting of wires was confirmed using the thin line painted around the circumference of a rope cross section. Illustrated in Figure 4.7a, the initial painting of the line marks the position of the strands before the rope is bent. Then, Figure 4.7b shows the position of the line after the rope has been installed onto the test bench with a pretension of about 3% of MBL. Here, it can be clearly seen that the strands have shifted relative to each other in the bending process.

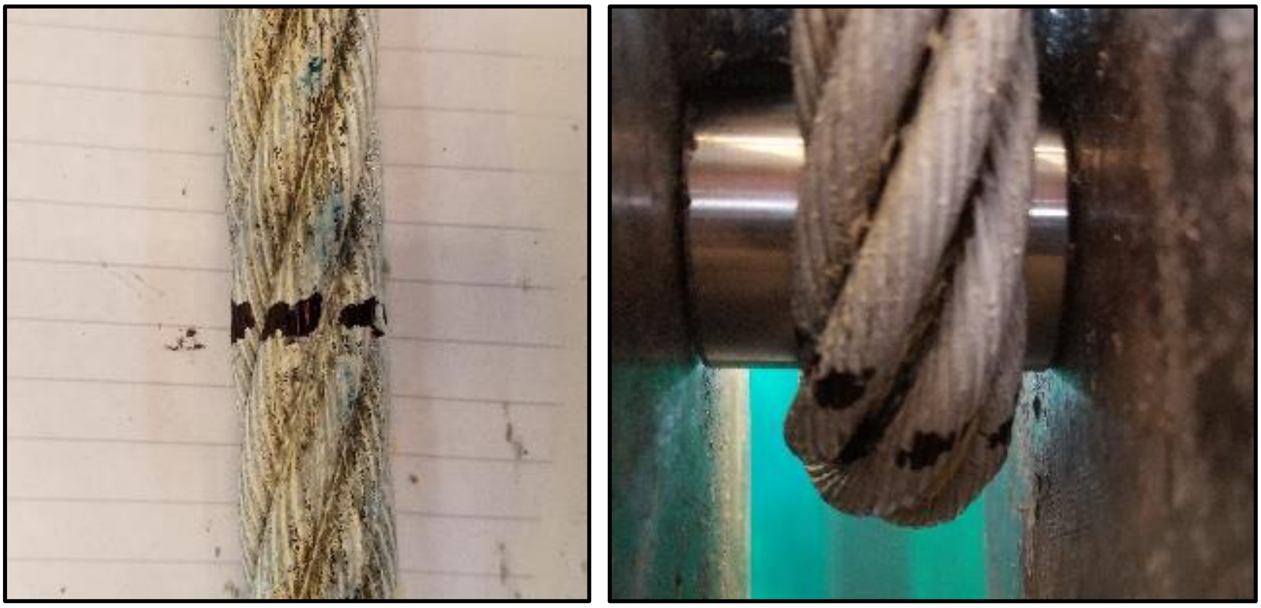

Figure 4.7 - Line marker before bending (a). Line marker after bending and pretension (b).

The white spray paint also provided some interesting insights. As the rope was being loaded, some of the outer strands begin twisting due to the torque produced from elongation. This became clearly evident since the white spray paint was only applied to the outer half of the strand. Therefore, as the strands started twisting, the unpainted portion became visible. This phenomenon is best observed with video, but Figure 4.8 also provides a good example of the difference before and after loading is applied.

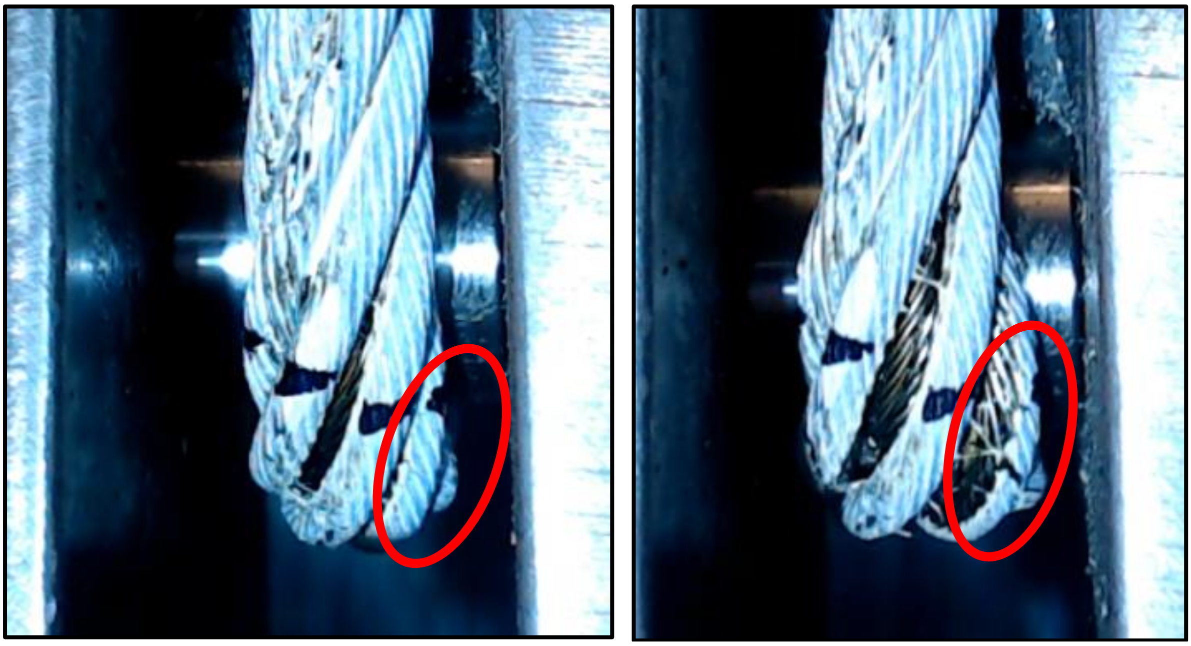

Figure 4.8 – Change in positioning of select strands at start and end of loading.

One of the clearest observations was the ovalization phenomenon. As explained in Section 2.3, the rope cross section starts to take an oval shape as it tries to conform around the shape of the pin due to the applied loading. Figure 4.9 clearly illustates the drastic change in the rope cross section before and after loading is applied.

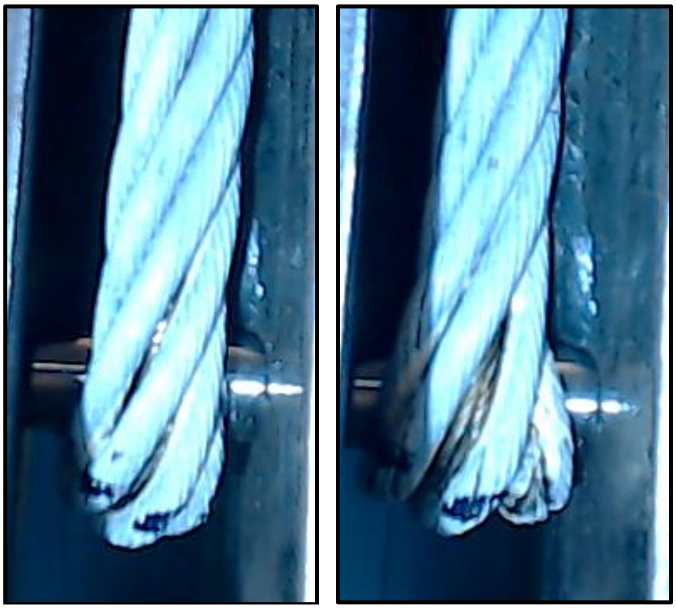

Figure 4.9 - Ovalization of rope before and after loading is applied.

Perhaps one of the most intriguing observations was that the origin of rope failure was more or less the same for all specimens, regardless of *D/d* ratio. The location where rupture occurred was consistently traced back to the strands illustrated by the callout in Figure 4.8. These rightmost strands were almost always the first to rupture in all samples.

4.1.5 Additional study

Given the results found in the bending test, it was decided that a study on the ovalization of the wire rope could also yield interesting insights. As the rope conforms around the curvature of the pin, it also wants to conform to the shape of the pin in the direction perpendicular to the rope axis. The question posed is how would the results be affected if the rope were to be constrained in the perpendicular direction to prevent the rope from ovalizing? To test this, Figure 4.10 shows how the bending setup had to be modified by inserting two spacer plates near the rope bend in order to prevent ovalization. The distance between the two spacer plates was approximately 24 mm.

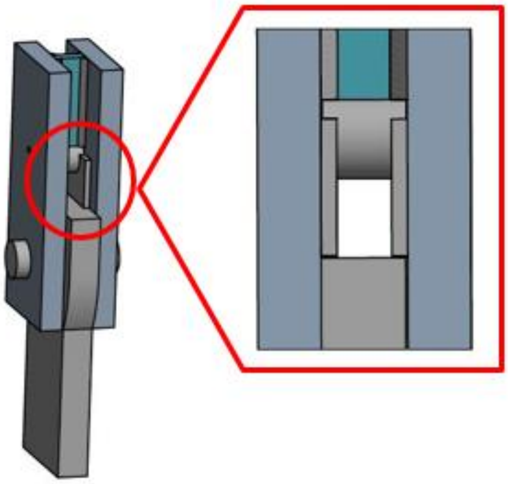

Figure 4.10 – Bending setup modification for ovalization study.

Table 4.5 provides a list of the samples that were used in this study. The 20 mm 6x36WS-IWRC-x rope type naming convention is used to differentiate this rope from the one used in [37] since their geometric properties are slightly different and they are made by different manufacturers. The first three samples were tested in the same bending setup as described in 4.1.3, while the last three samples were tested with the modification applied. The reason this rope type was chosen for this study was because it has a lay angle that is almost identical to the 6x25F-IWRC rope. Hence, the results could also be used to directly compare the two configurations by keeping the lay angle constant.

Table 4.5 – Description of test samples used in the additional study.

Rope Type	Diameter (mm)	# of Samples	Total Length (mm)	D/d	Setup Type
6x36WS-IWRC-x	20	3	1200	2	Original
6x36WS-IWRC-x	20	3	1200	2	Modified

The results of the additional study are summarized by Table 4.6. The reduction in capacity was calculated using Equation (29). The measured proof load used in the calculation was assumed to be the same as the results obtained from the 6x25F-IWRC tests. The certificates of both ropes provided by the manufacturer indicated that the difference between the two certified measured proof loads was negligible. More information about the properties of the 6x36WS-IWRC-x rope as well as the load-elongation curves can be found in Appendix D.

Table 4.6 - Summary of experimental results from additional study.

Sample	Setup	Capacity reduction	Avg. capacity reduction
C1	Original	38.2%	37.4%
C2	Original	35.5%	
C3	Original	38.6%	
C4	Modified	34.5%	36.0%
C5	Modified	37.2%	
C6	Modified	36.4%	

Generally, the results show that, based on the samples tested, the modification slightly improved sling capacity by 1.4% on average. Although this difference is small, it is important to note that the setup did not technically fully restrain the rope from ovalizing.

Using the observations obtained from the original experiments, special attention was put on the origin of failure. Figure 4.11 shows a before and after failure image of one of the samples. The origin was previously identified to consistently fail at a certain location indicated by the black mark in the before image. Looking at the after image in combination with video, it was quite apparent that the marked strand was indeed the first to fail. This technique was applied to a majority of the samples and the relationship consistently stayed true.

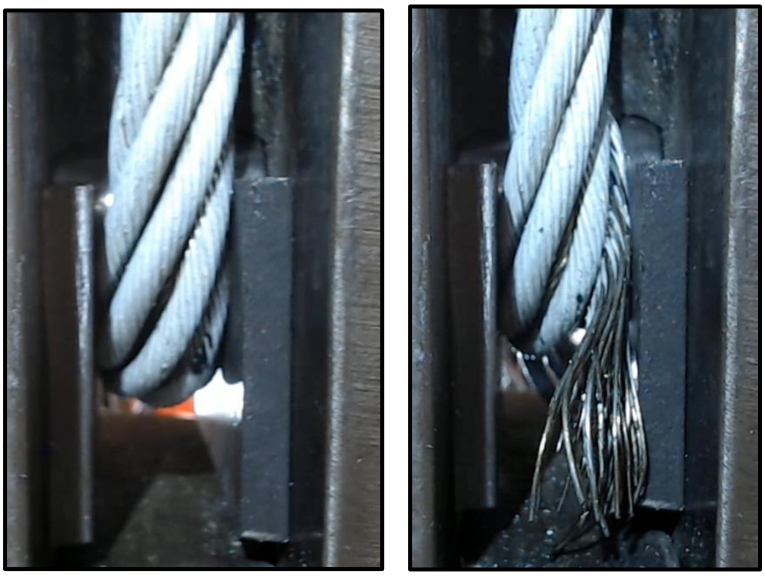

Figure 4.11 - Before (left) and after (right) image of marked failure location technique.

4.1.6 Statistical analysis

A brief statistical analysis was conducted on the results of the small-scale experiment. It is important to note that the data obtained should be considered as a small sample of a much larger population. The statistical values calculated here may deviate from those of the actual population, however, they are accurate enough to draw reasonable trends and conclusions.

Table 4.7 provides a summary of the statistical values concerning the proof load test. As mentioned previously, Sample P3 was omitted due to the premature failure mode of the rope. Overall, the remaining two samples exhibited consistent failure characteristics with very little deviations.

Table 4.7 - Summary of statistical values for 20 mm 6x25F-IWRC proof load test.

Sample	Break load [kN]	Machine elongation	Sensor elongation
P1	326	0.0548	0.0374
P2	324	0.0540	0.0357
Average	**325**	**0.0544**	**0.0366**

Using the three samples per *D/d* ratio, several statistical parameters were derived from the data obtained from the bending test. Table 4.8 provides a summary of each statistical variable calculated for the three different *D/d* ratios. A 95% confidence interval (t-test) was constructed to give a relative idea of the range of capacity reductions based on the experimental data.

Table 4.8 - Statistical summary of capacity reduction due to bending for 20 mm 6x25F-IWRC slings.

	D/d = 1	D/d = 1.5	D/d = 2
Average	43.3%	45.5%	42.3%
Sample standard deviation	0.7%	3.1%	2.3%
95% Confidence interval (+)	45.0%	53.1%	48.1%
95% Confidence interval (-)	41.7%	37.9%	36.5%

Figure 4.12 illustrates these statistical findings in comparison with the DNVGL and IMCA formula. The overall behavior as the *D/d* ratio increases shows a smaller reduction in capacity. However, this behavior was not as pronounced as predicted by DNVGL and IMCA standards. Moreover, the average of *D/d*=1 is lower than *D/d*=1.5. This is a rather obscure observation that may be the result of insufficient data points. Perhaps if the number of samples increases, the averages would balance to follow the expected relationship. Nevertheless, the most important observation from this plot is the fact that the majority of samples had a higher capacity reduction than that predicted by both standardization societies.

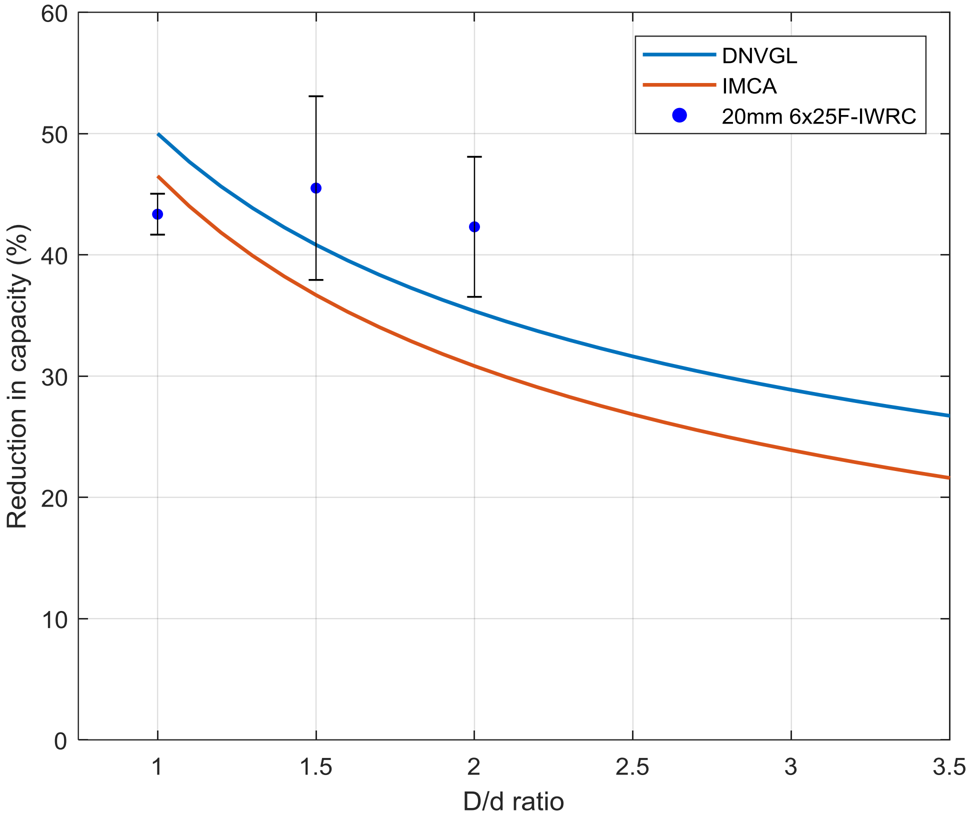

Figure 4.12 - 95% confidence intervals for capacity reduction of 20 mm 6x25F-IWRC sling experimental results.

4.2 FULL-SCALE EXPERIMENT

The full-scale experiment is done on 77 mm 6x36WS-IWRC steel wire rope slings. This experiment is of great significance because one of the main research questions of this thesis is to determine the actual capacity of large diameter slings used in the offshore industry. A total of four tests were conducted. The first tests were used to determine the measured breaking load and the rest tested the sling capacity in a bent configuration. *D/d* ratios of approximately 1.5, 2 and 2.5 were observed. A 1000-ton test bench at the Stevin II Laboratory located in the Delft University of Technology was used to perform all the tests. Custom components had to be designed for the test setups in order to create the desired loadcases.

4.2.1 Setup #1 – Proof load test

Again, the purpose of the proof load test is to determine the actual breaking capacity of the steel wire rope under investigation. The loading scenario is illustrated by Figure 4.13. A more detailed overview of the setup including dimensions can be found in Appendix E. The loading is applied by the hydraulic cylinder which pushes up on the topmost block transferring the force through four pull rods. These four pull rods are attached to a custom padeye block which acts as the anchor point for one end of the sling. On the other end, the sling is restrained via a pin, which transfers the force through custom plates that are rigidly attached to the test bench columns to create a fixed connection point.

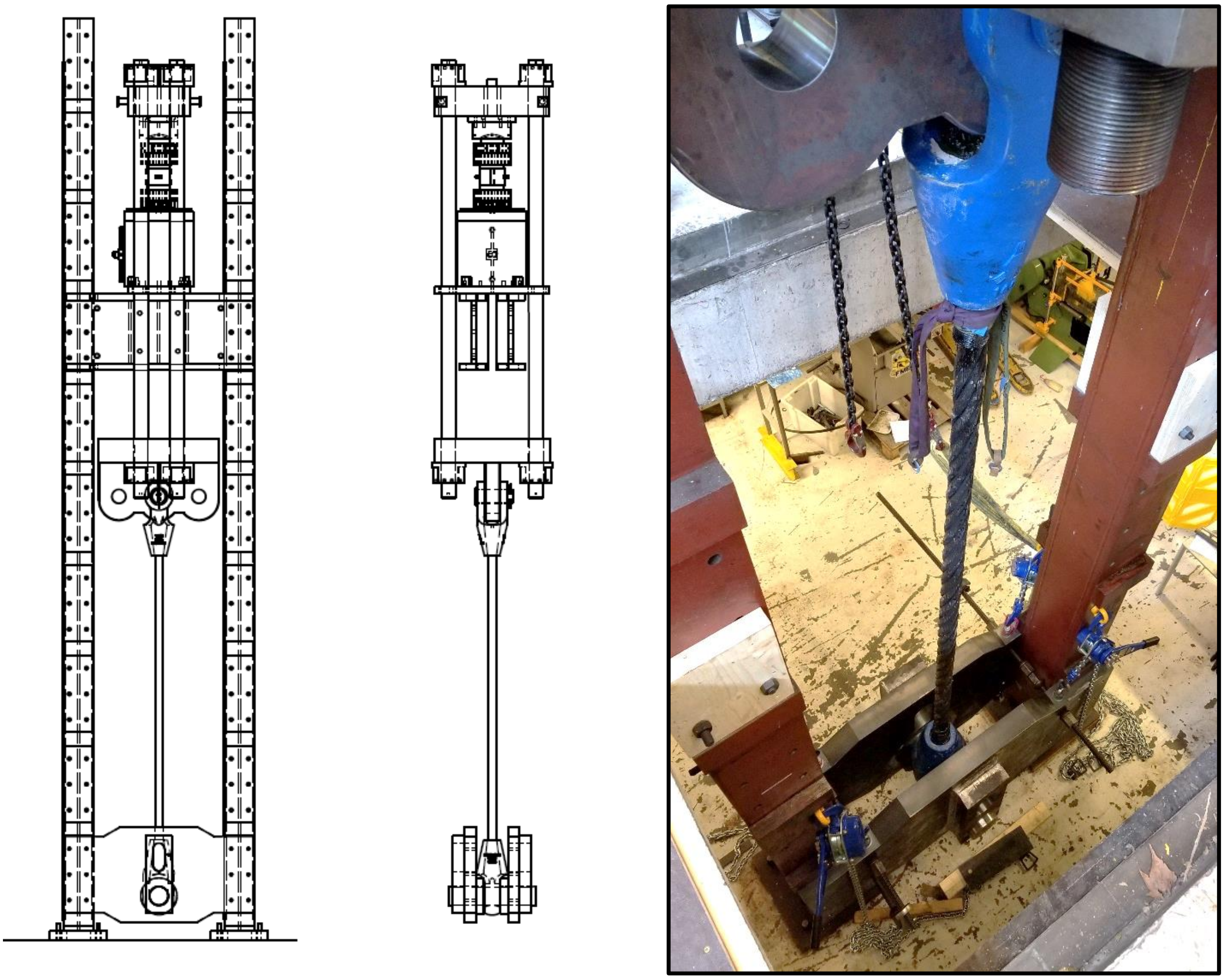

Figure 4.13 - Setup of proof load test for 77 mm 6x36WS-IWRC sling.

The measured breaking load and load-deformation behavior were again the main priority of this test. The machine can provide all this data, however, the actual elongation of the specimen was also checked by attaching LVDT sensors similarly as in the small-scale test. Table 4.9 briefly describes the parameters of the sling tested.

Table 4.9 - Sample description of full-scale proof load test sling.

Parameter	Value
Rope type	77 mm 6x36WS-IWRC
MBL	4751 kN
Rope length	3000 mm
LVDT measurement length	3000 mm
Pre-stretch	10% MBL

4.2.2 Results of proof load test

The proof load test was conducted on one sample of a 77mm 6x36WS-IWRC steel wire rope sling. The main parameters of interest are given in Table 4.10.

Table 4.10 - Summary of proof load test results for 77 mm 6x36WS-IWRC sling.

Parameter	Value
Measured break force	5138.1 kN
Measured elongation at break (machine)	0.0492
Measured elongation at break (sensor)	0.0394
Loading speed	0.175 mm/s

The test followed all requirements set by ISO 10425:2003(E). The break point was estimated to be around 1900 mm from the nearest socket, which constitutes a clean break as described in section 4.1.2. The measured break force was found to be about 8% higher than the MBL, which is within the predicted range of possible values. As expected, the rope did not completely sever in half. Two outer strands remained intact while the rest had total separation. A vast majority of the wires failed in necking with a few wires failing in shear (Figure 4.14a). The core strand also severed completely, which is expected since it usually experiences more stress than the outer strands. Interestingly, many of the wires in the core failed in shear (Figure 4.14b). This can be attributed to the fact that the helical contraction of the outer strands produces a high normal force on the core, which increases the friction and introduces shearing stresses on the wires.

Figure 4.14 - Typical failure mode of outer strand wires due to necking (a) and core wires due to shear (b).

The load-elongation curve illustrated by Figure 4.15 also showed an expected relationship. A relative elongation difference of about 1% was found between the machine and sensor output. Again, this error can be attributed to the elastic deformation of all the components of the test bench. The region where initial settlement occurs is barely noticeable indicating that the preload applied to the rope beforehand was successful. Wire breaks began to occur once the rope entered the plastic region, which can be identified by the small dips in force seen in the plot. This made sense since the rope was loaded for the first time whereas wire breaks can usually be heard earlier during a break test of an older rope.

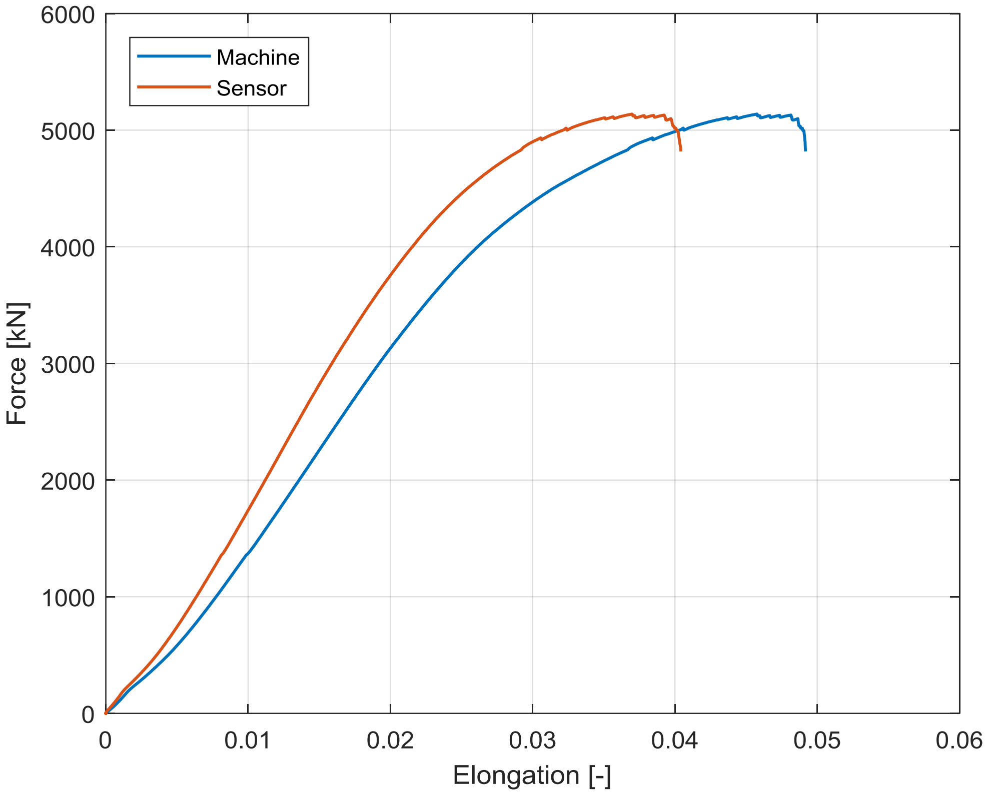

Figure 4.15 - Load-elongation curve of proof load test for 77 mm 6x36Ws-IWRC sling.

4.2.3 Setup #2 – Bending test

The setup for the bending test utilizes the same custom pieces built for the proof load test. The loading scenario is illustrated by Figure 4.16. More detailed information and drawings can be found in Appendix E. To achieve this, the custom plates had to be reoriented and repositioned on the test bench columns. The two sling ends were both attached to the custom padeye block and bent around a custom pin. The shape of the pin resulted from the need to resist the large forces while also achieving the desired *D/d* ratios.

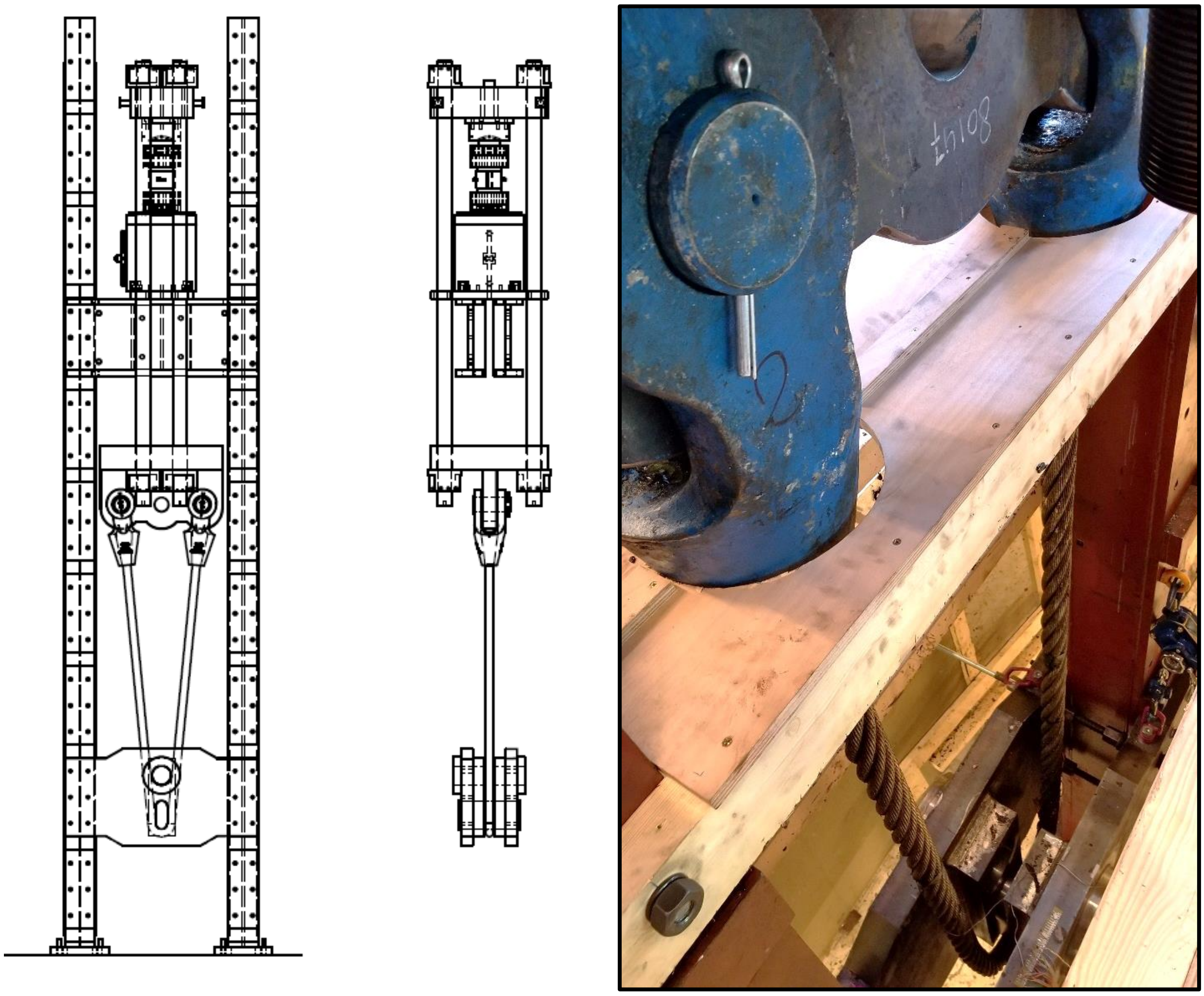

Figure 4.16 - Schematic overview of bending test setup for 77 mm 6x36WS-IWRC slings.

Test setups with different *D/d* ratios were created by utilizing custom-made sleeves. These sleeves are illustrated by Figure 4.17 and are made to fit around the custom pin as shown. Using both the custom pin and custom sleeves, *D/d* ratios of 1.5, 2 and 2.5 were achieved. This differed from the small-scale tests because ratios below 1.5 were difficult to achieve practically in the full-scale setup due to the high forces involved.

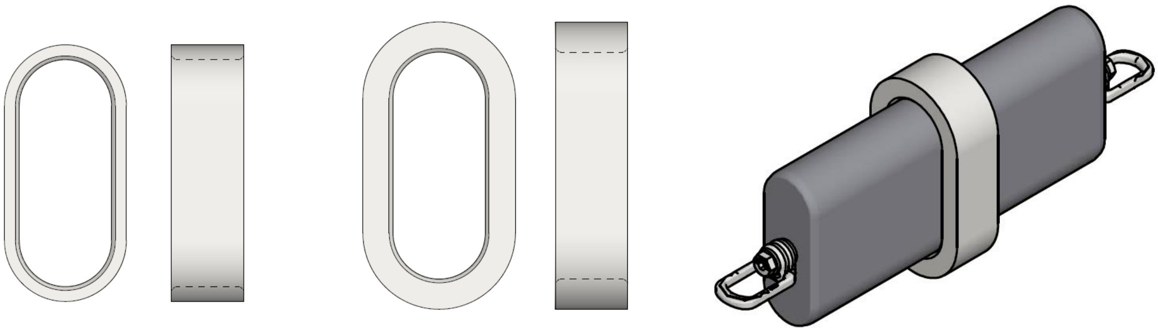

D/d = 2

D/d = 2.5

Figure 4.17 - Custom sleeve pieces used to achieve desired D/d ratios for full-scale bending test.

In addition to the break load, several other measurement techniques were implemented to gain more insight into the behavior of the rope. Using the machine displacement and applied loading, a force-displacement relationship was observed for each sample. In Sample S3 & S4, eight strain gauges were attached at various locations throughout the rope as indicated by the red marks in Figure 4.18. Two strain gauges were attached to arbitrary wires in the west and east leg roughly 125 cm from each socket end and acted as control measurements since wires in that part of the rope experience stresses due to only the axial loading of the rope. Three strain gauges were attached to each side of the bend where wires experience stresses due to bending, contact and axial forces in the rope. The locations of the wires along the cross-section of the rope are illustrated by the figure.

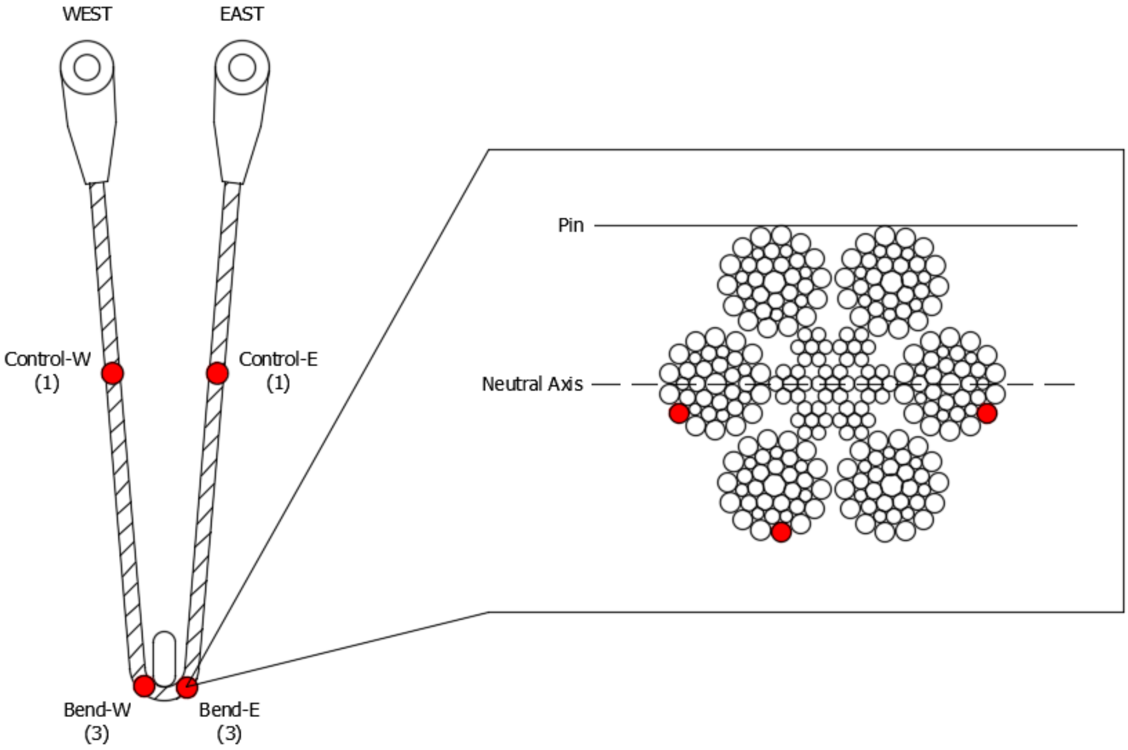

Figure 4.18 - Typical wire strain gauge locations throughout 77 mm 6x36WS-IWRC slings.

In addition to strain gauges, Sample S4 was outfitted with another measurement technique. The six outer strands of the rope were spray painted different colors in the vicinity of the bend as seen in Figure 4.19. The main purpose of this technique is to easily keep track of strand continuity after failure. Typically, several strands completely sever in half near the bend and flail out from their original position making it difficult to match the ends together. However, with the painting technique, the strand ends can be intuitively matched using the corresponding colors.

Figure 4.19 - Spray paint technique applied to outer strands near bend of 77 mm 6x36WS-IWRC sling.

A total of three samples were tested in this bent scenario with three different *D/d* ratios. Table 4.11 provides a description of the samples tested as well as any additional measurement techniques applied.

Table 4.11 - Description of full-scale bending test samples.

Sample	Rope Type	D/d	Rope Length (mm)	Additional Measurement Technique
S2	77mm 6x36WS-IWRC	1.5	5720	-
S3	77mm 6x36WS-IWRC	2	5770	Strain gauges
S4	77mm 6x36WS-IWRC	2.5	5820	Strain gauges, painting

4.2.4 Results of bending test

The results of the bending tests conducted are summarized in Table 4.12. All samples were preloaded up to 10% MBL and bent around a 110 mm radius of curvature by the rope manufacturer before delivery for ease of installation in the test bench at the Delft University of Technology. It is important to note that the test setup constrained the rope from ovalizing to a certain extent. The influence of this was tested in the additional study conducted in the previous chapter (4.1.5). The conclusion was that the influence in performance was negligible so there was no adjustments made to the results presented here.

Table 4.12 - Summary of results from the bending tests conducted on 77 mm 6x36WS-IWRC slings.

Sample	D/d	Break force (kN)	Machine elongation (-)	Reduction in capacity
S2	1.5	5981	0.0427	41.5%
S3	2	6689	0.0439	34.6%
S4	2.5	6802	0.0439	33.6%

Figure 4.20 shows the load-elongation diagrams of each bent sample tested. The measurement for each sample started with a preload of roughly 53 kN. Then, each specimen experienced elongation with a relatively small force applied as the rope was forming around the pin. It can be seen that as the *D/d* ratios increases, the duration of this phenomenon decreases. This is because a higher *D/d* ratio requires less change in rope curvature to fully form around the pin than a lower *D/d* ratio. Additionally, this can also be used to define the region where the change in rope curvature takes place. On average, this change ends between 20-25% of the MBL at which point the rope has taken on the curvature of the pin and begins to elongate elastically as seen in the figure. Observing the jagged lines at the end of the curves, Samples S2 & S4 had a relatively defined plastic region where multiple wire breaks were heard before rupture. On the other hand, Sample S3 had a more brittle behavior with only a few wire breaks before complete failure.

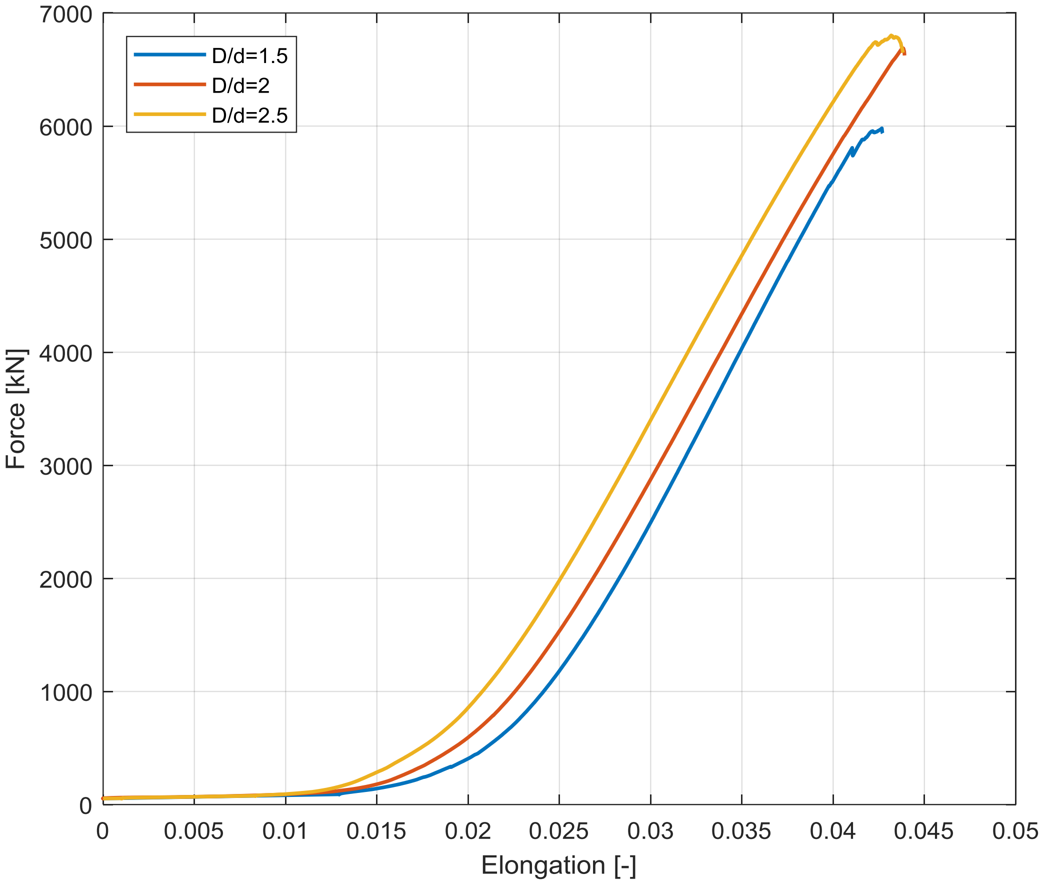

Figure 4.20 - Load-elongation plots for bending tests of 77 mm 6x36WS-IWRC slings.

The failure mode of wires in all samples was predominantly shear. Figure 4.21 displays a typical strand failure after a bending test. The wires near the breaking point are all unwound from their original position due to the large release of force at rupture. It is interesting to note that many wires show signs of shear in combination with cup-and-cone type of failure. This can be expected since the primary forces inside the wires near the rope bend are a combination of tensile, bending and contact.

Figure 4.21 - Typical shear failure mode of wires after full-scale bending test.

The origin of failure was consistent throughout all samples as observed in the small-scale experiment. Although the exact break location is difficult to determine, an educated approximmation yielded reasonable accuracy. The origin of rupture was again consistently observed to happen at the outer strands indicated by the red callout shown in Figure 4.22. The images represent both side views around the rope-pin interaction. Interestingly, these regions also correspond to the rightmost strands of a right hand ordinary lay (RHOL) rope.

Figure 4.22 – West (left) and east (right) elevation views of the rope bending around the pin.

An insight into contact stresses was discovered while observing the rope after failure. As seen in Figure 4.23, there is a pattern of local deformations along wires in an outside strand. This can be directly related to the contact stresses between the core and outer strand wires that results from the helix shape and contact pressure from the pin-rope interaction. Furthermore, the core and outer strands are helically laid in such a way that their wires cross each other causing high local contact stresses. Due to the fact wires in the core are generally smaller than those in the outer strands, they create stress concentrations and cause the local deformations seen in the image. Additionally, these deformations were most prominent near the break location of the wire, indicating that these contact stresses could play a significant role in its failure.

Figure 4.23 - Local contact deformations on outside strand wires of 77 mm 6x36WS-IWRC sling after bending test.

Local contact deformations were also observed on some of the custom pieces made for the test bench. Figure 4.24a shows the damage experienced by the custom pin after testing Sample S2. Here, high concentrated stresses induced by the hardened steel wires have imprinted onto the custom pin. Figure 4.24b displays the custom sleeve after testing Sample S3. The deformation phenomenon due to the steel wires is even more evident in this case. Here, the imprints can be used to distinguish the exact locations of wires and strands in contact with the sleeve. Part of the reason the imprints were so well defined was because the sleeve was made from a lower grade steel than the custom pin. Interestingly, these imprints extended past the bend and up to the straight portion of the sleeve indicating that a full wrap angle of 180° was achieved although the test setup places the rope into a V-shape as seen in Figure 4.16. This can possibly be explained by the fact that the contact area increases as the rope tries to conform around the pin due to the high loading applied.

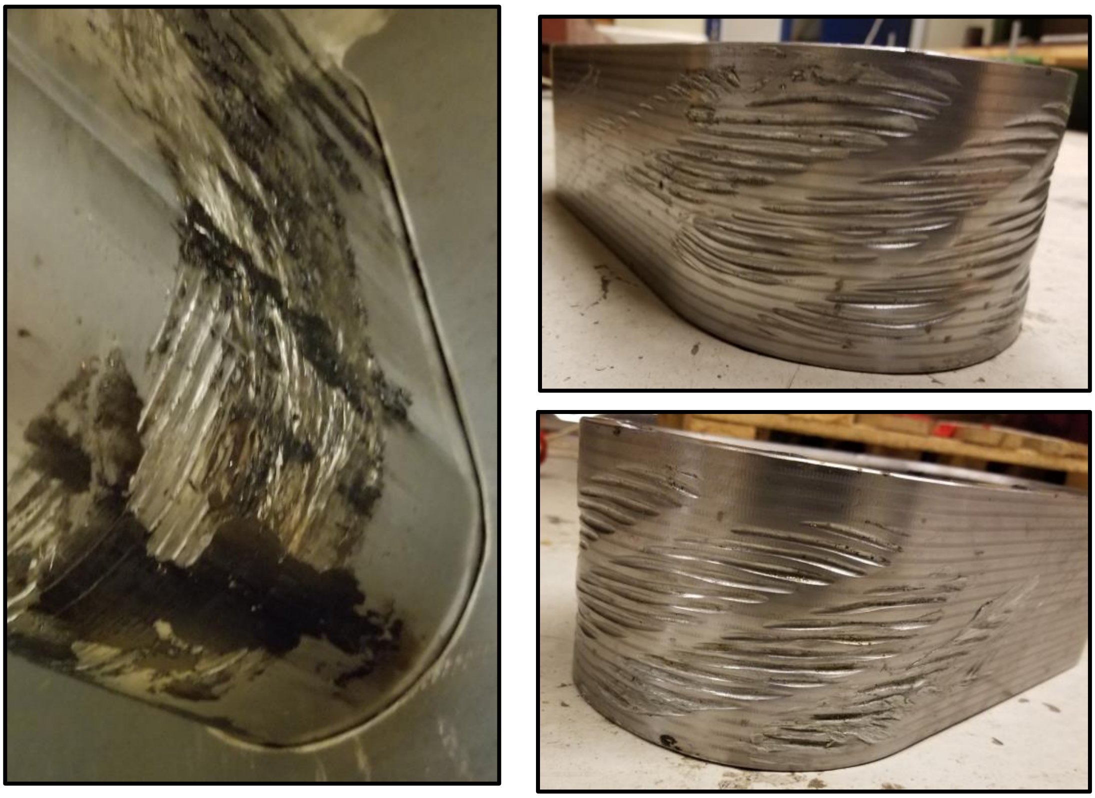

(a) (b)

Figure 4.24 - Local contact deformations due to wires on (a) custom pin and (b) custom sleeve.

5.0 RESULTS AND DISCUSSION

Using the results obtained both analytically and experimentally, a comparison can be made between the two methods. Based on the rope types and sizes of interest as well as the observations found during the experiments, the main relationships that can be discussed are:

- Proof load failure for all rope types;
- Reduction in capacity between all rope types;
- Experimental insights and observations.

5.1 PROOF LOAD FAILURE

The first step in determining the reduction in capacity of the slings is to obtain the actual breaking load of the rope. As discussed previously, these sorts of proof load tests are very common in the industry and are used to come up with the MBL of the rope, which is often used as a design parameter in engineering applications. However, the MBL is a conservative measure and normally not a good indicator of the actual rope capacity. Table 5.1 provides a summary of how the MBL compares to values predicted by the analytical model and the capacities obtained from the experiments.

Table 5.1 - Proof load capacity of rope configurations based on analysis method.

Rope Configuration	MBL	Analytical Model	Experiment	Lay Angle
20 mm 6x25F-IWRC	279 kN	336 kN	325 kN	18°
20 mm 6x36WS-IWRC	279 kN	330 kN	322 kN [37]	20°
77 mm 6x36WS-IWRC	4751 kN	5210 kN	5138 kN	17°

Overall, results showed good correlation to what was expected. The MBL was indeed lower than capacities obtained both analytically and experimentally. Additionally, the analytical model was consistently higher than the measured capacity obtained from experiments. This difference can be explained by the omission of additional coupling stresses due to torsion, bending and shear caused by the helical structure of the rope. The influence of these stresses varies depending on the lay angle as exemplified by Figure 2.25. This conclusion coincides with a study by Chen et al. [38] where it was found that as the lay angle increases, the tensile stiffness decreases and the torsional stiffness increases. Observing the resulting errors, inclusion of these additional stresses should be considered in the analytical model to obtain more accurate predictions.

5.2 REDUCTION IN CAPACITY

Part of the main research question is to investigate how the reduction in capacity due to bending varies with rope configurations of different sizes. This was achieved by considering a 6x36WS-IWRC rope configuration with two different sizes (20 mm & 77 mm) and then calculating the capacity reduction both analytically and experimentally. Figure 5.1 plots the corresponding results and compares them to the expressions recommended by both DNVGL and IMCA standards. The 20 mm 6x36WS-IWRC experimental data with a 95% confidence interval was obtained from previous research [37].

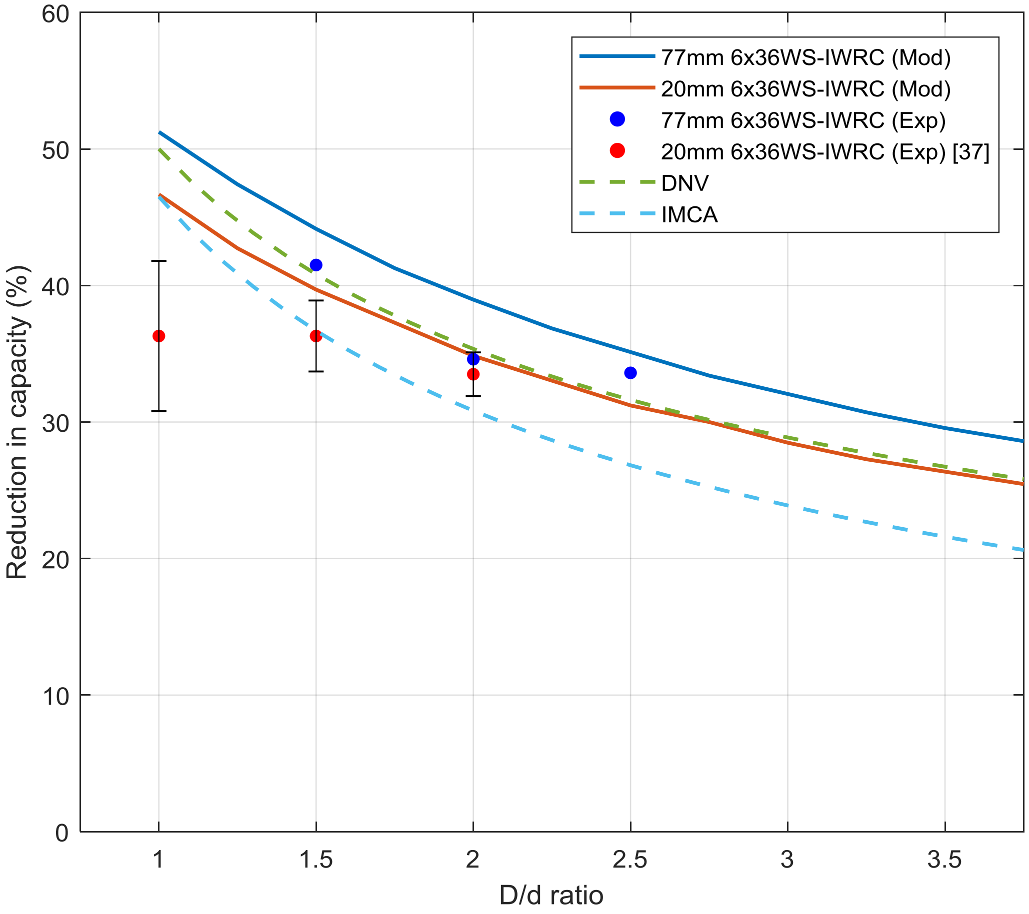

Figure 5.1 - Reduction in capacity comparison based on different rope diameters.

Generally, the results show that the 77 mm rope has a higher reduction in capacity than the 20 mm rope. Referring to the analytical study conducted in 3.2.3, it was deduced that the difference in capacity reduction was mainly due to the outer strand lay angle. The 77 mm rope has a smaller lay angle, which translates to higher bending strains that lower its capacity. The experimental results also follow this relationship when comparing the corresponding *D/d* ratios. With more data points, the relationship can be confirmed with higher confidence.

The other main part of the research question is to discover how the reduction in capacity varies with different rope configurations. In order to investigate this, two different steel wire rope configurations were chosen (6x25F-IWRC & 6x36WS-IWRC) and then the reduction was calculated both analytically and experimentally. Figure 5.2 displays the different capacity reductions and also plots those predicted by DNVGL and IMCA standards. The experimental values displayed in the figure are based on a 95% confidence interval extracted from 4.1.6 (6x25F-IWRC) and previous research (6x36WS-IWRC) [37].

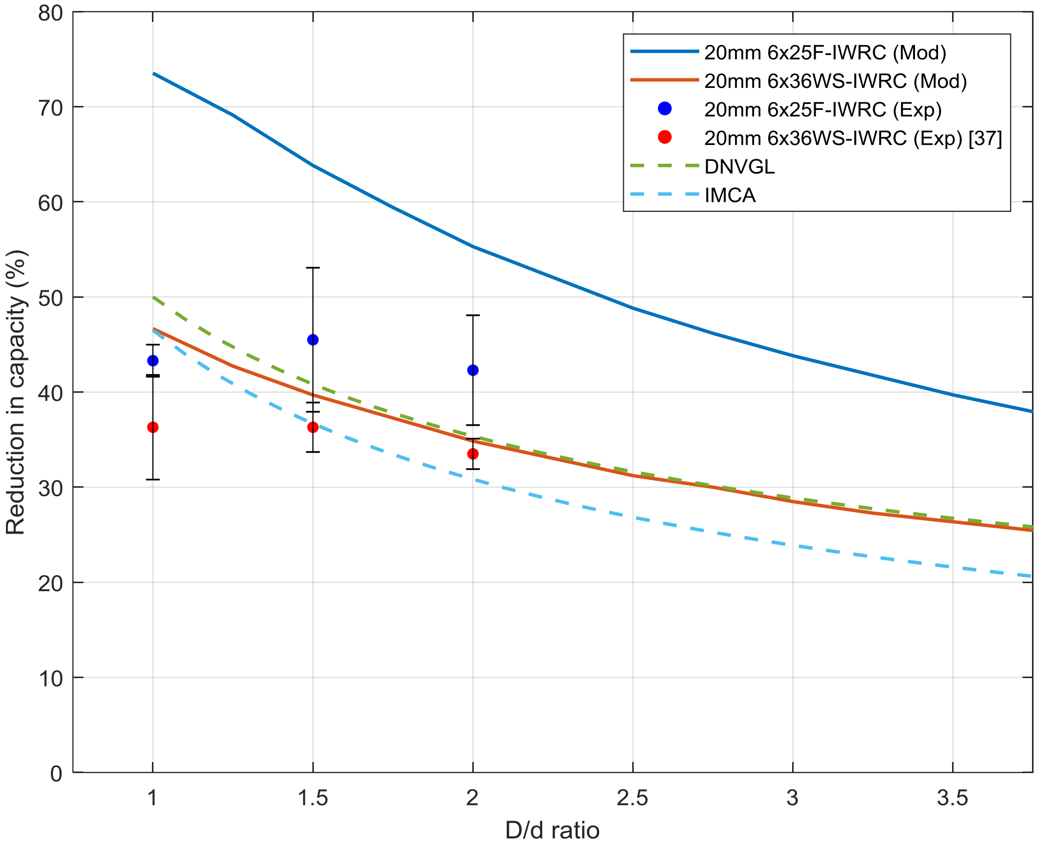

Figure 5.2 - Reduction in capacity comparison based on different rope configurations.

The most evident observation that can be made from this plot is the consistent difference in capacity reduction between the two different rope configurations. Analytically, the 6x25F-IWRC rope has a reduction that is significantly higher than the reduction of the 6x36WS-IWRC. Based on the study discussed in 3.2.3, it was concluded that the higher capacity reduction of the 6x25F-IWRC was mainly due to increased bending strains caused by larger outer strand wire diameters and a smaller outer strand lay angle. This relationship was confirmed experimentally, however, the difference was not as pronounced as seen from the analytical model.

For both studies, the differences between the analytical model and experimental results could be due to several factors. Firstly, the analytical model is heavily influenced by the bending stresses. As discussed in Chapter 2, there have been several approaches to calculating these bending stresses, but all of them consider scenarios with significantly smaller loading and curvatures. This means the method used in the analytical model as described in 3.1.2 may not be accurate enough for the scenario considered in this research.

The results also show that the analytical model predictions were higher by the same proportion for the 6x36WS-IWRC ropes, but not for the 6x25F-IWRC. This again could be attributed to the sensitivity of bending strain calculations. Furthermore, this also shows that the wire diameter ratios play a major role in the bending strains.

Another important observation to highlight is that many of the analytical and experimental results shown here actually exceed the reductions in capacity suggested by DNVGL and IMCA standards. This is rather obscure as it would be expected that the suggested reductions have a level of conservatism built-in. The source of error is difficult to assess without knowing the background into how these expressions were derived. However, some explanations for these differences could possibly be related to experimental setup. Although the experiments in this thesis followed the guidelines specified by ISO 10425:2003(E), there are no testing standards established for the bent configuration. Hence, possible sources of error are:

- Ovalization restriction at bend (pin verses sheave);
- Loading speed;
- Rope configuration;
- Friction between rope and pin surface.

5.3 EXPERIMENTAL INSIGHTS

In addition to the main parts of the research question, there were several noteworthy insights that were gained throughout the experiments.

Mentioned consistently in the experimental observations was the failure location. It was noticed that the failure regularly originated within specific strands throughout both the small and full-scale experiments. Figure 5.3 illustrates a simplified 3D model of the 20 mm 6x36WS-IWRC rope as it is bent with a *D/d*=2. Here, the two blue colored strands represent the locations where initial rope failure seemed to constantly occur.

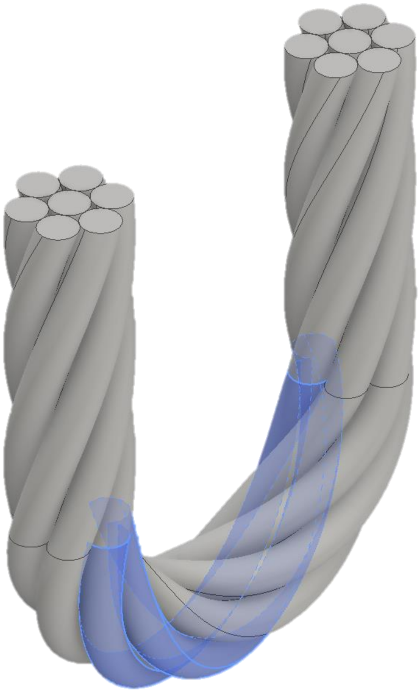

Figure 5.3 - Simplified 3D model of bent 6x36WS-IWRC with a D/d=2.

There are several observations that might help to explain this consistent behavior. First, these locations always correspond to be the rightmost strands of a RHOL rope when considering a side view of the bend. More importantly, these strands also tend to be furthest from the pin throughout the majority of the bend. Another consistent observation made throughout the experiments was that the strands closest to the pin were usually the ones that remained intact after failure. These are the strands not shaded in blue as depicted by Figure 5.4.

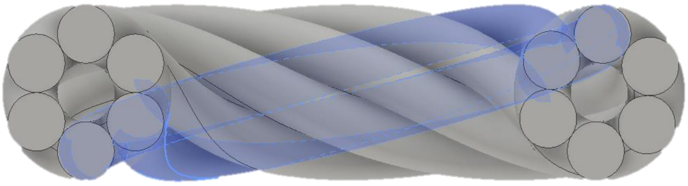

Figure 5.4 - Top view of simplified 3D model of bent 6x36WS-IWRC with a D/d=2.

These strands experienced heavy deformation as they were forced to conform around the shape of the pin with increasing load. Resulting from this interaction, high normal forces are created between the wires, which also causes an increase in friction. If the friction generated is high enough, this will prevent wires from sliding against each other. Consequently, the wires can be considered to bend around the strand or rope neutral axis rather than their own. This causes the wires on one half of the strand or rope to go into compression. However, this compressive force in the individual wires is constantly being offset by the increasing tensile axial loading applied by the test bench. This phenomenon is illustrated by Figure 5.5.

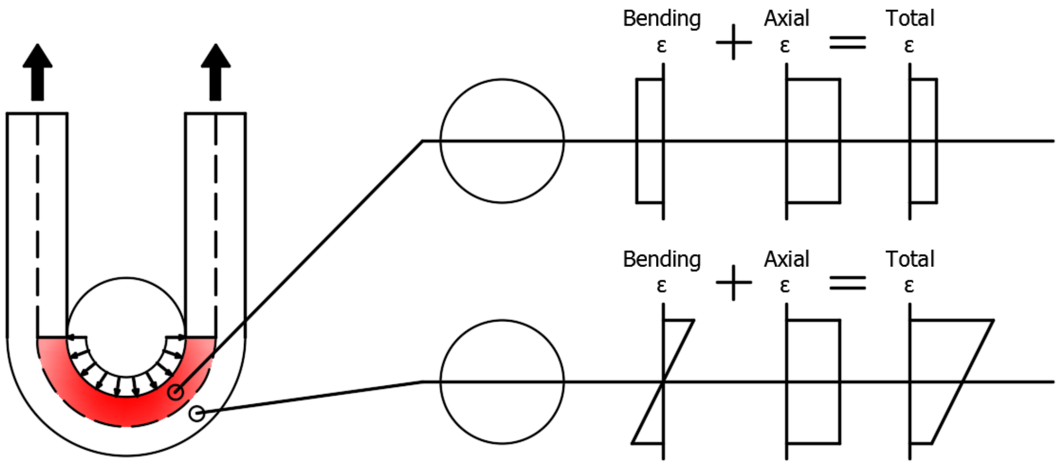

Figure 5.5 - Strains experienced by wires in different sections of the rope during loading.

Considering that wires farther away from the pin have more mobility and are less affected by the pin-rope interaction, they do not develop this uniform compressive force and thus experience the full onslaught of the increasing tensile axial loading. Globally, this causes wires closest to the pin to be less stressed than those on the outside, which may be the reason why the strands depicted in Figure 5.3 are the ones to fail first. This theory may exagerate this effect and can be considered comparable to the rope having a beamlike behavior, but the main idea behind it is that these specific types of nonlinear interactions between wires are what will govern how the rope will behave during bending.

The ovalization phenomenon was another important observation made throughout the experiments. In the additional study conducted in 4.1.5, it was concluded that restricting the rope from conforming to the pin shape (ovalizing) gave a slight increase in capacity of 1.4% on average. However, since the rope was not fully restricted, some ovalization was allowed to occur. The analytical relationship described in 2.3.4 showed that the ovalization stress increased greatly when the groove radius initially became bigger than the rope, but then gradually decreased (Figure 2.23 & Figure 2.24). Consequently, it could be possible that this increase in capacity is also bigger if the restraint was closer to the rope diameter.

Another insight was gained from the tests done in the additional study regarding the reduction in capacity. Since the specimens used for the tests were a different 20 mm 6x36WS-IWRC rope than the original one, the results could be used to make additional observations. Figure 5.6 below plots the average capacity reduction with a *D/d*=2 of all four rope types used throughout these experiments.

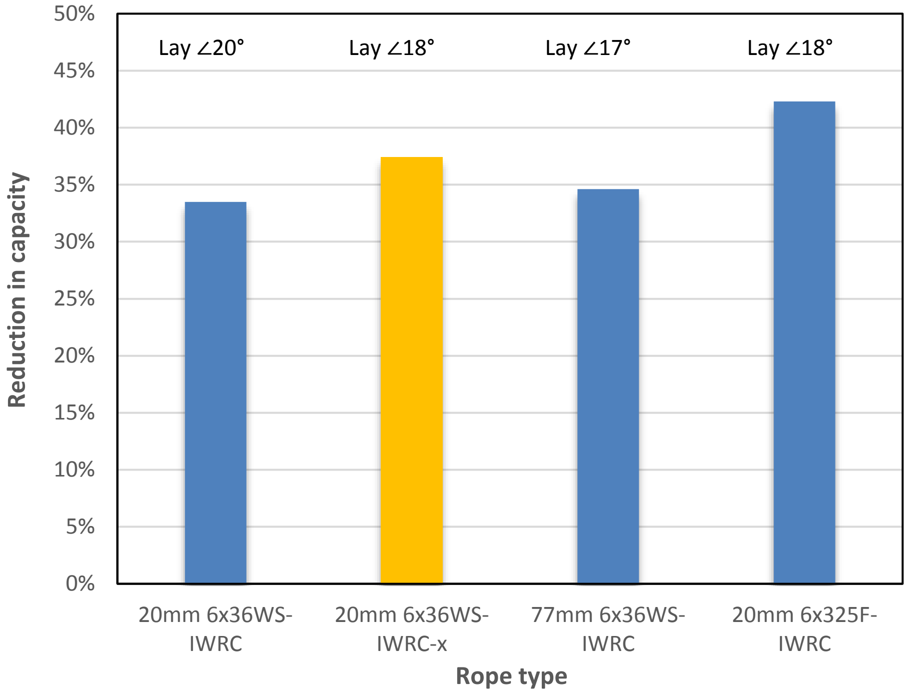

Figure 5.6 - Average reduction in capacity of all four rope types with a D/d=2.

The rope type yielding new information is the one highlighted in yellow. An important characteristic of this rope is that it has the same lay angle as the 20 mm 6x25F-IWRC. Comparing the two configurations directly using the plot above reconfirms that the wire diameter ratios play an important role in capacity reduction. Furthermore, when compared to the original 20 mm 6x36WS-IWRC, it has a slightly higher capacity reduction. This supports the conclusion that a lower lay angle reduces capacity. Although, when compared to the 77 mm 6x36WS-IWRC, this relationship does not hold, their lay angles are very close and the single data point from the full-scale experiment may not be a good representation of the actual average.

5.4 ADDITIONAL OBSERVATIONS

In addition to the insights mentioned, there were several observations made throughout the research process that raised further questions and could be of interest to investigate.

The strain gauges applied to Sample S3 & S4 yielded obscure results. The corresponding force-strain curves for both samples can be found in Appendix F. The strain output from the wires used as a control were either higher or equal to wires around the bend. Additionally, some strain gauges were damaged throughout the process. Further post-processing of this data is necessary and may result in more logical findings.

Several observations relating to contact stresses were made throughout the experiments. As discussed in section 4.2.4, there were several instances of local deformations near the failure location of wires in the outer strands. These deformations formed a pattern that can be related to the cross lay contact between wires in the outer and core strands. The occurrence of these deformations was observed throughout most samples in all experiments so it would be useful to investigate the influence of this phenomenon on the rope performance.

The boundary condition set by the pin-rope interaction exhibited several effects. One that was consistently observed was twisting of some of the outer strands during loading. Depending on the strand location, the extent of this twisting varied, but was difficult to quantify. Away from the bend, along the straight portion of the sling, the overall helical twisting of the outer strands was noticed to visibly occur only once the rope had fully conformed to the curvature of the pin. The influence of these observations on wire stresses was not considered, but could be worthwhile to further investigate.

6.0 CONCLUSION

The main objective of this study was to investigate the reduction in capacity of steel wire rope slings subjected to forced bending. The approach to answering the main research question involved doing a literature study, creating a predictive analytical model and then performing experiments for validation. Each aspect of the approach was completed successfully, and insights gained from each one led to the conclusions drawn to answer the main research question.

The literature study consisted of investigating past research done on steel wire ropes. Here, different approaches to modelling wire ropes were observed. Using equations mainly obtained from the thin-rod theory modelling approach, the main parameters that governed the behavior of wire ropes were identified. Short sensitivity studies were conducted on these constitutive equations and it was shown that properties such as lay angles, wire diameters and stress-strain relations played a vital role.

Based on the findings of the literature study, an analytical model was created that aimed to predict the reduction in capacity of steel wire ropes due to bending. This model analyzed the behavior of each individual wire when subjected to loading and then applied a failure criterion to determine when the entire rope cross-section would fail. The case studies investigated by the model yielded that the individual wire diameter to rope diameter ratio was the governing parameter along with a smaller contribution from the lay angle when considering bent ropes.

Conducting experiments was the final step in the project. First, small-scale experiments were done to test the reduction in capacity due to bending of 20 mm 6x25F-IWRC slings. The tests were successfully executed and results for three different *D/d* ratios were obtained (*D/d*=1, 1.5, 2). During testing, several observations were noted about rope behavior such as relative strand displacement, strand twist and failure location consistency. Additionally, full-scale tests were conducted on 77 mm 6x36WS-IWRC slings used in the offshore industry. These tests also yielded observations that were consistently found in the small-scale experiments and more. An additional study was performed using the small-scale test setup to examine influence of the rope ovalization on capacity.

Using findings from the literature study, analytical model and experiments, conclusions regarding the main research question were drawn. First, the results of the analytical model yielded reductions that were consistently higher than experimental results for all rope types and sizes under investigation. The errors were relatively small and could be used as a conservative estimate given the limited number of experimental data points. However, the error for the 20 mm 6x25F-IWRC was significantly high and suggests that more accurate calculations of the bending strains are required to improve model accuracy. Overall, the following insights were gained when considering the reduction in capacity of slings subjected to bending based on the findings in this thesis:

- Rope configurations play a vital role in capacity reduction. The number of wires in an outer strand determines the diameters of those wires. A smaller amount of wires means that the diameters will be larger causing the bending strains to also be higher. Ultimately, this causes a higher reduction in capacity.
- The lay angle of the outer strand also has an effect on rope capacity. Analytically, it was observed that a higher lay angle results in lower bending strains when calculating the change in curvature of individual wires sliding against each other. Overall, the analytical model predictions and experimental results supported this relationship.
- The diameter size of the wire rope proved to have little influence on the reduction in capacity due to bending. The difference in capacities between the 6x36WS-IWRC configurations was assumed to be caused by the difference in lay angles.
- An additional study was done to examine the effect of rope ovalization. The results showed little influence if this was prevented, but there are grounds for further investigation.
- The expressions recommended by DNVGL and IMCA require further clarification as results in this thesis show they are not conservative enough for certain *D/d* ratios and ropes.

7.0 RECOMMENDATIONS

Resulting from the research conducted to investigate the reduction in capacity due to bending of steel wire ropes are several recommendations for improvements and future research. The main topics include improvements to the analytical model, utilizing numerical modelling approaches, conducting more experiments and investigating alternative approaches.

Analytical Model Improvements

As with most analytical models, the one presented in this thesis does not perfectly represent reality. The potential flaws and possible sources of error have already been discussed. Some suggested improvements include:

- Incorporation of additional stresses such as torsion, moment and shear resulting from the helical structure of the rope should be implemented into the current model. This would help improve the prediction of the actual breaking load for both proof load and bending type tests.
- Calculation of the bending stress should be improved by considering more complex methods which accurately incorporate the double helical structure of the stranded rope configurations.
- The resulting contact stresses from the pin-rope interaction have proven to influence wires near the bend and should therefore be incorporated into the model. Consequently, this would also likely mean that the friction forces generated will increase due to the higher normal forces between layers.
- A strain area approach should be implemented to find the stress state of individual wires during each load step. This could help improve the failure criteria by more accurately incorporating the wire cross-sectional strain resulting from the different loadings. This would also yield a better representation of how the bending strains affect the individual wire capacity.
- The current model simplifies calculations by considering only the governing outer strand. Expanding the model to make the calculations for every wire in every strand while also finding a way to effectively visualize this data could bring forth interesting insights.

A new approach to the analytical model should also be considered. As discussed in previous research, there are many different techniques that have been used by authors to model steel wire ropes. Some have been proven more beneficial in modelling certain aspects than others. For instance, the semi-continuous models could be used to model the outer strands as spiral ropes while the core can be modelled using thin-rod theory. Overall, finding a way to compatibly combine some select theories into an analytical model could yield more accurate results.

Numerical Modelling

Conducting a numerical analysis could prove to be the next best step in discovering more insights into the behavior of steel wire rope. Specifically, gaining more knowledge about the effects of the pin-rope interaction could help in discovering the governing stresses that ultimately cause failure of the wires. As pointed out earlier, numerical modelling of wire ropes involves an enormous amount of computational power. To overcome this, a researcher should start with a simple model, verify the resulting behavior and then gradually increase complexity. Special attention should be made into exploring the use of different element types and friction models. Additionally, custom scripts may need to be implemented into FEA software to model effects such as the redistribution of loading after a wire failure.

Experiments

Performing experiments is one of the best ways to gain insights and validate the behavior of steel wire ropes. Even though the experiments conducted throughout this thesis have yielded valuable discoveries, they have also sparked interest in additional studies such as:

- The short additional study on the rope ovalization raised questions that require further investigation. An experiment can be set up where a bent sling is tested with different levels of restrictions. The results can then be compared to the theoretical predictions discussed in 2.3.4 to see how the sling capacity is affected, especially when no ovalization is allowed to happen.
- The stress-strain relationship of wires in all layers is an interesting parameter that is also important for the analytical model. Although the manufacturer provides the ultimate strength of the wires, their stress-strain relationship is not disclosed. Hence, conducting tests to obtain this data would provide

valuable input for the analytical model. Conducting these wire tests for several different rope configurations may lead to a general pattern between wire behavior and layer location in the rope. If this is achieved, general stress-strain relationships can be defined and used for ropes without having to conduct individual wire tests every time. In conjunction with these tests, strain gauges should be implemented to determine if they can indeed be used to accurately measure wire elongation.

- An experimental insight showed that the failure consistently originated within two specific strands as depicted in Figure 5.3. Since all the ropes tested in this thesis were RHOL, it would be interesting to see if the same strands, but on the opposite side of the rope axis would be the ones to fail consistently for a LHOL rope.
- There is a definite need for additional data points. Hence, repeating certain tests in order to gain more data would give a better statistical overview that would allow the researcher to draw conclusions with more confidence.
- There is also interest in performing new experiments that test different rope configurations and/or lay angles that would help validate if the conclusions drawn here hold true.

Although not specifically related to this research, the reusability of slings is also an interesting topic. Currently, bent slings used in engineered lifts are commonly disposed after only a single lift. These lifts always adhere to the proper working load limit of the slings so it is plausible to assume that any reduction in capacity resulting from one load cycle is minimal. Hence, it would be interesting to investigate the extent of this reduction and test if the integrity of the sling remains. The results can either be used to inspire confidence in sling reusability or help justify the slings being considered consumable after one load cycle.

Alternate Approaches

In addition to common approaches such as analytical and numerical models for predicting wire rope capacity, a possible alternative option is utilization of neural networks. As discussed, accurate analytical models are both difficult and time consuming to create while full numerical models are too computationally intensive to run. Alternatively, when it comes to very nonlinear data sets, neural networks are becoming a very popular approach and their benefits have been implemented into many different applications. The idea behind this machine learning method is to use an existing data set to "train" a computer model, which can then be used to estimate a desired output when given new data. More specifically, data from experiments such as the ones conducted in this thesis can be used to train the model with the goal of predicting rope capacity. One key issue that must be investigated is choosing the proper input variables that are considered critical to predicting rope capacity. This could be rope configuration, global rope stress (S/d^2), D/d ratio, lay angle, etc. These parameters should be carefully chosen using previous research as well as insights discussed in this thesis. Obtaining the amount of quality data that can be used to train the model is also a challenge. To do so, it may be suggested to form a partnership with a rope manufacturer to obtain data or carry out more tests. Once this has been overcome, the next step would be selecting the proper machine learning algorithm that is suitable for the data set and desired output. After the model has been trained, new data should be presented to verify how close the resulting model estimate is to actual capacity.

REFERENCES

[1] R. Vereet, "A Short History of Wire Rope," PR GmbH, Aachen, 2004.

[2] D. Sayenga, "Modern History of Wire Rope," 1999. [Online]. Available: http://atlantic-cable.com/Article/WireRope/Sayenga/wirerope4.htm.

[3] R. Vereet, "Steel Wire Ropes for Cranes," PR GmbH, Aachen, 2005.

[4] "Lifting & Rigging Learning Center," 2018. [Online]. Available: https://www.mazellacompanies.com.

[5] K. Feyrer, Wire Ropes, Tension, Endurance, Reliability, Springer-Verlag Berlin Heidelberg, 2007.

[6] "Manufacturing Process," 2018. [Online]. Available: http://www.gabaswire.com/en/overview/manufacturing-process.html.

[7] "DNVGL-ST-N001 Marine operations and marine warranty," DNVGL, 2016.

[8] "IMCA LR008, M179-2016 The Manufacture and Safe Use of Cable-laid Slings and Grommets," International Marine Contractors Association, 2016.

[9] V. Spak, G. Agnes and D. Inman, "Cable Modelling and Internal Damping Developments," *Applied Mechanics Reviews 65, ASME,* pp. 1-18, 2013.

[10] F. Hruska, "Calculation of stresses in wire ropes," *Wire and wire products,* pp. 766-767, 1951.

[11] J. Lanteigne, "Theoretical estimation of the response of helically armored cables to tension, torsion, and bending," *Journal of Applied Mechanics 52,* pp. 423-432, 1985.

[12] M. Lutchansky, "Axial stresses in armor wires of bent submarine cables," *Journal of Engineering 91,* pp. 687-691, 1967.

[13] C. Jolicoeur and A. Cardou, "A numerical comparison of current mathematical models of twisted wire cables under axisymmetric loads," *Journal of Energy Resources Technology,* pp. v113, 241-249, 1991.

[14] G. Costello and J. Phillips, "Effective modulus of twisted wire cables," *Journal of Engineering Mechanics Division, ASCE 102,* pp. 171-181, 1976.

[15] A. Love, A Treatise on the Mathematical Theory of Elasticity, New York: Dover Publications, 1944.

[16] G. Costello, Theory of Wire Rope, New York: Springer-Verlag, 1990.

[17] S. Velinsky, Analysis of wire ropes with complex cross sections, University of Illinois at Urbana-Champaign, 1981.

[18] S. Velinsky, G. Anderson and G. Costello, "Wire rope with complex cross sections," *Journal of Engineering Mechanics, ASCE 110,* pp. 380-391, 1984.

[19] K. O. Papailiou, "Bending of helically twisted cables under variable bending stiffness due to internal friction, tensile force and cable curvature," EIDGENÖSSISCHE TECHNISCHE HOCHSCHULE ZURICH, 1995.

[20] K.-J. Hong, A. D. Kiureghian and J. L. Sackman, "Bending Behavior of Helically Wrapped Cables," *Journal of Engineering Mechanics,* pp. 500-511, 2005.

[21] M. Raoof and R. Hobbs, "The Bending of Spiral Strand and Armored Cables Close to Terminations," *Journal of Energy Resource Technology,* pp. v106(3): 349-355, 1984.

[22] C. Jolicoeur and A. Cardou, "Semicontinuous mathematical model for bending of multilayered wire strands," *Journal of Engineering Mechanics,* pp. 112(7): 643-650, 1996.

[23] M. Raoof and I. Kraincanic, "Critical examination of various approaches used for analysing helical cables," *Journal of Strain Analysis,* pp. v29-1: 43-55, 1994.

[24] W. Jiang, M. Warby and J. Henshall, "Statically Indeterminate Contacts in Axially Loaded Wire Strand," *Eur. J. Mech. Solids,* pp. v27, pg. 69-78, 2008.

[25] E. Imrak and C. Erdonmez, "On the problem of wire rope model generation with axial loading," *Mathematical and Computer Applications,* pp. vol.15: 259-268, 2010.

[26] D. Zhang and M. Ostoja-Starzewski, "Finite Element Solutions to the Bending Stiffness of a Single-Layered Helically Wound Cable With Internal Friction," *Journal of Applied Mechanics,* pp. 1-8, 2016.

[27] S. Timoshenko, Strength of Materials Part II - Advanced Theory and Problems, New York: D. Van Nostrand Company, Inc., 1940.

[28] Reuleaux, Der Konstrukteur, Braunschweig: Vieweg-Verlag, 1861.

[29] G. Schiffner, "Spannungen in laufenden Drahtseilen," University of Stuttgart, Stuttgart, 1986.

[30] L. Wiek, "Facts and figures of stresses in steel wire ropes," in *Proceedings of the Round Table of OIPEEC*, Milan, 1973.

[31] R. Hobbs and S. Nabijou, "Changes in wire curvature as a wire rope is bent over a sheave," *Journal of Strain Analysis,* pp. vol. 30, pg. 271-281, 1995.

[32] Leider, "Die Bestimmung der Zusatzspannungen bei der Biegung von Drahseilen und ihr Einfluss auf die Seillebensdauer," Diss. TH Karlsruhe, 1975.

[33] Hütte, des Ingenieurs Taschenbuch, 28.Auflage, Berlin: Verlag Wilhelm Ernst und Sohn, 1955.

[34] S. Kmet, E. Stanova, G. Fedorko, M. Fabian and J. Brodniansky, "Experimental investigation and finite element analysis of a four-layered spiral strand bent over a curved support," *Engineering Structures,* no. 57, pp. 475-483, 2013.

[35] V. Fontarini, M. Benedetti and B. Monelli, "Elasto-plastic behavior of a Warrington-Seale rope: Experimental analysis and finite element modeling," *Engineering Structures,* pp. v82, pgs. 113-120, 2015.

[36] E. Czitary, Seilschwebebahnen, Wien Springer, 1952.

[37] B. C. d. Jong, "Analytical and experimental analysis of the capacity of steel wire ropes subjected to forced bending," TU Delft, Allseas Engineering B.V., Delft, 2015.

[38] Y. Chen, F. Meng and X. Gong, "Full contact analysis of wire rope strand subjected to varying loads based on semi-analytical method," *International Journal of Solids and Structures,* pp. 51-66, 2017.

APPENDIX A: USER INPUT

The behavior of steel wire ropes is heavily dependent on their geometric properties. Hence, the user input is an important step in ensuring that the results from the analytical model are valid. A summary of the required parameters that must be given by the user in order to reconstruct the rope geometry in the model can be found below. A figure is also provided for clarity.

Wire rope build-up

- number of strand layers
- number of strands in a layer
- strand winding radius
- strand lay length
- MBL
- applied force per time step

Individual strand build-up

- number of layers in strand
- wire diameter of each layer
- number of wires in each layer
- lay length of wires in strand

Stress-strain data

- ultimate stress
- ultimate strain
- stress-strain plot/data points

Material properties

- friction coefficient between strands
- friction coefficient between wires
- poisson ratio for strands
- poisson ratio for wires

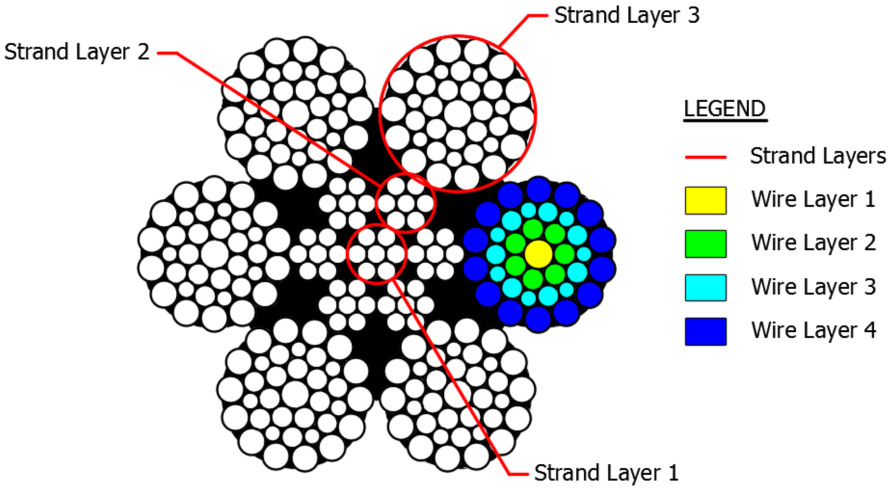

6x36WS-IWRC

APPENDIX B: SMALL-SCALE EXPERIMENT TEST SETUP

The test setup for the small-scale experiment involved designing custom pieces in order to achieve the desired loadcases. This setup was originally designed by de Jong [37]. The pieces required for the proof load test are presented first followed by the pieces for the bent sling. The slings were all fitted with standard open spelter sockets for a 20 mm rope.

Proof load test

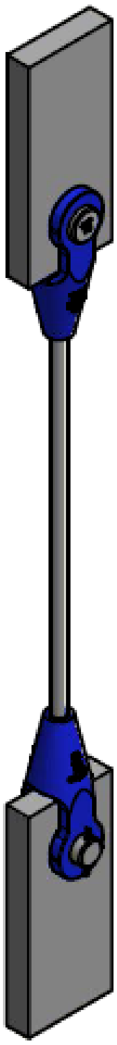

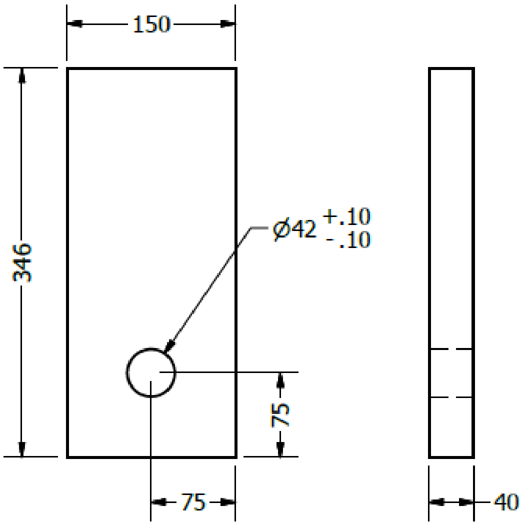

Fixation plates

Bending test

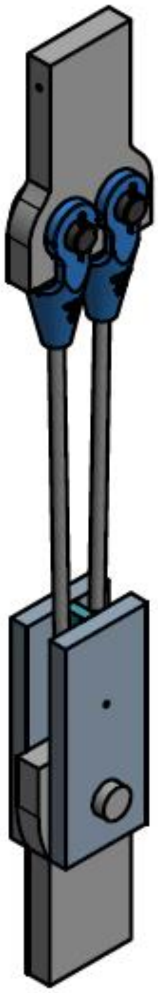

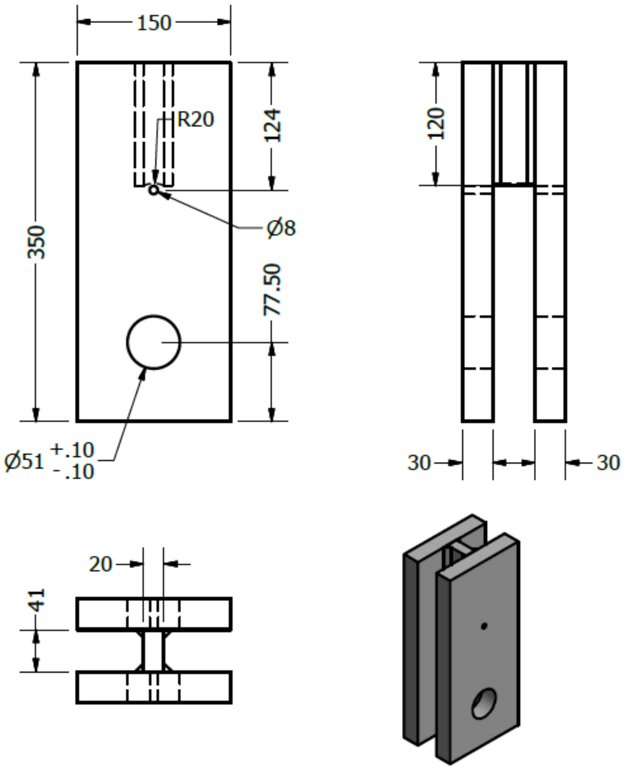

Main plate assembly

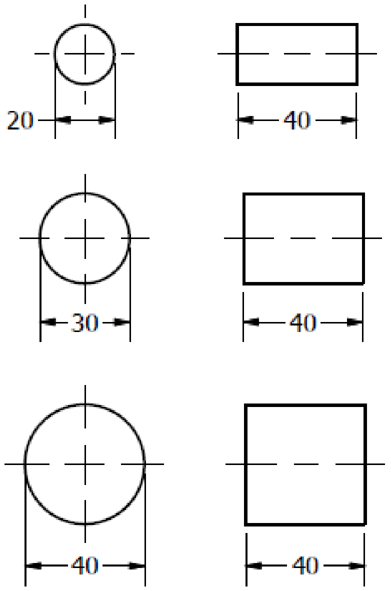

D/d pins

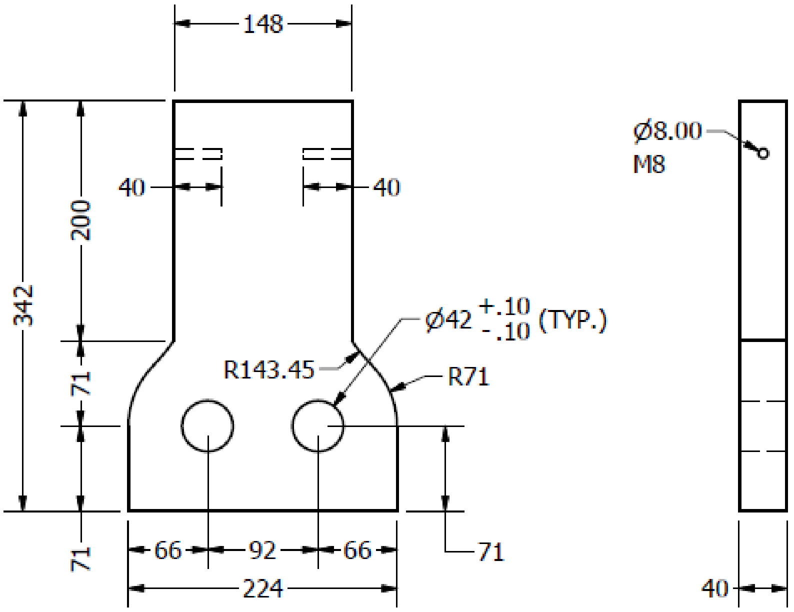

Top fixation plate

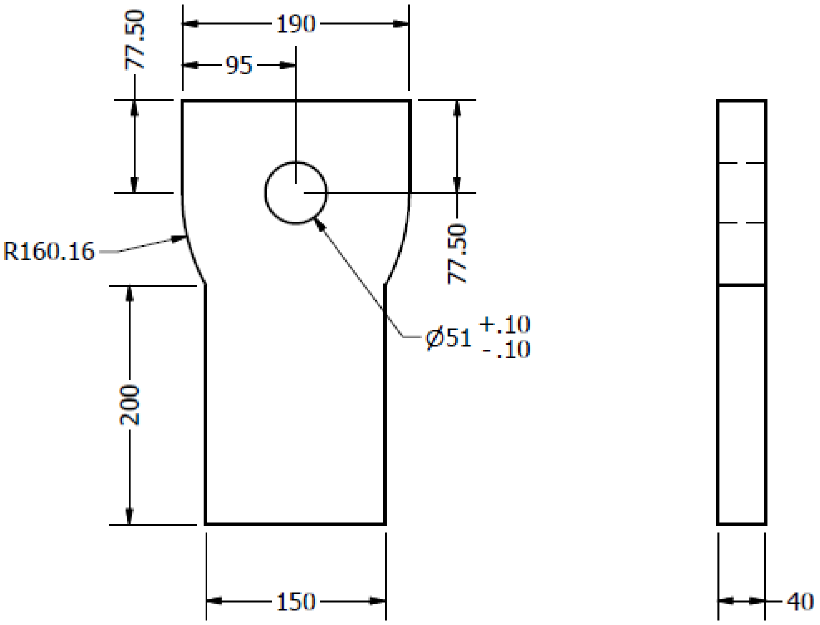

Bottom fixation plate

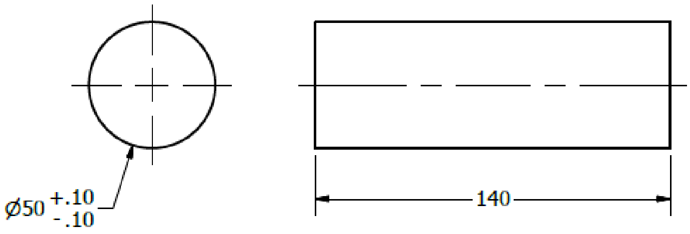

Main assembly pin

APPENDIX C: LOAD-ELONGATION PLOTS (SMALL-SCALE EXPERIMENT)

The load-elongation curves for all samples in the small-scale experiments are presented here. The first three figures show the plots for proof load samples P1, P2 and P3, respectively. Both the test bench output and average LVDT sensor reading are shown for each sample.

The remaining figures are related to the bent samples tested in the small-scale experiment. Each plot compares the resulting test bench output of the bent samples based on the *D/d* ratio.

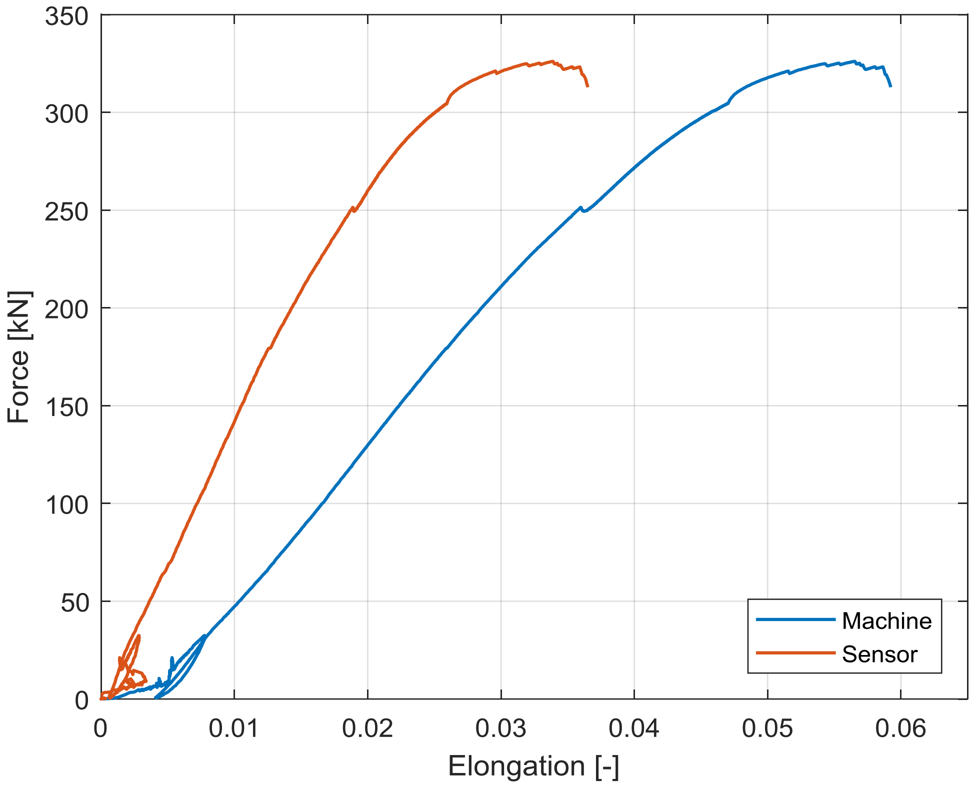

Figure C.1 – Load-elongation curves of Sample P1 from small-scale experiment.

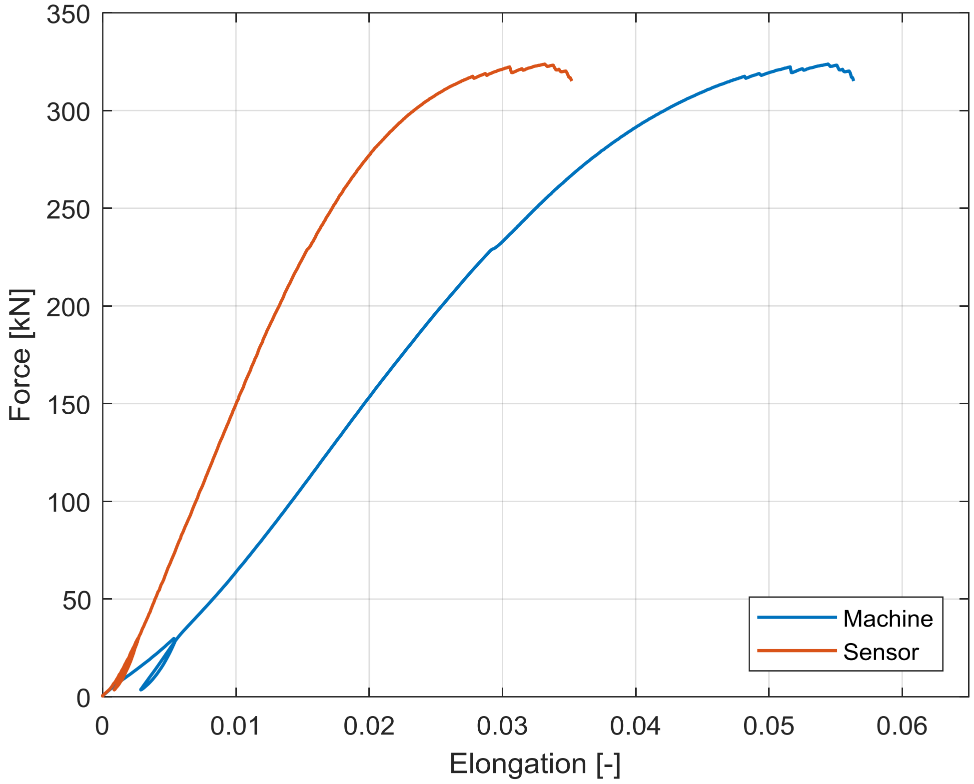

Figure C.2 – Load-elongation curves of Sample P2 from small-scale experiment.

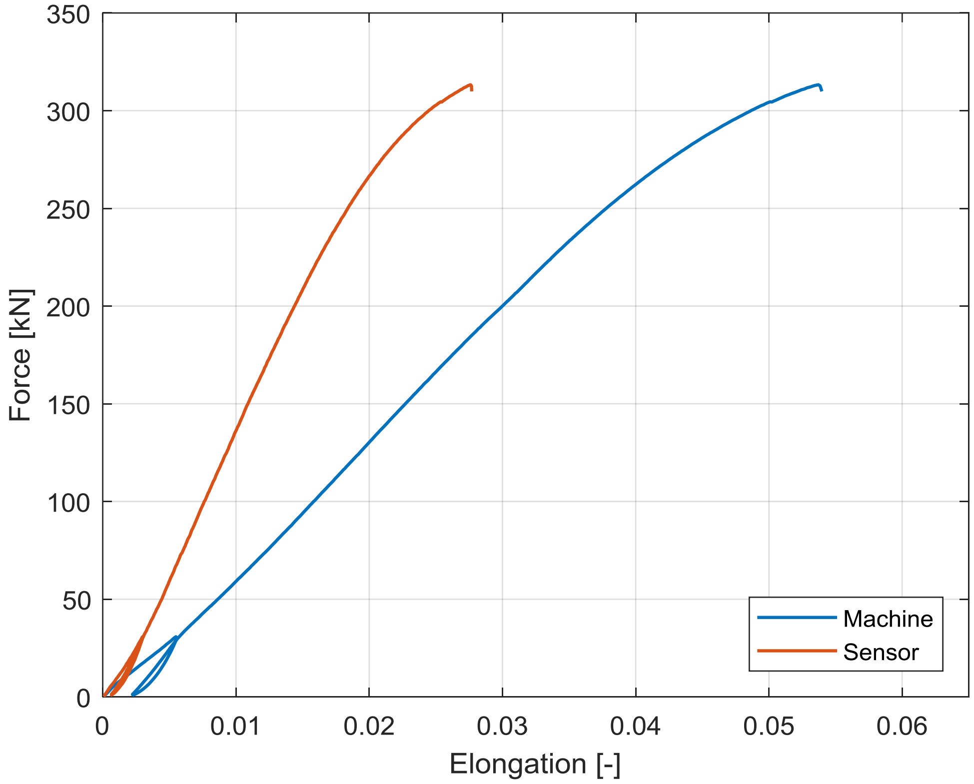

Figure C.3 – Load-elongation curves of Sample P3 from small-scale experiment.

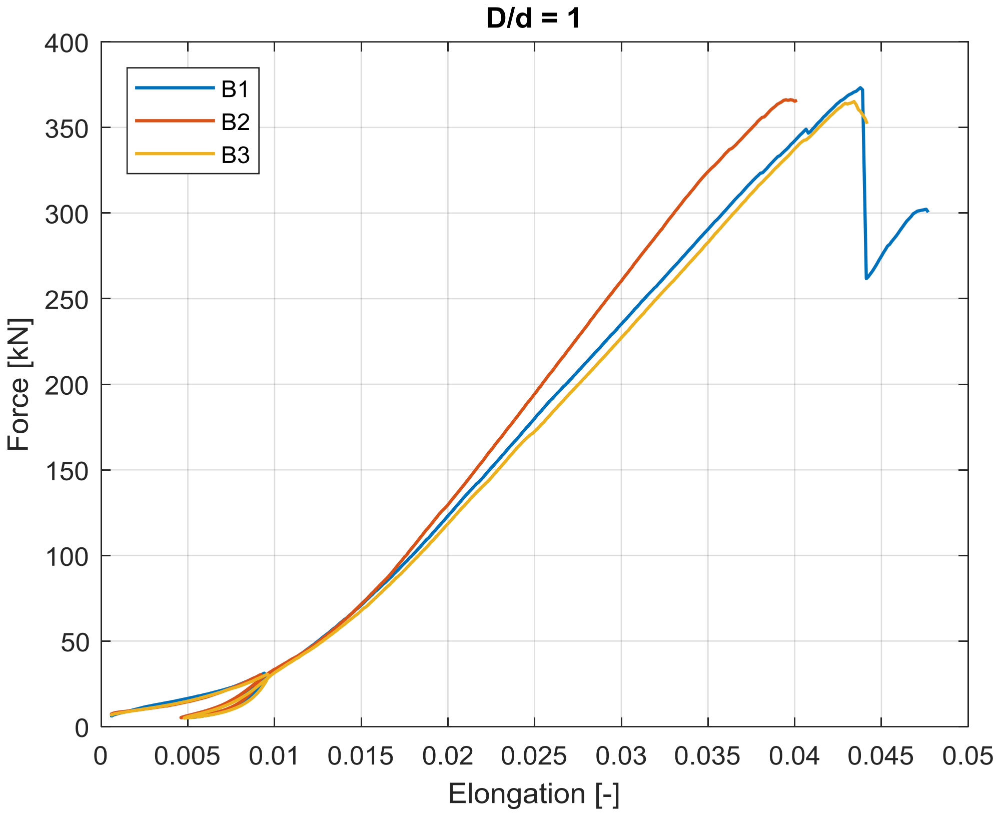

Figure C.4 - Load-elongation curves of bent samples with D/d=1 from small-scale experiment.

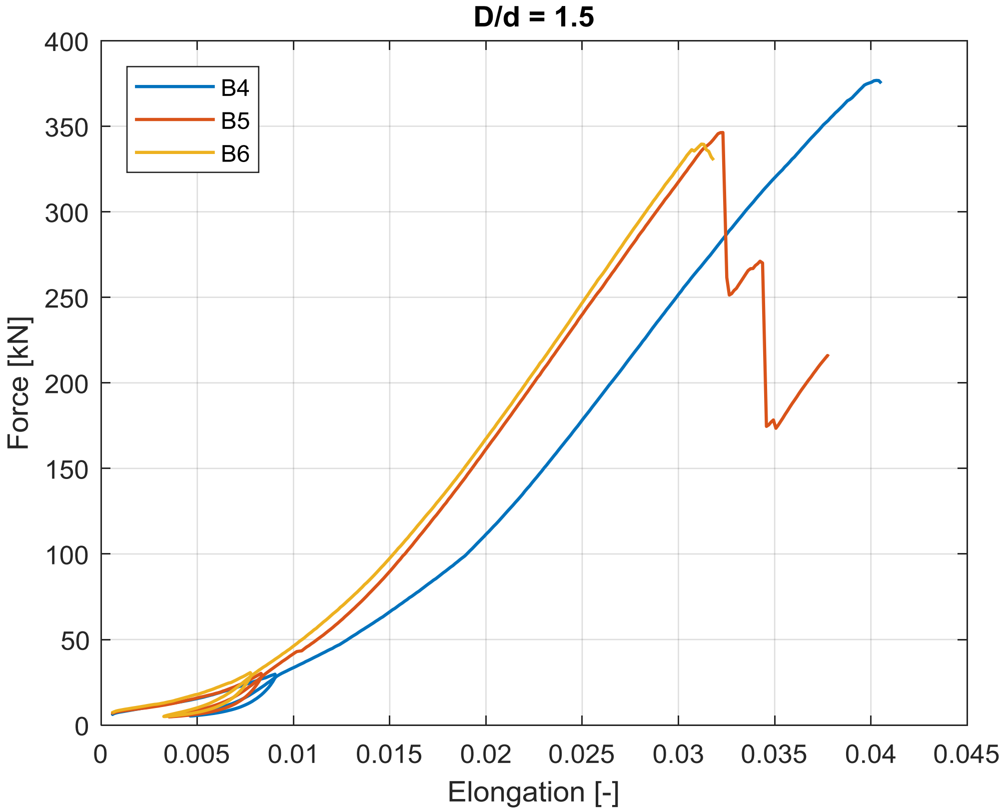

Figure C.5 – Load-elongation curves of bent samples with D/d=1.5 from small-scale experiment.

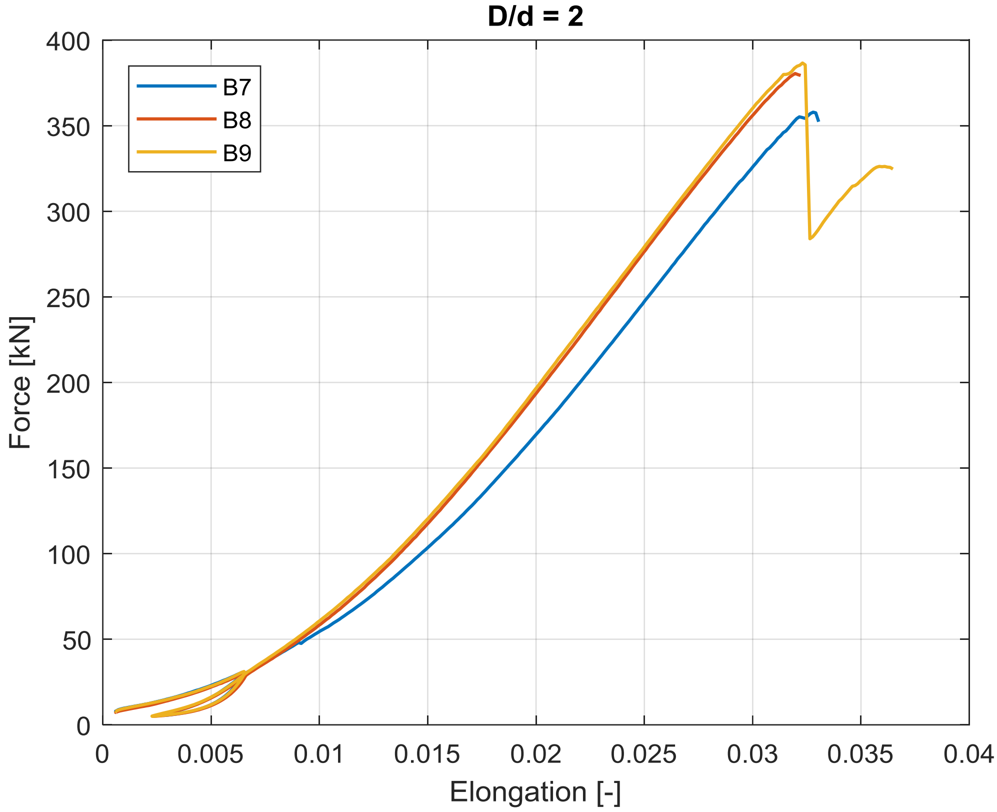

Figure C.6 – Load-elongation curves of bent samples with D/d=2 from small-scale experiment.

APPENDIX D: ADDITIONAL STUDY SUPPLEMENT

The information presented here provides additional information about the 20 mm 6x36WS-IWRC-x rope used in the additional study described by section 4.1.5. Two tables summarize the major rope characteristics and geometric properties obtained from the certificate provided by the manufacturer. The subsequent figures represent the resulting load-elongation curves from the tests conducted for the additional study.

Table D.1 – Rope properties of 20 mm 6x36WS-IWRC-x.

	20 mm 6x36WS-IWRC-x
Lay type	RHOL
Strand lay angle	18°
Strand construction	1-7-7+7-14
Grade	1960 N/mm^2
Coating	Galvanized
Lubrication	A2

Table D.2 – Individual wire properties in outer strand of 20 mm 6x36WS-IWRC-x.

Wire Diameter (mm)	Ult. Tensile Strength (N/mm^2)
1.10	2013
0.91	2157
0.70	2141
0.94	2050
1.26	2046

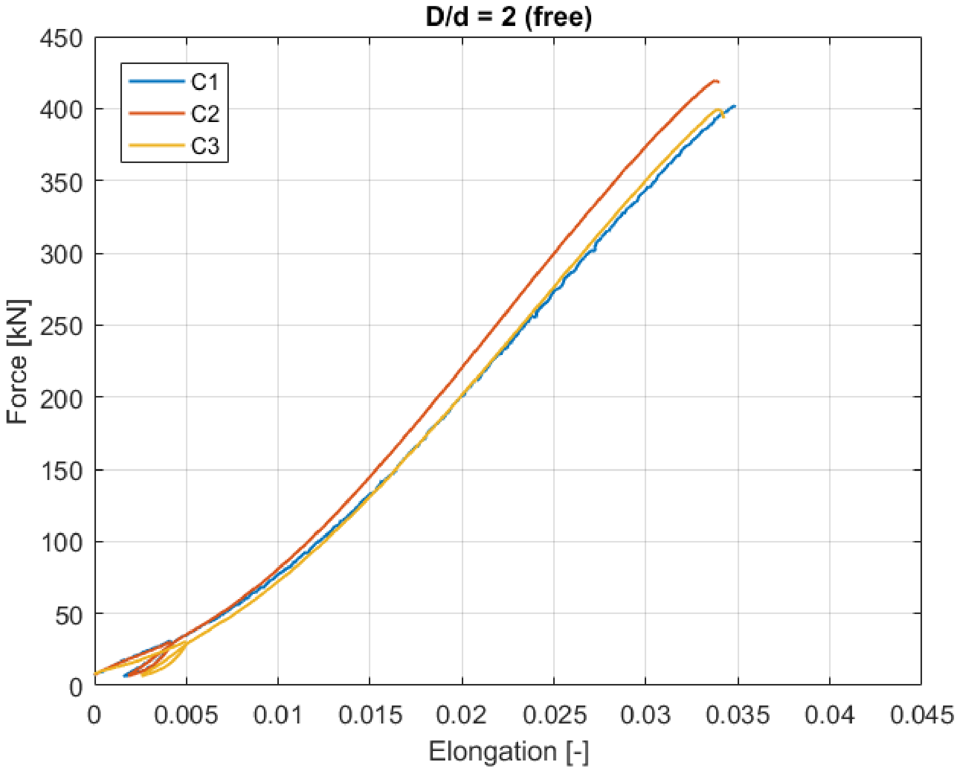

Figure D.1 – Load-elongation curves of samples with D/d=2 from additional study without restraints for ovalization.

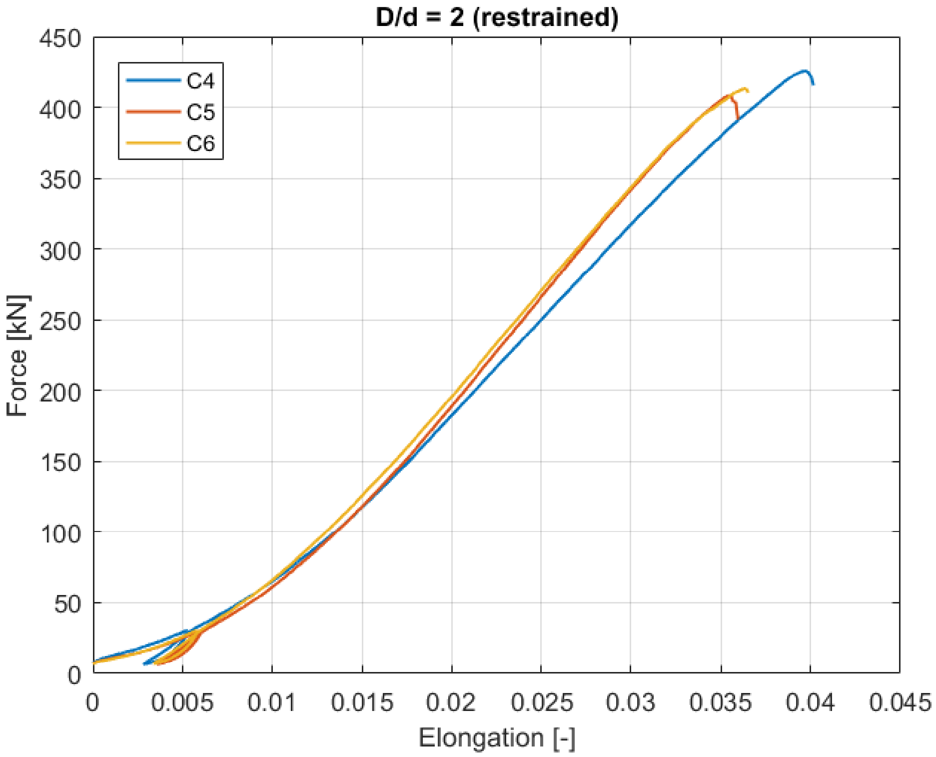

Figure D.2 – Load-elongation curves of samples with D/d=2 from additional study with restraints for ovalization.

APPENDIX E: FULL-SCALE EXPERIMENT TEST SETUP

The test bench used for the full-scale experiment is illustrated by the figures below. Additional custom pieces had to be designed in order to be able to test the desired loadcases and are labelled by the appropriate callouts. Dimensions for the custom pieces can be found in the subsequent figures, which were taken from detailed drawings created at Allseas.

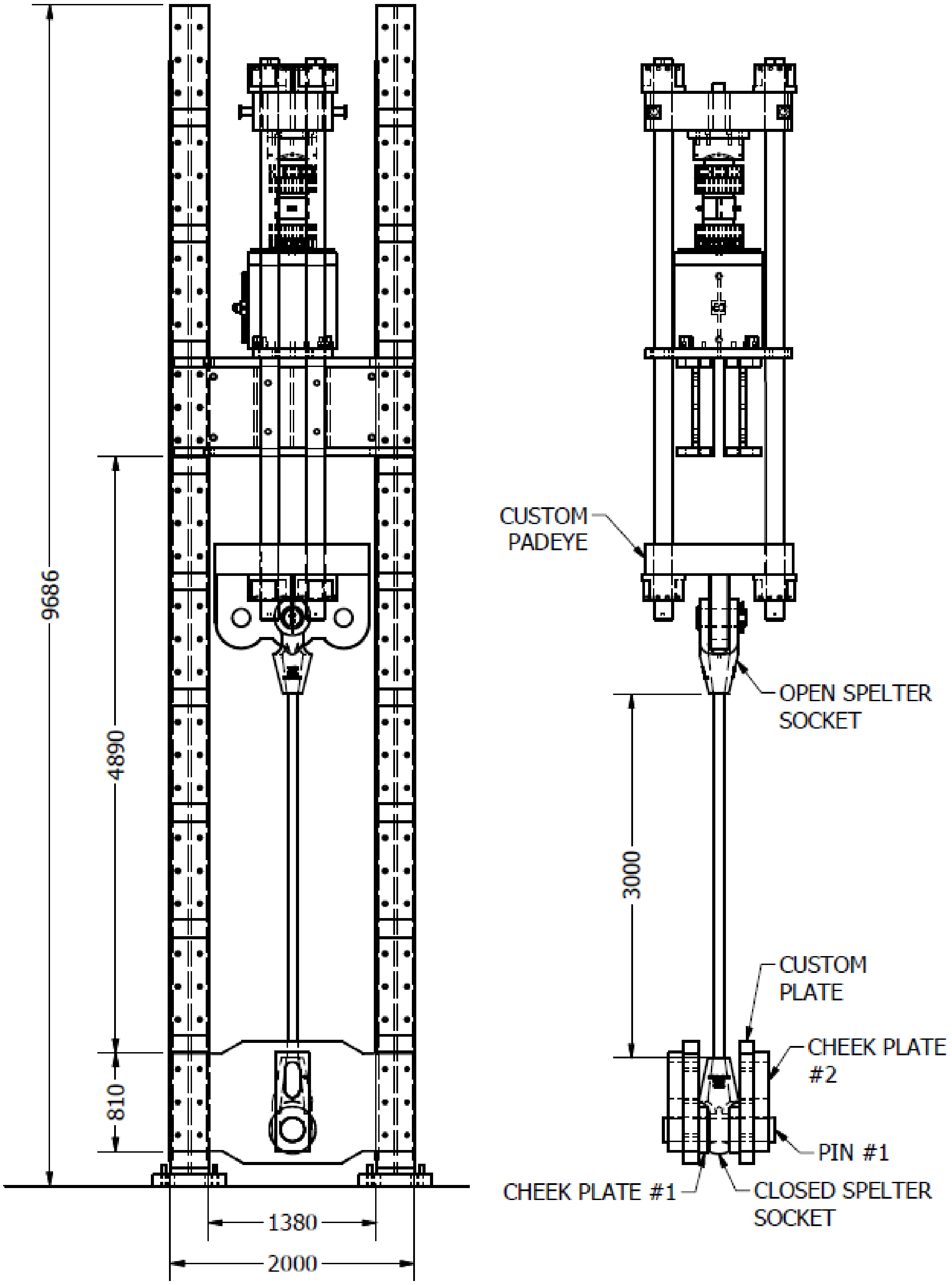

Figure E.1 – Overview of proof load test setup for full-scale experiment.

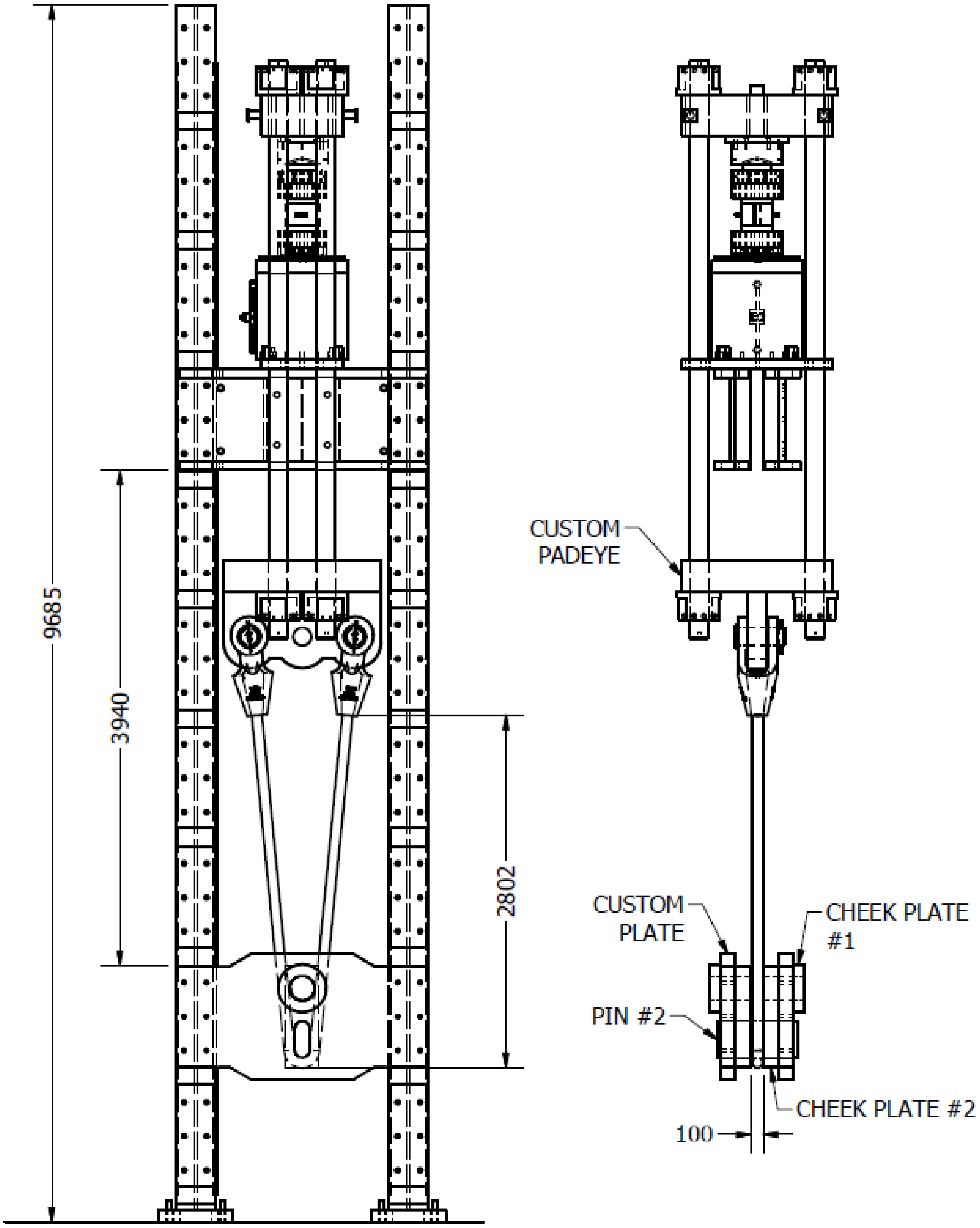

Figure E.2 – Overview of bending test setup for full-scale experiment.

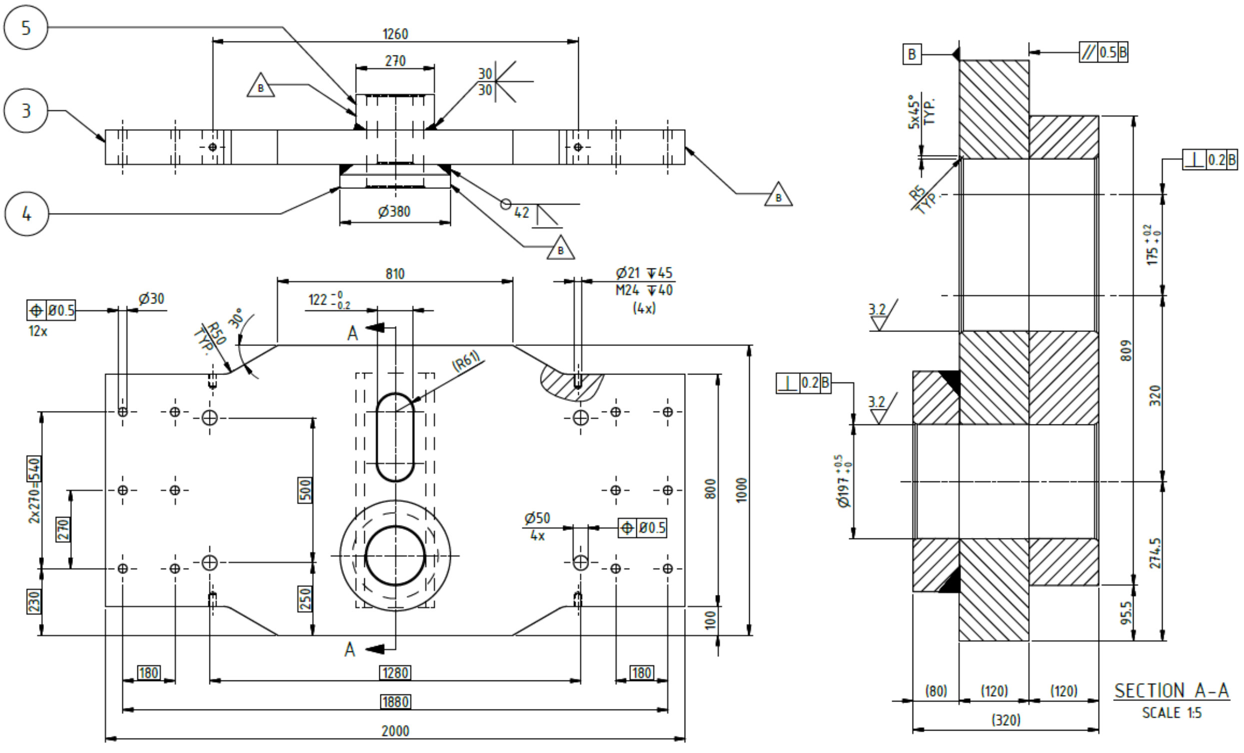

Figure E.3 – Custom plate and custom cheek plate #1 & #2 assembly.

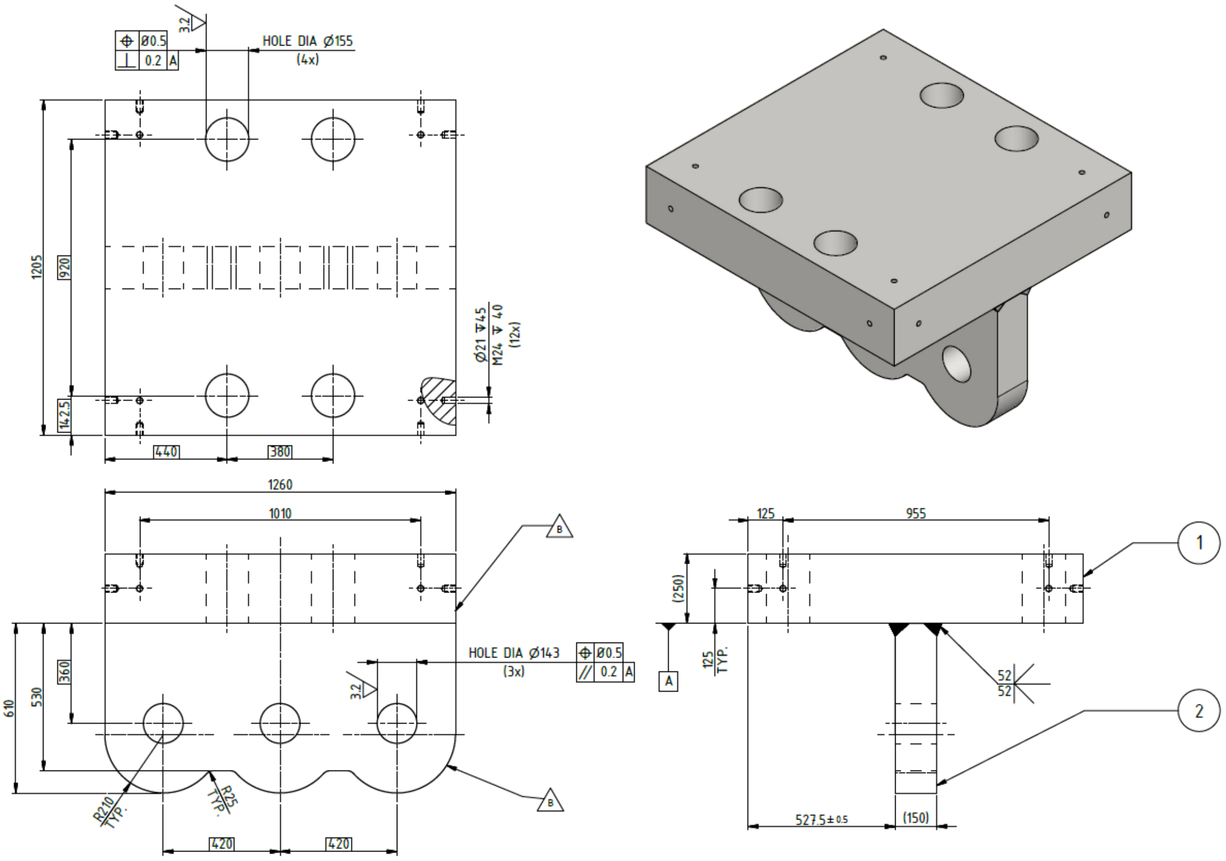

Figure E.4 – Custom padeye.

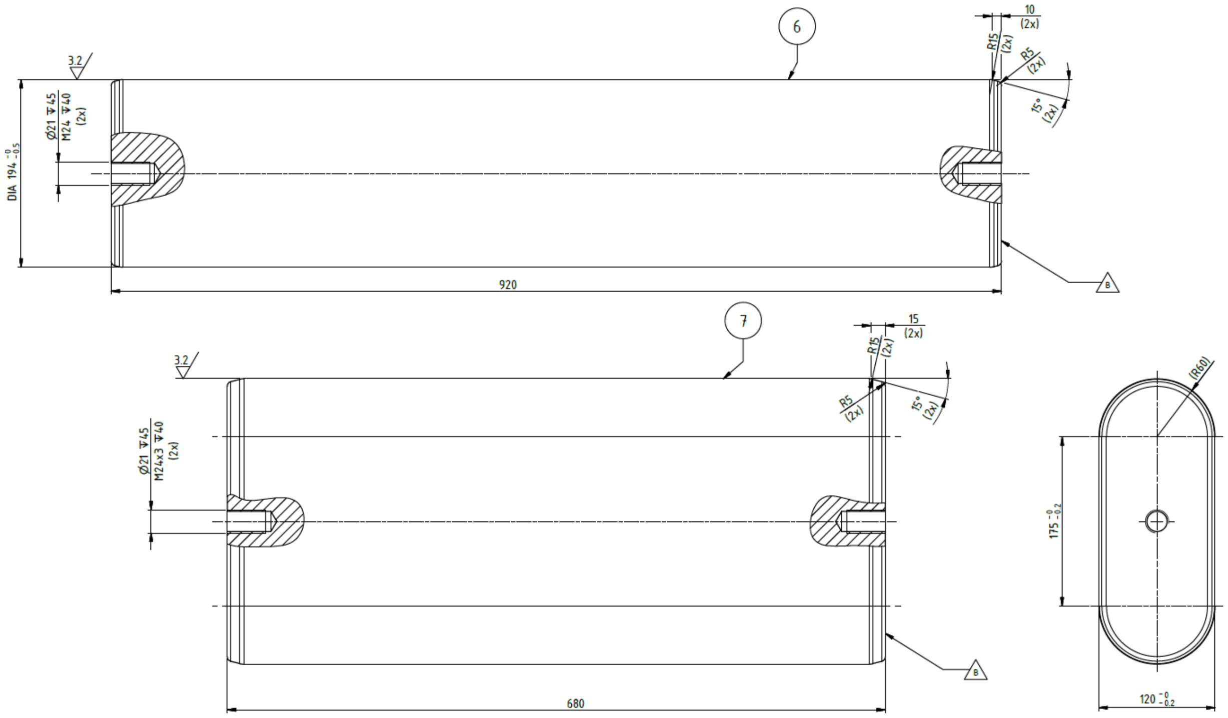

Figure E.5 – Custom pin #1 (top) and pin #2 (bottom).

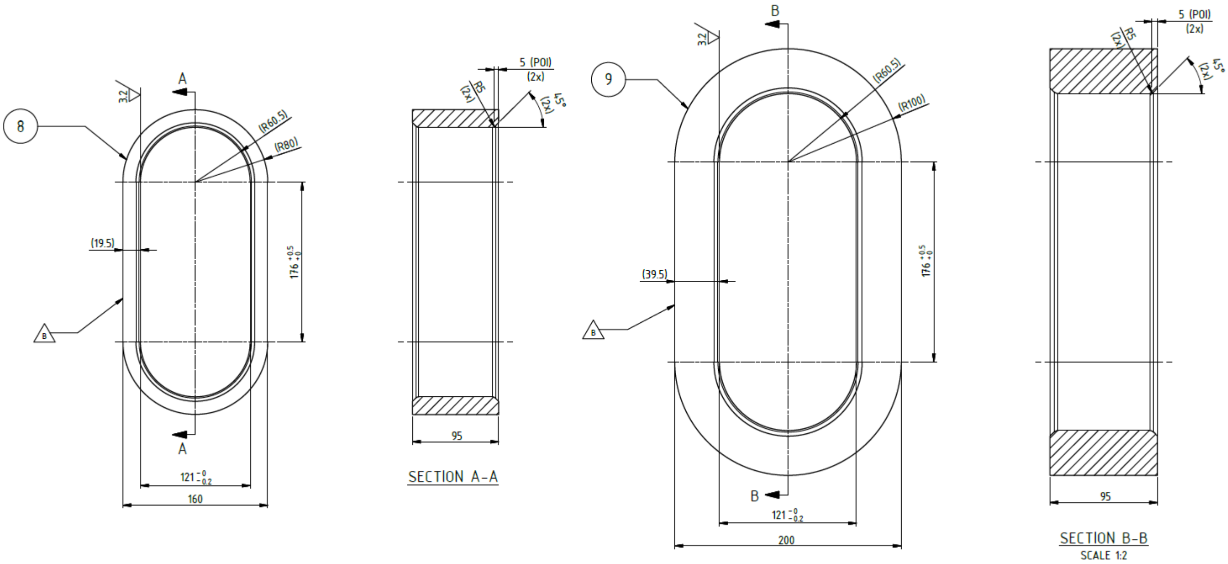

Figure E.6 – Custom sleeves for D/d=2 (left) and D/d=2.5 (right).

APPENDIX F: STRAIN GAUGE DATA

Data from the strain gauges can be found in the figures below. The strain gauge locations are based on Figure 4.18 and the nomenclature for the units around each bend are defined by the corresponding compass direction. In Sample S3, six out of the eight strain gauges were functional while only five of eight units worked for Sample S4. The plots show the test bench force output against the strain gauge output.

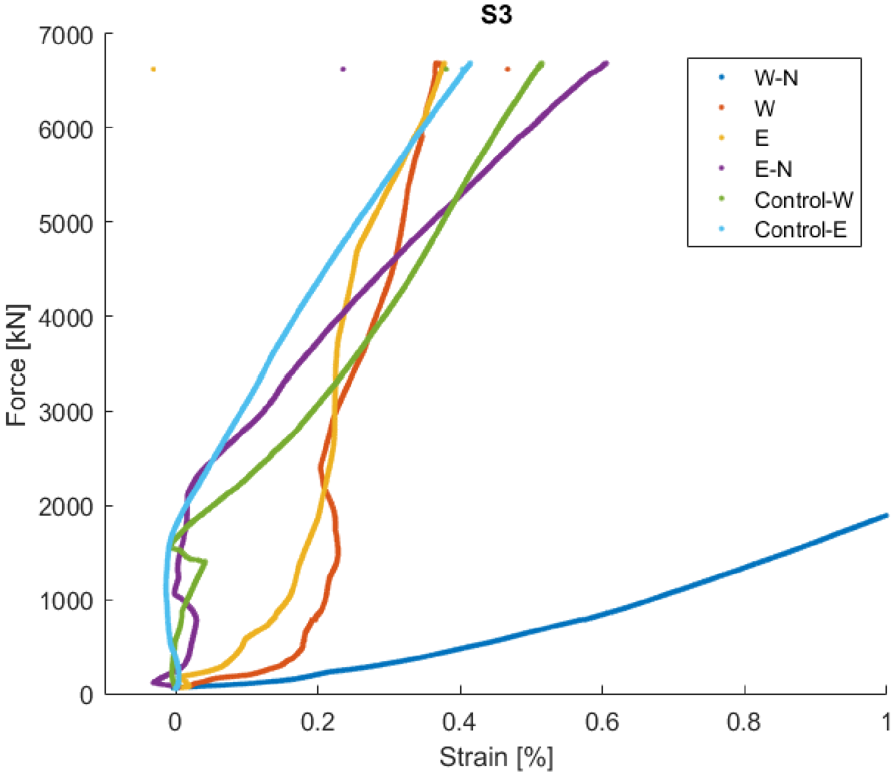

Figure F.1 – Force-strain curves of strain gauges in Sample S3.

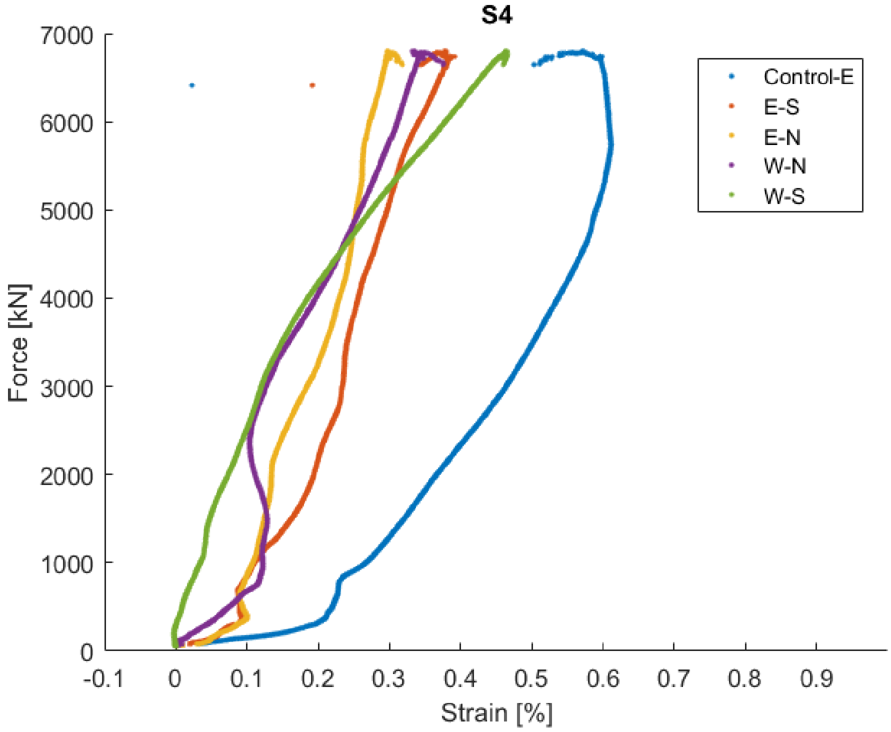

Figure F.2 - Force-strain curves of strain gauges in Sample S4.